Estudio de las propiedades magnéticas, electrónicas y estructurales de perovskitas de manganeso y su interrelación.

Memoria presentada por
Juan Ignacio Salafranca Laforga
Instituto de Ciencia de Materiales de Madrid (CSIC)

para optar al grado de
Doctor en Ciencias Físicas.

por la Universidad Autónoma de Madrid
Facultad de Ciencias
1 Enero de 2008

Structural, Magnetic and Electronic properties of Manganites and Their Interplay

by

Juan Ignacio Salafranca Laforga

Instituto de Ciencia de Materiales de Madrid (CSIC)

in Partial Fulfillment of the Requirements for the Degree of

Phylosophical Doctor in Physics

at the Universidad Autónoma de Madrid

Faculty of Science

January 15, 2008

Introducción

Óxidos de metales de transición

Los óxidos de metales de transici'on constituyen una familia de materiales muy interesante. A menudo, cristalizan en estructuras simples, como la estructura de perovskita ilustrada en la Fig. 0.1, o sus derivados. A pesar de su simplicidad química y estructural, los óxidos de metales de transición exhiben una importante variedad de fenómenos físicos, entre ellos, algunos no son bien esntendidos hoy en día. Por ejemplo, $LaTiO_3$ es un aislante de Mott [Iliev 04], la exhaustivamente estudiada *familia* de los Cupratos con estructura del tipo $La_{1-x}Sr_xCuO_4$, presentan antiferromagnetismo, superconductividad de *alta temperatura crítica*, y un estado conductor que es incompatible con la teoría del líquido de Fermi. En el caso de las manganitas, el objeto de esta tesis, $LaMnO_3$ permanece ordernado hasta temperaturas del orden de 750 K y $TbMnO_3$ exhibe fases magnéticas inconmensuradas. (ver Capítulo 3) que coexisten con ferroelectricidad. Fases más exóticas se encuentran, por ejemplo, en titanatos y rutenatos [Mochizuki 04, Nakatsuji 00].

Otra interesante característica compartida por los óxidos de metales de transición es la ectremada sensibilidad a ciertos parámetros físicos, como el desorden. Existen numeros y bien documentados ejemplos. En la familia de lso rutenatos, Fig. 0.4(a), la substitución de Ca por el elemenot isovalente Sr produce una gran variedad de fases, a pesar de la similitud química de los compuestos [Nakatsuji 00]. $SrTiO_3$, un aislante de bandas, se torna ferroeléctrico en láminas delgadas a temperatura ambiente [Kim 07], y a bajas temperaturas, aparece una transición superconductora cundo la composición es deficiente en Óxigeno. Las propiedades de las manganitas son muy sensibles as desorden y al doping, y exhiben respuestas sorprendentemente grandes a campos magneéticos (discutidas en la sección 1.4). En ciertas manganitas, consideradas en principio ordenadas, el desorden sútil que produce la posición aleatoria de dos iones muy similares, (Ba^{2+} y La^{3+}) tiene importantes consecuencias para la transición magnética (Capítulo 4). Los experimentos muestran que estas pequeñas desviaciones del ordenamiento prefecto pueden alterar el diagrama de fases de manera sustancial. (ver Fig.0.3).

La teoría de bandas es, en general incapaz de predecir la estabilidad de estas fases exóticas, y las respuestas extremas a estímulos pequeños o moderados. La pequeña extension espacial de los orbitales d, (especialemnte de los orbitales 3d) produce una compleja combinación entre interaciones que surgen del carácter localizado de los electrones, y efectos debidos a la hibridación. Los acoplos electron-electron y electron-red son importantes y

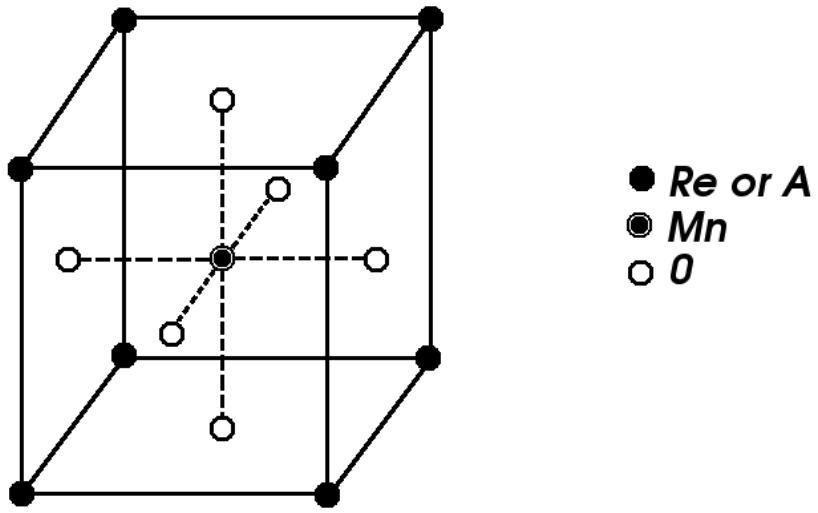

Figura 0.1: Estructura de perovskita no distorsionada,[Jonker 50]. En las manganitas, el Mn occupa la posici'on B, el Ox'igeno la O y la X es ocupada por distintas combinaciones de elementos alkalinos o tierras raras.

el estuio de los óxidos de metales de tensición constituyen una parte significativa y muy activa del campo de los *electrones fuertemente correlacionados.*

Manganitas

Nos concentraremos en las manganitas: fenómenos extraordinarios y un gran cuerpo de observaciones experimentales las convierten en especialmente atractivas a nuestro entender. A principios de los 90's Jin y colaboradores [Jin 94] informaron de un cambio de 3 órdenes de magnitud en la resistencia eléctrica de una lámina delgada de manganita cuando un campo magnético era aplicado. Esta inusitada y espectacualar magnetoresistencia, colosal como fue pronto bautizada, y, especialmente la posibilidad de aplicaiones en dispositvos electrónicos comerciales, estimul]'o en gran medida la investigación en manganitas.

La magnetoresistencia es una propiedad muy interesante de los materiales magnéticos desde el punto de vista tecnológico ya que permiten el diseño, por ejemplo, de sensores magnéticos. Desde entonces, estos materiales se han estudiado muy a fondo y también se ha encontrado otros con magnetorresistencia similar, como las dobles perovsquitas, los pirocloros de óxido de manganeso o el hexaboruro de europio. Estos materiales no son sólo importantes por las posibles aplicaciones tecnológicas de la magnetorresistencia colosal sino que, además, presentan una complejidad tal que suponen un reto tanto teórico como experimental.

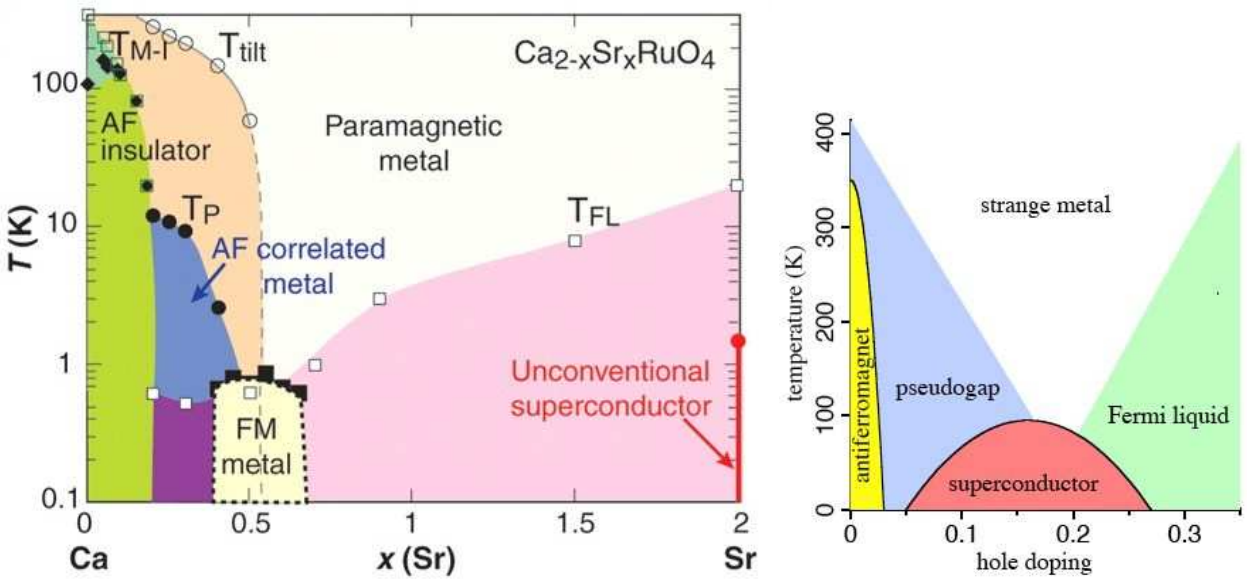

(a) Diagrama de fases de los rutenatos tipo Ca_2RuO_4 (b) iagrama de fases de los cupratos

Figura 0.2: Diagrama de fases de dos familias de compuestos, que ilustran el rico diagrama de fases y la senibilidad a distintos parámetros. (a) Diagrama de fases de los rutenatos con estructura laminado, de fórmula química $Ca_{2-x}Sr_xRuO_4$. Distintas fases electrónicas, desde aislantes a superconductoras, distintos ordénes magnéticos, y distintas transiciones estructurales aparecen. Notar que el dopante Sr es isovalente al Ca, Para más detalles consultar [Nakatsuji 00] y [Dagotto 05]. (b) Diagrama de fases esquemático de los cupratos, paradigma de los sitemas de electrones fuertemente correlacionados. Los huecos (el eje orizontal) son introducidos en el sistema mediante dopaje químico. Tomado de [Dagotto 05].

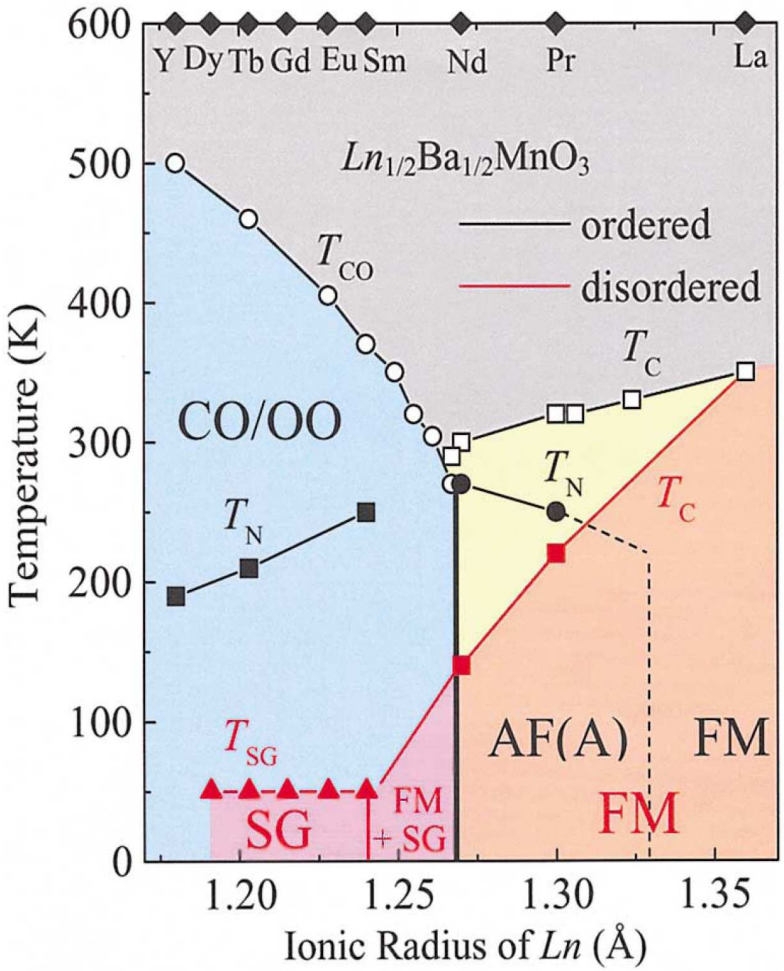

Figura 0.3: Alteraciones en el diagrama de fases de las manganitas a dopaje mitad debidas al desorden que surge de la posición aleatoria de los cationes situados en las posición A. CO/OO, FM, y SG denotan estados con oden de carga y orbital, ferromagnetico, and vidrio de espín, repectivamente. T_{CO}, T_C, y T_{SG} repesentan las correspondientes. Los compuestos con radio iónico mayor (hacia la derecha en el eje horizontal) tiene un ancho de banda mayor. El ión divalente, Ba en todos los compuestos y los diferentes lantánidos, (Ln) en el caso de los compuestos ordenados están situados en planos atómicos alternados (lineas y símbolos negros); por contra, ocupan posiciones de la red al azar en los desordenados, (lineas y símbolos rojos, y area sombreada en rojo). Tomado de [Akahoshi 03].

Antes de aparecer estos materiales, ya se había conseguido obtener valores grandes de magnetorresistencia en superestructuras de capas alternas de metales magnéticos y no magnéticos. Se denominó magnetorresistencia gigante. De hecho, estos sistemas ya se están utilizando en la industria para hacer cabezas lectoras de grabaciones magnéticas. Valores mayores de la magnetorresistencia permitirían el aumento de la densidad de almacenamiento de datos en memorias magnéticas.

La magnetorresistencia colosal (desde ahora utilizaré las siglas en inglés CMR) se encontró en las manganitas dopadas que presentan una transición metal-aislante a casi la misma temperatura que la transición magnética. Por tanto, a bajas temperaturas, el sistema es ferromagnético y metálico y por encima de la temperatura de la transición magnética T_c es paramagnético y aislante. Las temperaturas críticas experimentales van desde 100 K a 500 K. En el punto de la transición, la resistividad presenta un pico muy abrupto que desaparece progresivamente cuando se aplican campos magnéticos del orden de Teslas . Es decir, la CMR está limitada a la región próxima a T_c y, además, precisa de campos muy altos para ser realmente grande. Esta es la llamada magnetorresistencia intrínseca. Más interesante desde el punto de vista práctico es la magnetorresistencia extrínseca de muestras policristalinas y multicapas. Aparece para campos magnéticos pequeños, mucho menores que 1 Tesla y en un rango de temperaturas amplio por debajo de T_c. La magnetorresistencia extrínseca está asociada con la polarización de espín de los materiales. De hecho, tanto las manganitas como las dobles perovsquitas, entre otros, son *medio metálicos*. Esto significa que todos los portadores de corriente tienen un mismo espín. Esto se da en la fase ferromagnética ya que el acoplo Hund obliga a todos los electrones de un orbital parcialmente lleno de un ion a colocarse paralelos unos a otros. Es decir, tanto los electrones localizados en el ion (que configuran el espín del ion) como los de conducción tienen la misma orientación de espín. Por tanto, dos de estos sistemas ferromagnéticos puestos en contacto, ofrecerán una resistencia al paso de corriente muy grande si no están paralelos. Un pequeño campo magnético los orientaría convenientemente y reduciría la resistividad dando lugar a una magnetorresistencia grande. Dominar este carácter medio metálico es crucial para conseguir tener magnetorresistencia extrínseca con campos bajos a temperatura ambiente. Desafortunadamente, la polarización de espín se anula a temperaturas mucho más bajas que la crítica. La solución puede estar en los materiales con T_c muy alta, como las dobles perovsquitas ($T_c > 500K$).

Estos materiales no son sólo interesantes por las posibles aplicaciones tecnológicas. Las manganitas son por sí mismas muy interesantes porque son el prototipo de sistema en el que muchas interacciones distintas compiten de igual a igual y dan lugar a unos diagramas de fases muy complejos. La fórmula de estos óxidos de manganeso con estructura de perovsquita es $A_{1-x}B_xMnO_3$ donde A es una tierra rara trivalente y B es un alcalino divalente. El oxígeno está en el estado de oxidación O^{2-} y tiene su última capa p llena. x nos da la proporción de iones A y B en el compuesto. El manganeso puede presentar valencia +3 ó +4. Su proporción se controla directamente con x: por neutralidad de carga, el número de iones A^{3+} es igual al de iones Mn^{3+} y el de B^{2+} al de Mn^{4+}. La última capa d del Mn está incompleta. Los cinco orbitales d están degenerados en el

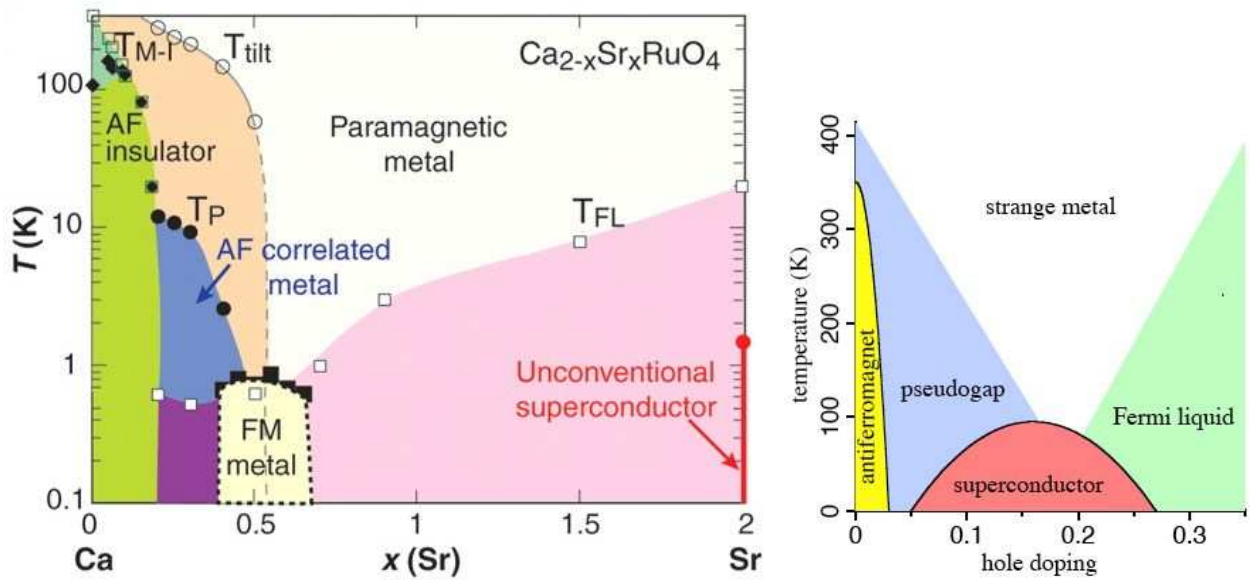

(a) Phase diagram of layered Ruthenates (b) Phase diagram of Cuprates

Figura 0.4: (a) Diagrama de fases de los rutenatos, para mas detalles ver [Nakatsuji 00] y [Dagotto 05]. (b)Diagrama de fases esquematico de los cupratos. [Dagotto 05].

átomo aislado pero en una red cúbica, como la de las manganitas, se separan en tres t_{2g} y dos e_g (ver Fig. 0.5). Los t_{2g} tienen menor energía por razones de simetría. El Mn^{4+} tiene tres electrones en su última capa que se colocan paralelos (regla de Hund) en los niveles t_{2g}. Estos electrones están localizados en el ion y sus espines se suman para dar un espín total $|S| = 3/2$. Los orbitales e_g son los únicos activos para el transporte (se hibridan con p del oxígeno dando lugar a la banda de conducción) y en el caso del Mn^{4+} están vacios. Por otra parte, el Mn^{3+} tiene un electrón extra que se coloca en un orbital e_g con el espín paralelo al de los t_{2g} ($|S| = 2$). x es, por tanto, la densidad de huecos en la banda de conducción. Los orbitales e_g del Mn^{3+} rompen su degeneración debido al teorema de Jahn-Teller que dice que un estado fundamental degenerado se deforma de manera espontánea para disminuir su simetría a no ser que la degeneración sea sólo de espín (más abajo veremos en qué consisten las deformaciones Jahn-Teller).

La estructura cristalina es la de perovskita (Fig. 0.1). Los Mn forman una red cúbica. Cada Mn está rodeado de seis oxígenos que forman un octahedro. Tenemos entonces una red cúbica de octahedros. Los iones A y B están en los huecos entre octahedros. Lo más importante a destacar por ahora es que los iones de Mn están unidos por medio de un O.

Entonces, si $x = 0$, sólo hay Mn^{3+} en el sistema, por tanto, la banda de conducción está llena y el sistema es aislante. Además es un antiferromagneto. La interacción antiferromagnética proviene de la interacción de superintercambio entre los espines localizados en los orbitales t_{2g}. Si, por el contrario, $x = 1$, sólo hay Mn^{4+}, la banda de conduc-

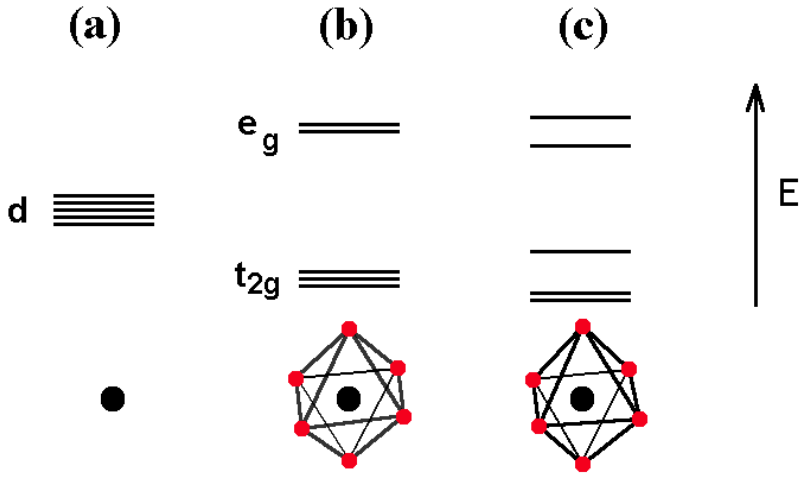

Figura 0.5: Esquema de enrgías de los niveles d, en un átomo aislado, a) , en un entorno octhédrico como el de las manganitas, b), y tras una distorsión uniaxial simétrica. c).

ción está vacía y también es aislante y antiferromagnético. Para x intermedio, la banda está parcialmente llena y el sistema es metálico y ferromagnético. La correlación estre ferromagnetismo y metalicidad la explicó Zener [Zener 51, C.Zener 51] en los años 50 por medio de su modelo de *doble intercambio*. En el estado de valencia mixta, es decir, cuando hay tanto Mn^{3+} como Mn^{4+}, el proceso de conducción se produce por medio del orbital p completo del O: un electrón se transfiere de un Mn al O a la vez que un electrón del O se transfiere al otro Mn. El nombre de doble intercambio se debe a la necesidad de dos procesos simultáneos. Los estados

$$\psi_1 : Mn^{3+}O^{2-}Mn^{4+}$$
$$\psi_2 : Mn^{4+}O^{2-}Mn^{3+}$$

están degenerados en energía si los espines localizados en los t_{2g} están paralelos (es decir, ordenados ferromagnéticamente). Entonces, los electrones de los e_g, que están fuertemente acoplados a los t_{2g} por la regla de Hund y que no cambian su espín en el proceso, se pueden mover fácilmente por el sistema. Si los espines localizados estuvieran antiparalelos, los electrones e_g no podrían pasar de uno a otro y el sistema sería aislante.

Ya he comentado que los espines localizados en los Mn son grandes (3/2) por lo que es una buena aproximación considerarlos clásicos. Esto lo hicieron Anderson y Hasewaga [Anderson 55] para formalizar el modelo de doble intercambio partiendo de un solo par de Mn. En la Fig. 0.6 podemos ver que si tratamos los espines como clásicos, el electrón, cuando se transfiere de un Mn al vecino, se tiene que projectar en la dirección del nuevo espín $\vec{S}_2$. Generalizándolo a una red cúbica de espines, tenemos el Hamiltoniano

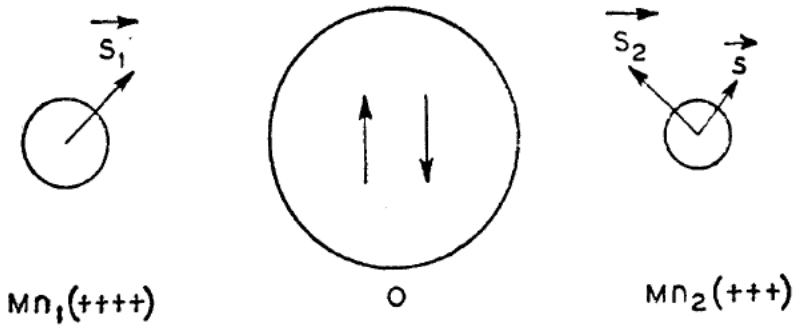

FIG. 1. Model for double exchange.

Figura 0.6: Modelo semi-clásico del doble intercambio según Anderson y Hasewaga [Anderson 55]. Los espines S se consideran grandes (clásicos) y se les trata como vectores tridimensionales.

$$H = t \sum_{ij} cos\frac{\theta_{ij}}{2} d_i^+ \, d_j \tag{0.1}$$

donde i y j son primeros vecinos y θ_{ij} es el ángulo relativo entre $\vec{S}_i$ y $\vec{S}_j$. d_i^+ es el operador de creación de un electrón en el sitio i con su espín paralelo al del ion. t es el parámetro de "hopping" que está directamente relacionado con el ancho de la banda de conducción $W = 12t$.

Más recientemente, Müller-Hartmann y Dagotto[Müller-Hartmann 96] señalaron la importancia de considerar la fase de Berry, es decir, la fase que adquiere un electrón cuando se mueve en circuitos cerrados. Partiendo del Hamiltoniano tipo Kondo

$$H = -t \sum_{\langle i,j \rangle \sigma} C_{i,\sigma}^+ C_{j,\sigma} - J_H \sum_i \vec{\sigma}_i \vec{S}_i \tag{0.2}$$

donde J_H es el acoplo Hund, $C_{i,\sigma}^+$ es el operador creación de un electrón en el sitio i con espín $\sigma = \uparrow, \downarrow$. Haciendo el límite $J_H >> t$, es decir, proyectando el espín del electrón de conducción en cada sitio sobre el correspondiente espín localizado,

$$H = -t \sum_{\langle ij \rangle} \left(cos\frac{\theta_i}{2} cos\frac{\theta_j}{2} + sin\frac{\theta_i}{2} sin\frac{\theta_j}{2} e^{i(\phi_i - \phi_j)} \right) d_i^+ d_j \tag{0.3}$$

donde θ_i y ϕ_i son las coordenadas polares de los espines clásicos. [1]

El modelo de doble intercambio puede explicar la correlación entre ferromagnetismo y metalicidad que ya se había descubierto en los años 50 pero la magnetorresistencia colosal queda fuera de su alcance: la transición metal-aislante precisa de la existencia de interacción con la red (fonones) (Millis *et al* [Millis 98]). Así mismo, el estado de valencia mixta es sólo ferromagnético para $0{,}2 < x < 0{,}5$ y para valores diferentes de x se han encontrado distintas fases aislantes. Estas nuevas fases aparecen porque hay otras interacciones, aparte de la de doble intercambio, que pueden dominar el sistema en algunos casos. Para empezar, la fuerza del doble intercambio se ve mermada por el desorden del sistema. Los iones A y B suelen ser de distintos tamaños y esto hace que los octahedros se inclinen con respecto a la red cúbica. Entonces, las ligaduras Mn-O-Mn dejan de estar en línea recta y forman ángulos distintos de 180^o. Consecuentemente, el solapamiento de los orbitales disminuye y la banda de conducción se estrecha. Esto es muy importante porque en el modelo de doble intercambio, la T_c depende de la anchura de la banda. Por ejemplo, la T_c del $La_{0,7}Sr_{0,3}MnO_3$ es $350K$ y la del $La_{0,7}Ca_{0,3}Mn_3O$ es $\sim 250K$. Otra fuente de desorden es la diferencia de tamaño entre los iones Mn^{3+} y Mn^{4+} que da lugar al modo respiratorio de distorsión de los octahedros. Los iones de Mn^{3+} también sufren deformaciones Jahn-Teller (Fig. 0.7) que llevan asociado el desdoblamiento de los niveles e_g. Todas estas deformaciones de la red compiten energéticamente con el doble intercambio. También está la interacción de superintercambio entre los espines localizados que es de carácter antiferromagnético.

El caso del $La_{0,5}Ca_{0,5}MnO_3$ puede ayudarnos a ilustrar la competencia de la que hablo. En principio, $x = 0{,}5$ corresponde al estado de valencia mixta ideal ya que hay tantos Mn^{3+} como Mn^{4+}. Sin embargo, el sistema no es ni metálico ni ferromagnético. Por el contrario, presenta orden de carga, de espín y de orbital. Este es el estado fundamental. Cuando se aplica un campo magnético grande, el sistema pasa a una fase ferromagnética y metálica, dando lugar a CMR.

Además, los sistemas no son homogéneos [van den Brink 99a]. Con esto quiero decir que fases ferromagnéticas y de orden de carga, por ejemplo, pueden coexistir al mismo tiempo. Esto es una prueba más de la competencia estricta entre los grados de libertad de espín, de carga y de la red. Las fases aislantes aparecen con más fuerza en los sistemas de banda de conducción estrecha. Además, la CMR es mayor cuanto más estrecha es la banda (o más pequeña es la T_c). Esto es consistente con algo que ya he comentado: el modelo de doble intercambio no puede explicar la CMR.

En este trabajo, estudiamos las propiedades del Hamiltoniano de doble intercambio con el objetivo de discernir aquellas propiedades de las manganitas que este simple modelo puede explicar. Además, es indiscutible, que esta interacción subyace al comportamiento general de las manganitas.

[1] En el proceso de proyección del espín del electrón de conducción sobre el espín localizado se pasa continuamente del operador $C^+_{i,\sigma}$ a d^+_i que está en la base local de cada ion.

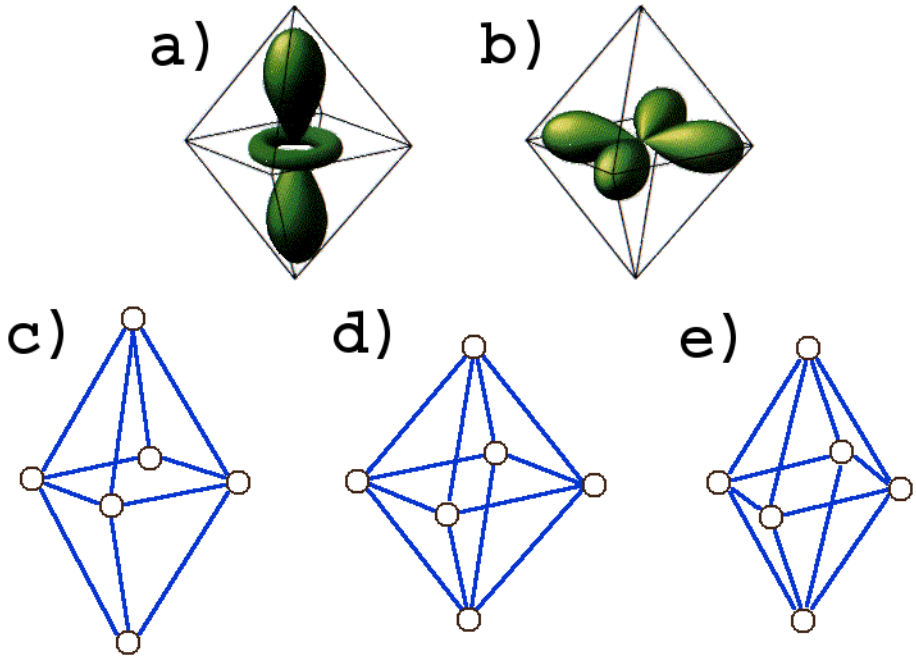

Figura 0.7: a) and b), Esquema de los orbitales d reales. $3z^2 - r^2$ (a) y $x^2 - y^2$ (b). d) octahedros regulares. c) and e): Los octahedros tras una disotrsion $Q_z > 0$ (c) y $Q_x > 0$. Los orbitales e_g orbitals (a) y b)) son afectados de manera distinta por estas distorsiones

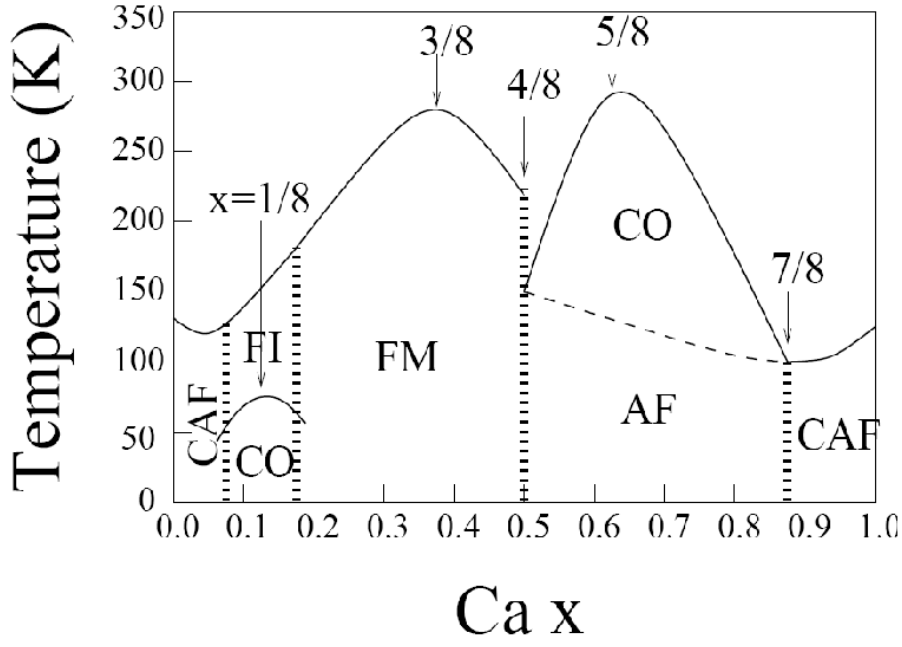

Figura 0.8: Diagrama de fases de la familia $LaCaMnO_3$ [P.Schiffer 95]. FM: ferromagnético metal, FI ferromagnético aislante, CO orden de carga, AF antiferromagnetico aislante, CAF canted antiferromagnetico aislante.

Conclusiones

Hemos estudiado las manganitas fijandonos principalmente en el modelo de doble intercambio, y en la competición entre las interacciones que favorecen la localización y el antiferromagnetismo, como el superintercambio y la interacción electrón-red frente a las que favorecen las fases ferromagnéticas y metálicas.

Hemos estudiado la relevancia de el acoplo electrón-red en las propiedades de trasnporte de las manganitas a dopaje óptimo, en el que se encontró la magnetorresistencia colosal. Así mismo, hemos provado que es necesario introducir desorden o algún otro ingrediente en el modelo para reproducir el pico en la magnetoresistencia que aparce en los experimentos

Esto está demostrado en el Capítulo 2. Allí calculamos la conductividad numéricamente con el formalismo de Kubo. Utilizamos simulaciones de Monte-Carlo para generar configuraciones de espín y de las posiciones de los oxígenos con las que calcular la conductancia a distintas temperaturas. Está, entonces, garantizado que las fluctuaciones de espín y de los modos Jhan Teller están incluidos apropiadamente y que el desorden no diagonal no es suficiente para hacer que los portadores de corriente se localicen.

El desorden es estudiado en el Capítulo 4 en relación a la transición ferromagnética-paramagnética en las manganitas metálicas. En él se demuestra que el desorden debido a los cationes dopantes tiene un papel importante en la reducción de la temperatura de Curie. El orden de la transición también cambía, para un grado desorden suficientemente grande, de primer orden a transicón contínua.

El campo de las manganitas está repleto de resultados sorprendentes. Uno de estos es el tratado en el Capítulo 3, las fases inconmensuradas observadas experimentalmente en las manganitas. Mediante cálculos analíticos y simulaciones numéricas, se muestras que estas fases surgen de la competición entre la interacción ferromagnética de largo alcance debida al Doble Intercambio y la interacción antiferromagnética de corto alcance debida al superintercambio. Adem'as, se estudia la variación de la periodicidad con la temperatura que reproduce cualtitativamente la de los experimentos. Se muestra que la fase inconmensurada se puede entender como paredes de dominio con correlaciones ferromagnéticas que separan regiones esencialmente conmensuradas con la red. Además establecemos un diagrama de fases del modelo para manganitas sin dopar, clarificando la naturelza del gap en las fases conmensuradas.

Finalmente, se han explorado las tremendas posibilidades que ofrecen los muy notables avances en técnicas de crecimiento de óxidos. En particular, en el Capítulo 5 se ha

propuesto y estudiado una heterostructura compuesta de manganitas ferromagnéticas y antiferromagnéticas, a dopajes cercanos al óptimo, como dispositivo útil para la espintrónica. Los cálculos indican que es posible, manipulando la magnetización de una de las capas, cambiar el estado electrónico de la capa vecina de metal a aislante. Además, se muestra que las presencia de las capas ferromagnéticas metálicas potencian la interacón de Doble Intercambio en la capa central, favoreciendo la aparición del estado metálico en determinadas condiciones. Así mismo se ha recuperado el resultado esperimental de que la magnetoresitencia de las multicapas de maganitas con ancho de banda pequeño se ve favorecido por la presencia de otras cuyo estado fundamental es ferromagnético y metálico.

Contents

Chapter 1

Introduction

1.1. Transition Metal Oxides

Transition-metal oxides constitute a very interesting family of materials, with challenging properties. Many oxides crystallize in simple lattice arrangements, such as the perovskite structure (Fig. 1.1). Despite the chemical and structural simplicity, transition-metal oxides display very different physical phenomena, among them, not all are well understood. For instance $LaTiO_3$ is a Mott insulator [Iliev 04], the intensively studied *family* of layered Cuprates, like $La_{1-x}Sr_xCuO_4$, present antiferromagnetism, *High Critical Temperature* superconductivity, and a conducting state non-compatible with fermi-liquid theory 1.2(b). In the case of manganites, the subject of this thesis, $LaMnO_3$ remains orbital ordered up to 750 K and $TbMnO_3$ shows magnetic incommensurate phases (see chapter 3) that coexists with ferroelectricity. More exotic phases are found, for example, in Titanates and Ruthenates [Mochizuki 04, Nakatsuji 00].

Other interesting characteristic shared by transition-metal oxides, is the tremendous sensitivity to certain physical parameters, such us doping, pressure, magnetic field, or disorder. There are numerous well documented examples. In the family of Ruthenates $Ca_{2-x}Sr_xRuO_3$, Fig. 1.2(a), substitution of Ca by the isovalent element Sr produces a great variety of phases, despite the chemical similarity of the compounds [Nakatsuji 00]. $SrTiO_3$, a band insulator, becomes ferroelectric in thin films at room temperature [Kim 07], and a metal-superconducting transition appears at low temperatures when the composition is oxygen deficient. Manganites properties are very sensitive to disorder and doping and show surprisingly large responses to magnetic fields (discussed in section 1.4). For certain manganites which were, in principle, considered as having an ordered structure, removing the subtle disorder which arises from the radom position of two very similar ions (Ba^{2+} and La^{3+}) has important consequences for the magnetic transition (chapter 4). Experiments show that these small departures from perfect ordering can change the phase diagram substantially (see Fig.1.3).

Band theory is, in general, unable to predict the stability of the *exotic* phases, and the huge responses to small or moderate stimulus. The small spatial extent of d orbitals (specially 3d orbitals) produces a complex interplay between interactions arising from

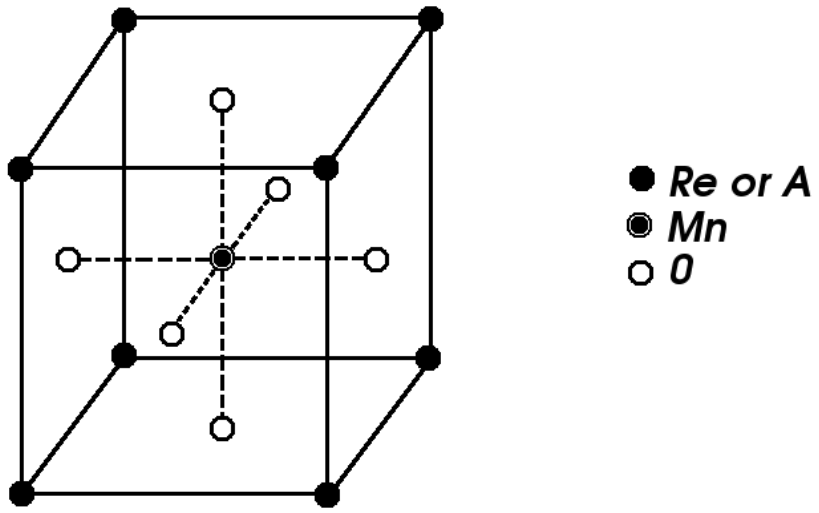

Figure 1.1: Undistorted perovskite structure as shown in Ref. [Jonker 50]. In manganites, Mn occupy the B position, Oxygen the O position, and different combinations of alkaline elements, Lead, or rare earth elements, the A position. The dotted lines mark the axes of a regular octahedra, formed by MnO_6 in manganites .

the localized character of the electrons and effects due to hybridization. Both electron-electron and electron-lattice coupling are significant and the study of transition metal oxides constitutes a substantial and very active part of the field of *strongly correlated electrons* .

1.2. Manganites

We shall concentrate in manganites: some *spectacular* phenomena and a large body of experimental work makes them specially attractive to us. In the early 90's Jin and collaborators [Jin 94] reported a change of 3 orders of magnitude in the electrical resistance of a manganite thin film when a magnetic field was applied. This extraordinary magnetoresistance, Colossal Magnetoresistance (CMR) as it has been named, and specially, its potential for application in commercial electronic devices, greatly stimulated research on manganites.

CMR is a remarkable phenomena, challenging our understanding, and much work is today devoted to it. However, it is doubtful that manganites can compete with *Nobel awarded* GMR multilayers [Binasch 89, Baibich 88] as base materials for magnetic memories read heads. From the point of view of applications, the most interesting property of manganites seems to be their half metallicity. It makes them good spin

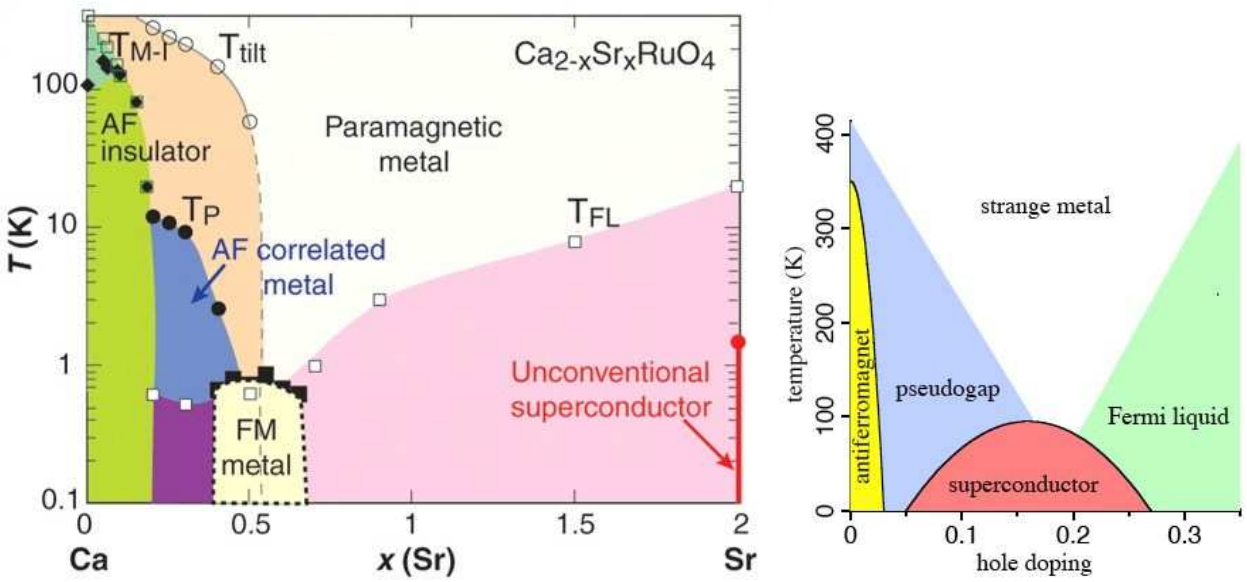

(a) Phase diagram of layered Ruthenates

(b) Phase diagram of Cuprates

Figure 1.2: Phase diagram of two families of compounds illustrating the wealthy phase diagram and the sensitiveness to different parameters. (a) Phase diagram of a family of layered Ruthenates, with chemical formula $Ca_{2-x}Sr_xRuO_4$. Different electronic phases, from insulating to superconducting, different magnetic orderings, and structural transitions appear. Notice that Sr dopant is isovalent to Ca. The notation is standard, for details see [Nakatsuji 00] and [Dagotto 05]. (b) Schematic phase diagram of Cuprates, paradigm of correlated electron system. Holes are introduced in the system by chemical doping. Taken from [Dagotto 05].

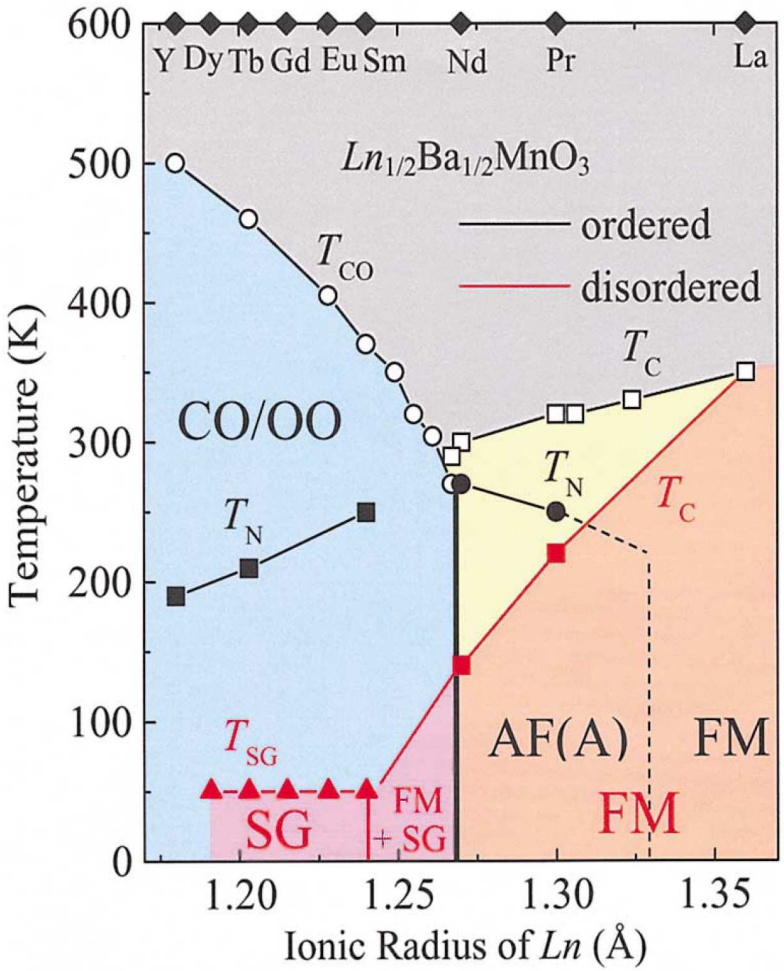

Figure 1.3: Changes in the phase diagram of half doped manganites introduced by disorder arising from the random position of the A-sitting cations. CO/OO, FM, and SG stand for the charge/orbital ordered, ferromagnetic, and spin-glass states, respectively. T_{CO}, T_C, and T_{SG} represent the corresponding transition temperatures. Compounds with bigger ionic radius (right of horizontal axis) have larger bandwidth. Divalent cation, Ba in all compounds, and different lanthanoids (Ln) are placed in alternative planes in the ordered compounds (black line and symbols) and randomly distributed in the disordered compounds (red line and symbols; the region shaded in red). Taken from [Akahoshi 03].

injectors for spintronics (see chapter 5), an appealing, promising, and fast developing field [Bibes 07].

May it be for the possible applications or because the extraordinary basic interest of these materials, a tremendous effort, involving hundreds of scientists, has been done in the last 15 years in manganites research. As a result, we have at our disposal precise experimental information and a large amount of data. This represents a great opportunity to improve our understanding of strongly correlated electron systems.

Before the important discovery of CMR, some works established the basic ideas and features of manganites. We shall go over these main characteristics, in an approximate order of chronological discovery, trying to give credit to the pioneer works.

1.3. Historic introduction

1.3.1. The 50's. Cornerstones

The first experimental work

The work of Jonker and Van Santen [Jonker 50, van Santen 50] constitutes the cornerstone of the field of manganites. In general, the two scientists were interested in the properties of the transition metal oxides growing in the perovskite structure. Indeed, posterior research has proven that this family of compounds is tremendously interesting [Dagotto 02, Tokura 00]. The perovskite structure is illustrated in Fig. 1.1. It corresponds to compounds with chemical formula ABO_3. The large cations occupy the corners of the ideally cubic unit cell, (positions labeled A in Fig. 1.1), the small cations, Manganese in the case of our interest, are in the center (B position) of the cube. Finally, there is one anion, usually oxygen, in the center of each of the faces (O position), forming a regular octahedra around the B position. In particular, Jonker and Van Santen were able to grow different manganese oxides with this structure and called the whole family manganites.

In their work, published back in 1950 [Jonker 50], they state: *Various manganites of the general formula* $La^{3+}Mn^{3+}0_3^{2-}$–$Me^{2+}Mn^{4+}O_3^{2-}$ *have been prepared in the form of polycrystalline products. Perovskite structures were found, i.a. for all mixed crystals* $LaMnO_3$–$CaMnO_3$, *for* $LaMnO_3$–$SrMnO_3$ *containing up to 70%* $SrMnO_3$, *and for* $LaMnO_3$–$BaMnO_3$ *containing less than 50%* $BaMnO_3$. The general formula is commonly expressed today as $La_{1-x}Me_xMnO_3$ and we will use this later notation throughout the thesis. As remarked in Ref. [Jonker 50], one important aspect of the perovskite structure of these compounds, is its ability to accommodate both divalent and trivalent cations in the A position. Then, when x is not 1 or 0, charge neutrality implies that the B sitting Manganese is in a mixed valence state, there must be Mn^{3+} and Mn^{4+} in the system. As it was soon clear, a key point is how this charge density gets distributed in

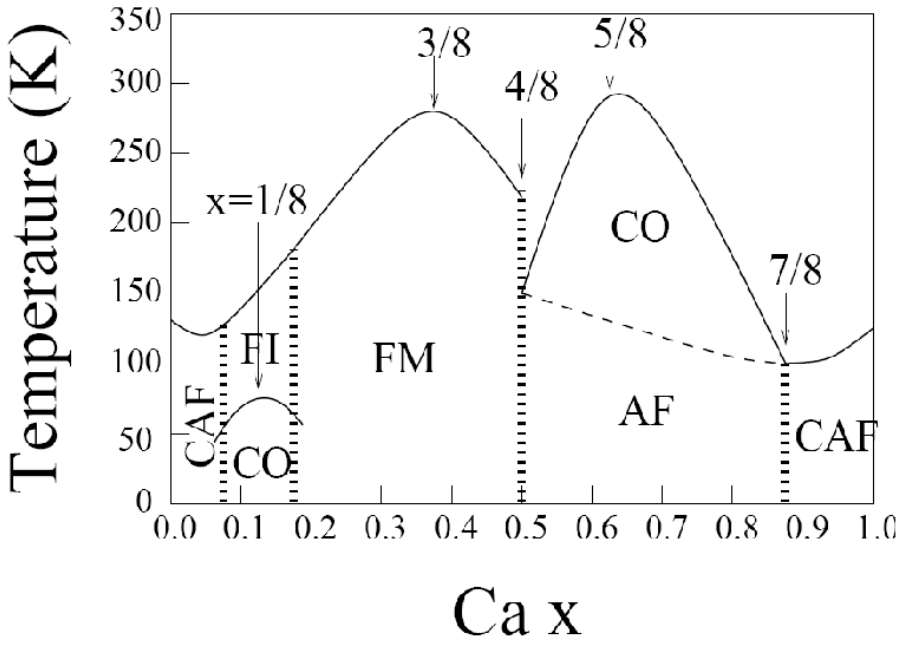

Figure 1.4: Phase diagram of the family $LaCaMnO_3$ as published in [P.Schiffer 95]. The different phases will be studied in detail along the thesis. FM: ferromagnetic metal, FI ferromagnetic insulator, CO charge order, AF antiferromagnetic insulator, CAF canted antiferromagnetic insulator. In this family, special features are observed when hole doping x is an integer multiple of 1/8.

the material. From the quotation, it can be inferred that the authors considered that proper proportions of manganese ions were in the 3+ or the 4+ states. This localized or ionic picture has been traditionally adopted, but recent experimental and theoretical work ([Dagotto 02], and references therein) shows that it is at odds with some aspects of manganite physics, and it is more correct to think of 4-x electrons per Mn. We will discuss how, of the 4-x electrons, three are strongly localized, but the rest only do get localized in particular experimental situations or compositions.

Two articles collect their early results, in the first one [Jonker 50], Jonker and Van Santen devoted different sections to the overview of the preparation method, considerations about the structure, and to magnetic properties, while the electrical properties where discussed in a second paper [van Santen 50]. The points they address are crucial to understand the behavior of manganites:

- the oxygen content of the sample depends closely on the preparation details, in particular on the composition of the atmosphere during preparation. They correctly realized that excess or defect of oxygen affected the average valency of the Manganese ions. This has been a subject of intense work, and, probably, a source of non exactly reproducible

results until recent years.

- It was already known, as thus they explained it, that the perovskite structure is stable only if the goldsmith tolerance factor, Γ, is close to unity. Γ is defined in terms of the average ionic radius of the species occupying the different positions of the structure (Fig. 1.1) $\Gamma=(r_A+r_O)/(r_B+r_O)\sqrt{2}$. For $\Gamma \sim 1$ the ideal perovskite with a cubic unit cell is obtained. As Γ differs from one, the MnO_6 octahedra begin to tilt and the Mn-O-Mn angle is no longer 180°. The importance of the small departures from the ideal perovskite structure could only be understood later, as explained below.

- Most importantly, they measured the Curie temperature, and the saturation magnetization as a function of the composition. They synthesized compounds where lanthanum was substituted by either Calcium, Barium or Strontium. For the approximate range of 25%- 35% of nominal Mn^{4+} composition, the saturation magnetization could be calculated assuming the contribution of all the spins of the manganese 3d electrons (and none from the orbital angular momentum). In the second paper [van Santen 50] they reported metallic like behavior and the highest conductivities in this so called optimal doping.

- They also discussed magnetic interactions between different Manganese ions, Mn^{4+} and Mn^{3+}. It was clear from their experiments that some kind of ferromagnetic interaction was induced when mixed valence manganese was present in the material. They also inferred that an antiferromagnetic interaction existed between two Mn^{4+} ions, and they reported that the interaction among Mn in a 3+ valence state should be small. Although they were right about the sign of the interactions, the work presented in this thesis, as in most articles in modern literature, indicates that the properties of manganites cannot be understood only in terms of pair like interactions, they are much better described if long range interactions, especially in the metallic regime, are considered.

In summary, Jonker and Van Santen established the main features of manganites and gave important indications for the growth and characterization. They started to unveil the rich phase diagram, but mainly, they demonstrated the close correlation between electronic transport and magnetism, crucially suggesting a common origin for both.

Zener and the Double Exchange Mechanism

Also in the early 50's, Zener published several theoretical papers about the magnetism of transition metals and their oxides, two of them are specially relevant for the physics of manganites. Ref. [Zener 51] appeared some months after the publication of the experimental work of Jonker and Van Santen, but, apparently, before Zener was aware of it. In order to explain the lattice structure and magnetism of some of the transition metals, Zener deduced three *principles*. The first one states that the electrons in the incomplete d shell will have their spin correlated so that the total spin will be maximum. This is equivalent to Hund's rule in atomic physics, and for manganites it implies that the Manganese ion is in a high spin state. That is, S= 3/2 for Mn^{4+} and S= 2 for Mn^{3+}.

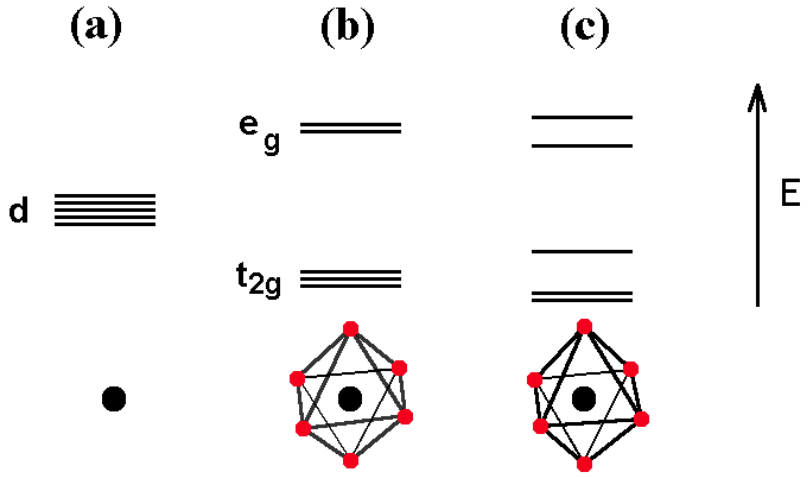

Figure 1.5: Scheme showing the energy (E) of d levels in an isolated atom a) , in an octahedral environment such as the one found in manganites b), and after a uniaxial distortion c). The symmetry of the environment is reduced from a) to c) as it is the degeneracy.

The second principle is that direct coupling between localized electrons in neighboring magnetic ions is always antiferromagnetic. Applied to the case of manganites, it explains how, in the absence of coupling mediated by conduction electrons (for insulating manganites), the ground state is antiferromagnetic. The last one refers to the role of those conduction electrons, they are strongly coupled to the spin of localized electrons, and the coupling tends to align all the spins ferromagnetically.

Zener applied these *principles* to manganites in a second paper [C.Zener 51]. Before we review it, a remark should be made about Zener's first *principle*. Here the well known quenching of d orbital momentum [Van Vlek 32] takes place. The situation is described in Fig. 1.5. For an isolated (gaseous) atom the d levels are degenerate due to the isotropic environment, the application of a magnetic field would lift the degeneracy, leading to Zeeman splitting and to an induced magnetic moment in which the orbital magnetic moment adds up to the spin magnetic moment [Bransden 80]. When the manganese ions are in an octahedral environment such as the one in the perovskite structure (see Fig. 1.1) the degeneracy of the d orbitals is removed even in the absence of a magnetic field. It can be shown [Dagotto 02] that three orbitals, named t_{2g} according to their symmetry (see Fig. 1.7) reduce their energy, while other orbitals, the e_g (Fig 1.7), point towards the negative charged oxygen and therefore have a higher energy. The expectation value of the z component of the orbital angular momentum for this wavefunctions is zero, in accordance with the observation reported by Jonker and Van Santen that only the spin magnetic moment contributes to the saturation magnetization. There is another physical consequence of this splitting. When the splitting is big compared with the

dispersion of the *band* formed by the lower t_{2g} orbitals, a band insulator will form for a filling of three d electrons per Manganese. This is just the case of $CaMnO_3$, one end member of the family of manganites discussed by Jonker and Van Santen. In fact, in manganites the three electrons in the t_{2g} orbitals form a localized 3/2 spin which is often called 'core spin' [Dagotto 02]. Although the detailed role of orbital degeneracy in d orbital systems was discussed later by Kanamori [J.Kanamori 60], we explain here these arguments which complement the analysis of Zener (further analysis of the work of Kanamori is given below, in section 1.3.2).

Zener realized the fact that his ideas, presented in [Zener 51], could explain the main aspects of manganites. That is the subject a second article, published also in 1951 [C.Zener 51]. He also considered the microscopic mechanism that made interactions in manganites similar to transition metals, despite the fact that magnetic ions are around 40% further apart in manganites, and an oxygen ion is between each two. In Zener's picture, an electron located in one Manganese ion has its spin parallel to the other d electrons in that ion (first principle). Since hopping preserves spin, when the spins of the Mn neighboring ions are parallel hopping process of one electron takes place between low energy configurations, and this favors ferromagnetic configurations. Therefore delocalizing of electrons is favored by a ferromagnetic order, and this mechanism explains the ferromagnetic coupling in manganites.

The essential ingredients of the mechanism that leads to ferromagnetic coupling are Hund's rule, coupling of spins of localized and mobile electrons, and spin preserving process between incomplete shells. How the electron transfer or hopping actually takes place is not important. Anyhow, Zener believed that the main contribution came from a process in which one electron hopped from the Oxygen to one Manganese, and simultaneously another electron hoped from the other Manganese to the hole in the Oxygen. This is why the name double exchange was applied to this mechanism, but this way in which strong coupling between carriers and localized spin induces ferromagnetism is more general.

Although Zener did not explore quantitatively his ideas, his physical intuition and his ability to *read* the important experimental results are quite remarkable. Posterior research has benefitted from the essential clues he provided.

Anderson and Hasewaga formalized the ideas of Zener and offered the community a quantitative approach to the physics of double exchange. Their work appeared in 1955 [Anderson 55]. They considered the two site problem both in semiclassical and quantum approximations. The semiclassical approach reduces to consider the transfer of one electron between two ions of large spin. In this way the quantization of the core spin can be ignored and a definite angle can be defined between the directions of the core spins of the two ions. The electron can be in two states in each ion, say either with its spin parallel or antiparallel to the core spin. As the hopping preserves spin, if one chooses a basis of localized orbitals and a common axis for the spins, the hopping matrix is diagonal in the spin index. However, in the limit of very large Hund's coupling, the only relevant orbitals are the ones for which the electron spin is parallel to

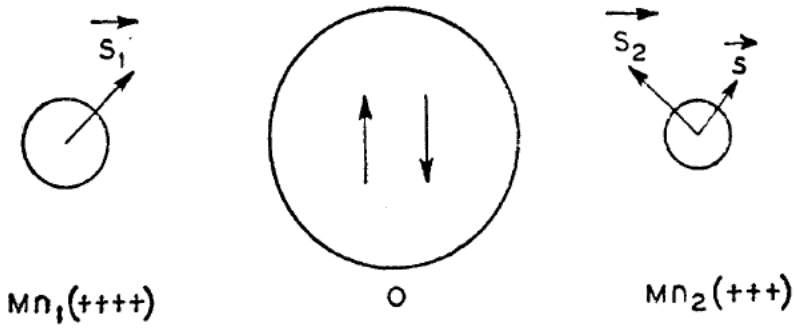

FIG. 1. Model for double exchange.

Figure 1.6: Scheme of the Double exchange model as seen by Anderson and Hasegawa [Anderson 55]. When an e_g electron hops form the manganese on the left side to the one on the right side, it retains the spin state.

the local core spin. It is convenient then to rotate the final states so that the quantization axis is defined by the core spin in each ion. As some of the possible final states are not relevant, the effective hopping is reduced. In the general case it can be shown [Müller-Hartmann 96] that the hopping amplitude t, becomes

$$t = t_0 \cos(\frac{\theta_i}{2}) \cos(\frac{\theta_j}{2}) + \sin(\frac{\theta_i}{2}) \sin(\frac{\theta_j}{2}) e^{-i(\phi_i - \phi_j)} \tag{1.1}$$

If the spins of the two ions are parallel, $\theta_i = \theta_j$, there is no need to rotate the quantization axis and the hopping is maximum and equal to its value in the absence of Hund's coupling, t_0, while if they are antiparallel, it is zero. This approximation, involving infinite Hund's coupling and classical core spins, (i.e. Eq 1.1) will be used along this thesis.

Wollan and Koehler

Another important step in the understanding of manganites was taken in 1955, when Wollan and Koehler published a neutron diffraction study of the La, Ca manganite series. They encountered an unexpectedly rich phase diagram. Some of the phases already discussed in that paper, and confirmed by posterior works, are important both for manganites and for the work presented in this thesis, and are discussed in the appendix. Let us remark that although the Manganese sites (which are the magnetic active sites in manganites) form a simple cubic lattice, the different phases observed by Wollan and Koehler break this symmetry in several different ways.

The competition between these phases is of great importance, and is probably responsible for the extremely large responses (*Colossal*) of manganites to moderate fields. Wollan

and Koehler also found signatures of charge order, other important issue in manganites, subject of intense debate and much work [Attfield 06].

1.3.2. The 60's and de Gennes

The variety of phases observed by Wollan and Koehler arose new questions that the ideas of Zener could not explain by themselves. De Gennes was the first one to consider theoretically the relative thermodynamic stability of different magnetic orders [de Gennes 60]. The work of de Gennes is cited most of the times relating to his prediction that canted phases should appear when doping the antiferromagnetic phase (in particular the A phase in Wollan-Koehler notation) with holes. But even more relevant for this work is the method of calculation. He used a mean field like virtual crystal approximation, in which, for each ordering, the hopping is assumed to be uniform and depends only on the magnetization of the sublattices corresponding to the particular ordering considered. The virtual crystal approximation is described in detail in chapter 3.

De Gennes also made an enlightening discussion about the different approximations made in the general problem of manganites. We shall do the same and give the modern view about the validity of those different approximations discussed in [de Gennes 60].

Degeneracy of the d orbitals

The fivefold degeneracy of the d band was neglected by de Gennes and earlier theoretical works [C.Zener 51, Anderson 55]. De Gennes pointed out that the consideration of orbital degeneracy *would only complicate matters by introducing more unknown parameters*. Certainly consideration of several d orbitals increases the number of parameters, makes the problem conceptually more complex and computational more difficult to address. When modern computers allowed numerical study of the double exchange model, a one orbital model was used [Vergés 02, Calderón 99b, Alonso 01c, Dagotto 02] to start with. We shall not give a complete account of the theoretical work on one or two orbitals (it can be found on [Dagotto 02]).

Let us remark, however, that the orbital degeneracy is of crucial importance to reproduce some phases already observed by Wollan and Koehler. In particular, the A phase present in undoped manganites such as $LaMnO_3$ (see chapter 3, and [Kimura 03]), or the CE phase [van den Brink 99a, L.Brey 05, Aliaga 03] appearing for compositions near half-doping. The fact that the orbitals involved present d symmetry and the anisotropy of the hopping between them stabilizes these phases. Therefore, we have considered orbital degeneracy throughout the thesis. It is also true that the one orbital model correctly reproducers some of the main features of the ferromagnetic metallic state, even the insulator metal transition found in $LaCaMnO_3$ at the optimal doping and other compounds [Vergés 02].

Quasi classical approximation.

The quasi classical approximation assumes two approximations discussed by de Gennes. The intratomic exchange is larger than the bandwidth, and the ionic spins are considered classical vectors. De Gennes describes them as *good starting approximations in all cases*. These approximations give the double exchange factor in the hopping, Eq.1.1. We agree with de Gennes and these approximations have been taken in all the work reported in this thesis. From the arguments presented in the last section, it appears that considering the t_{2g} electrons as a localized core spin is a sensible simplification. This would reduce the problem to the e_g orbitals coupled with a quantum 3/2 spin. However, little work has been done about the relevance of the quantum nature of the core spins[Müller-Hartmann 96, Kubo 72] for the phenomenology of manganites, and none to our knowledge includes the degrees of freedom within the t_{2g} subspace. As suggested by Millis [Millis 00] it would be interesting at least as a formal justification of the approximations commonly made.

Electron-Lattice coupling.

The coupling of electrons and lattice is of great importance in manganites, and much work has been devoted to it since the 60's. De Gennes remarked that this coupling would alter the effective masses and mobility of the carriers, but we know today that the effects are much more important. Two main types of distortions encountered in manganites are discussed next: (i) Distortions of the unit cell arising from changes in the network of the MnO_6 octahedra, and (ii) symmetric distortions of the octahedra, Jahn-Teller distortions. More complicated distortions do occur in particular cases, such as the ferroelectricity in some undoped manganites[Goto 04], but we will not discuss them here nor have they been studied in the rest of the thesis.

We discuss first type the conceptually simpler distortions of type (i). Often distortions of the unit cell can be well described as changes in the arrangement of the MnO_6 octahedra. The perovskite unit cell is ideally cubic, but this only happens if the tolerance factor is exactly one, that is, when the ions present in the material have perfectly matching sizes. When a bond is compressed, either by ionic size mismatch or by external pressure, it reacts by buckling. The Mn-O-Mn angle is then less than 180 degrees, and there is clear experimental evidence (see for instance [Fontcuberta 96]) that this strongly affects the the bandwidth of the e_g band, because it reduces the e_g hopping. The reduction of the bandwidth enhances the effects of other interactions competing with kinetic energy, mainly antiferromagnetic interactions and a second kind of electron phonon coupling, discussed next.

Jahn Teller distortions (type (ii)) are very important in manganites and have been the subject of numerous works. Probably the most influential, and the one that established the basis for the development of the subject, is the work of Kanamori [J.Kanamori 60]. Jahn Teller theorem [Jahn 37] states that a system having a degenerate ground state

will spontaneously distort unless this degeneracy due to electronic spin. The distortion lowers the symmetry and removes degeneracy so that, occupying only the lowest energy state, a new ground state with lower energy is reached. Fig. 1.5 shows that 4 electrons occupying the d levels of a Manganese ion in a octahedral environment corresponds to a degenerate ground state. The problem becomes more interesting in manganites, since neighboring octahedra share corners, distortions are coupled and Jahn Teller effect is cooperative. Kanamori studied cooperative distortions arising from Jahn-Teller theorem in different (undoped) compounds, such as $LaMnO_3$.

Cooperative Jahn Teller effect is best described with the aid of formalism shared from other phenomena. On one side, normal modes of vibration of a octahedra constitute an appropriate basis in which an arbitrary distortion can be expressed. Symmetry relations can be readily identified in this basis. On the other side, e_g orbitals constitute a two level system, any Hamiltonian within this subspace can be expressed in terms of the Pauli matrices allowing for the application of spin language to this pseudospin subspace.

e_g orbitals 1.7 are symmetric with respect to inversion of the coordinates or to a mirror relection with respect the planes containing any two axis. Therefore any distortion of the octahedra coupling linearly with them will have the same symmetry. The only two normal modes with this characteristic are the Q2 and Q3 modes described in Fig. 1.7. More details can be found in [Dagotto 02]. Kanamori defined the pseudospin states so that $|\uparrow>$ represents one electron in $|3z^2 - r^2>$ and $|\downarrow>$ represents one electron in $|x^2 - y^2>$. As usual, the combination of the power of the coordinates refers to the angular dependence of the orbitals. Opposing the linear coupling there is a quadratic elastic energy cost for the distortions. Kanamori expressed the Hamiltonian as:

$$H_{e-latt} = \sum -g/\sqrt{C}\,(\sigma_z\,Q_3 + \sigma_x\,Q_2) + C/2\left(Q_2^2 + Q_3^2\right)\ . \tag{1.2}$$

Where g is the coupling constant and C and elastic constant. The same Hamiltonian is used along this thesis, although the distortions, with a convenient normalization of the distortions and the couplings. If some parameter t (normally the hopping) is used as energy unit, Eq. 1.2 becomes:

$$\frac{H_{e-latt}}{t} = \sum -\lambda\,(\sigma_z\,Q_3 + \sigma_x\,Q_2) + \left(Q_2^2 + Q_3^2\right)\ . \tag{1.3}$$

Although Jahn Teller effects were already known, Kanamori was the first one to consider the cooperativeness of the distortions. In particular, he studied the most significant cases for undoped materials, pseudo-ferromagnetic and pseudo-antiferromagnetic ordered distortions. For doped manganites, the situation is complex, and can be addressed by applying a Hamiltonian like 1.3 to finite size cluster with periodic boundary conditions 2, and oxygen positions as independent variables.

The breathing mode,Q_0 is also considered in this thesis. It does not lift the degeneracy of the E_g orbitals, but it obviously couples to the charge in each ion (ρ), and it can be important for undoped manganites. Coupling to breathing mode can also be understood

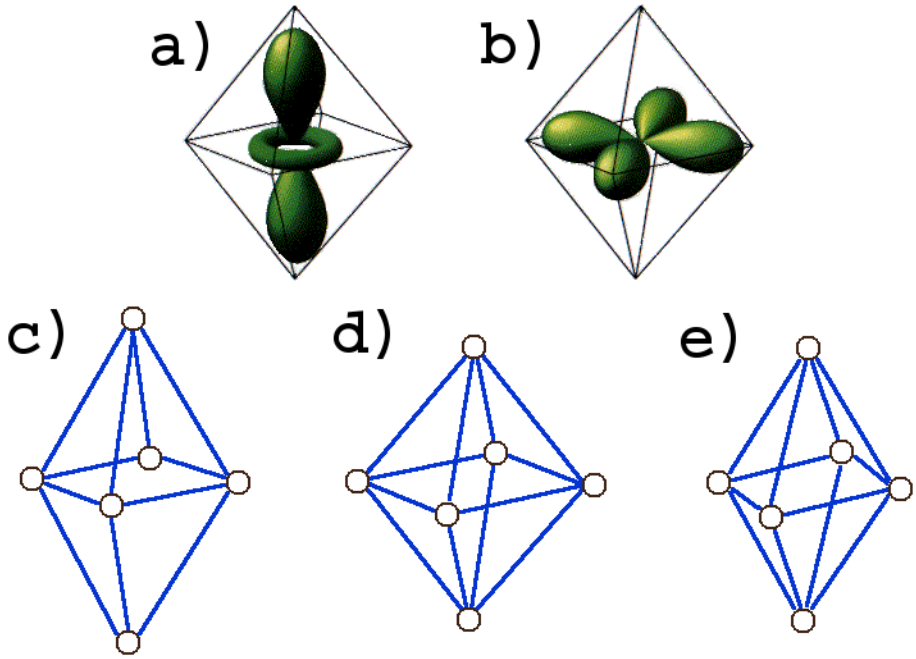

Figure 1.7: a) and b), scheme of the real d orbitals, $3z^2 - r^2$ (a) and $x^2 - y^2$ (b). d) regular octahedron. c) and e): The octahedron after a $Q_z > 0$ distortion (c) and a $Q_x > 0$ distortion. The e_g orbitals (a) and b)) are differently affected by the different distortions of the regular octahedra.

within Jahn Teller theorem, where the degenerate configurations are obtained by *placing* a hole in one site or the other. Along this thesis we shall use the following approximation (with the notation of Eq.1.3:

$$H = \sum \lambda(\rho Q_0) + \beta Q_0^2. \tag{1.4}$$

β measures the relative strength of the breathing and Jahn Teller distortions.

Coulomb Interactions

Coulomb interactions are known to be important in materials with narrow bands. Hund's rule in fact is a consequence of the importance of Coulomb repulsion, it accounts for the strong Coulomb repulsion of electrons in the same orbital. De Gennes justified the ignorance of other Coulombic terms because he was interested in the few carriers limit. Within the metallic state, it can be expected that Coulomb interactions will only renormalize the parameters of the quasi particles, but even this simple renormalization might affect the relative stability of different phases.

Interorbital interactions are significant. The inclusion of interorbital repulsion at a mean field level, stabilizes the experimentally observed A phase against the Ferromagnetic phase in undoped manganites.

Long range Coulomb interactions are important for phase separation. It is known that standard models in which it is not included lead to phase separation between phases with different density [van den Brink 99b]. A more detailed discussion about the role of Coulomb interactions in phase separation tendencies can be found in Ref. [Dagotto 02]

Both on site and long range Coulomb interaction have been taken into account in chapter 5. There, it is discussed how Coulomb opposes charge segregation.

Interactions with the counter-ions

De Gennes stated that ignoring the interactions between the A sitting cations and electrons is a drastic simplification. This issue is closely related to the subject of lattice distortions, since the size of the cations determines the tolerance factor. Important experimental work on this subject has been done by Rodriguez Martinez and Attfield. They showed that the charge of the counter-ions is not important, contrary to the opinion of the Gennes and interestingly suggesting some kind of screening. They were also able to clarify the important role of the variance of the size of the B cations quantifying it. In chapter 4 the subject of the influence of disorder arising from the B ions size and distribution is addresses and more details are given there.

1.4. CMR and disorder

Magnetoresistance is the change in resistance of a material when it is in a magnetic field H. We will use the definition:

$$MR(\%) = 100 \times \frac{\rho(H) - \rho(0)}{\rho(0)} \tag{1.5}$$

Where ρ stands for resistivity. For manganites ρ is always smaller for applied magnetic fields, so that MR is negative and less that 100%. An alternative definition, often called inflationary magnetoresistance, normalizes the difference dividing by the resistivity under magnetic field. In this way the value is, in principle, unbound and it can reach 10^4,10^5 [Jin 94]. This high values lead to the coining of the term colossal magnetoresistance, CMR (less spectacular but significant values of magnetoresistance in manganites had been measured in [Volger 54, Kusters 89, von Helmolt 93]. It also rose hopes, in the early 90's, of possible technological applications, that have not been realized so far. In this section we discuss the relation between CMR and disorder.

The importance of disorder in manganites has been emphasized by many different researchers [Dagotto 02, J.M.D.Coey 99, Akahoshi 03, Damay 97, Li 97, Motome 03,

Millis 03] . As the close balance of different (often coupled) degrees of freedom is believed to be responsible for the rich physics and phenomenology of manganites, disorder might play a crucial role. How exactly disorder affects this competition and CMR is an open question, both because the materials appear to be extremely sensitive to disorder and because the sources of disorder in the materials are difficult to identify and quantify.

Perhaps the most extended view is that exposed by Dagotto [Dagotto 02]. In the vicinity of a first order transition, disorder favors the coexistence of the two phases, thus producing phase separation (or phase coexistence, a names preferred by others). There is a strong experimental evidence for *textured* phases in manganites, mainly obtained by surfaces probes [Israel 07].

Colossal Magneto Resistance, as other *huge* responses to external perturbations in manganites, is a direct result of this coexistence in Dagotto's view. The application of a magnetic field favors the metallic ferromagnetic phase over the insulator antiferromagnetic one. CMR is then caused by the percolation of the metallic ferromagnetic droplets. Resistor network calculations [Mayr 01] give some insights on the mechanism behind this view. However, there is no direct evidence (experimental or theoretical) confirming this view.

In fact, a most recent work on thin films of manganites [Moshnyaga 06] apparently shows that phase separation is not the only mechanism behind C.M.R. The authors observed it both in a sample showing phase separation in other where phase separation was absent. If this results are confirmed similar conclusion might apply to other *colossal* effects in manganites.

An alternative view is suggested by Millis [Millis 03]. He refers to an experimental work where disorder is induced in a controlled manner by substituting Manganese ions by Aluminum [Sawaki 00b]. In that paper, after small threshold in disorder is reached, the properties of the materials change in an abrupt manner. Millis' interpretation is that the ubiquitous discussion about the influence of disorder in Manganese perovskites, come from their extreme sensitiveness to external perturbation. So that colossal effects are not caused by phase separation, but both of them are two of these huge responses to perturbations. Israel, Calderon and Mathur point in a similar direction [Israel 07]: *The role of phase separation in CMR is circumstantial, and not casual*

Although C.M.R. is probably the most spectacular physical phenomenom in manganites, and it is responsible for the great interest they raised. It is surely not the only interesting aspect of manganite physics. They display many other effects some of them also related to, or sensitive to, disorder. Among them there are two beautiful examples we would like to remark.

Going back to the picture of two close competing phases, a feature which is well stablish, disorder might affect them differently. If it disturbs more the phase with lower free energy, for instance the more symmetric one, the energy of this symmetric phase in the presence of disorder might now be higher than the less symmetric one thus producing a phase transition. The *disorder induced phase transition* was studied by [Motome 03].

Other remarkable phenomenom related to disorder, and which might be responsible from some of the *exotic* properties of manganites, is the Griffiths phase. It was studied by Griffiths, many years ago [Griffiths 69] in the context of the Ising model. He considered the role of the weaker interactions produced by disorder in a physical system. These effect might be relevant for magnetic interactions in manganites. For a strong enough disorder and at some finite temperature (lower than T^*, the critical temperature of the clean system). Some parts of the system might be effectively decoupled from the rest. In this scenario, the magnetization of the isolated clusters would point in random directions, and there would be no net magnetization in the system. Therefore a first aspect of the Griffiths phase is the lowering of the critical temperature T_c by disorder. A second characteristic is the non-analytical behavior of the susceptibility *above* T_c. At a temperature larger that the critical temperature of the disordered system T_c and smaller that the clean system critical temperature T^*, there are independent clusters internally joined by the *strong bounds*. The magnetizations of the different clusters would order under an arbitrarily small field. Although Griffiths results were derived for the Ising model, some experiments show that they might be relevant for the far more complex situation of manganites [Salamon 02].

1.5. Sketch of Contents

In this thesis, we have studied different and complementary aspects of manganites physics. Competition of different interaction is responsible for most of the spectacular and interesting effects found in manganites. One of the contending interactions is double exchange, it explains the coupling between magnetism and transport and the big portion of the phase diagram that ferromagnetic metallic phases occupy. In describing the kinetic energy, the Manganese ions are considered as the electronic and magnetic active sites, and their d levels the relevant orbitals. Although some hybridization with oxygen probably takes place, the success of this model suggest that, in a tight biding approach, it can be described by a proper renormalization of the hopping parameter. A tight binding approach is well suited due to the limited spatial extent of the 3d orbitals . Orbital degeneracy and the precise symmetry of the e_g orbitals is important. Localizing tendencies oppose kinetic energy. These are favored by the electron phonon coupling and superexchange interactions, which also promotes antiferromagnetic correlations.

Chapter 2 exposes the results about the magnetic and electronic phase diagrams of the model, and several dopings are studied. Emphasis is done in the role of different localizing effects: Coupling of the octahedra distortions with the electronic degree of freedom, and superexchange interactions between the localized electrons. Montecarlo algorithm allows us to study the behavior at finite temperatures. A detailed study of the conductivity for the different range of parameters is performed.

Undoped manganites are the subject of chapter 3. The competition between short range antiferromagnetic superexchange interaction and the long range ferromagnetic double

exchange interaction gives rise to an interesting phase diagram. We recover the essential features of the experimental results, interestingly, incommensurate magnetic phases and temperature induced commensurate-incommensurate phase transitions.

The A site in the perovskite structure is often occupied by two or more chemical species. Most of the times an average *virtual* ion with average charge and size is included in the models. Experiments suggest that, although this is a good approximation regarding the charge is not in respect to size. The effect that size disorder in the cations surrounding manganese ions has on the magnetic properties of manganites is the subject of chapter 4. We show how the Curie temperature and the order of the transition are strongly affected by disorder.

The results of this thesis, and many others, show that certain maturity in the understanding of bulk manganites and some other transition metal oxides, has been achieved. This, but mainly the extraordinary precise control of the growth of thin films and heterostructures has encouraged the rapid development of the field of heterostructures of transition metal oxides. Several groups in the world are able today to growth multilayers where the different materials are a few unit cells thick. In chapter 5 we study these heterostructures. Since some manganites are half metals and have been used in spintronics, we study the magnetic and transport properties of an all-manganite spin valve. It consists of a thin antiferromagnetic and insulating manganite sandwiched between two ferromagnetic and metallic manganite electrodes.

Chapter 2

Phase Transitions Due to the Formation of Polarons

2.1. Introduction

Metal-insulator transitions (MIT) have been observed in different materials [Imada 98] as a function of several control parameters. Some aspects make the case of the temperature induced trasition in manganites particularly interesting. The insulating phase survives for a wide range of band fillings, while tipically Mott-Hubbard and Pierls insulators are quite sensitive to this parameter. Futhermore, the high temperature phase is the insulating phase. Electrons are localized in these conditions, and distort the lattice. A naive guess would predict that this is the less symmetric (and the low temperature) phase. Anomalous thermal expantion [Teresa 97] around the MIT remmark the role of the lattice. The magnetic degree of freedom is also important, around the trasition, the metallic phase is ferromagnetic, and the insulating behavior is found in the paramagnetic phase. A prominent peak in the resitivity as a function of temperature is also found near the Curie temperature, T_C. The detailed study of this phase transition, considering the magnetic and lattice degrees of freedom is the subject of this chapter.

Manganites display a great variety of physical properties as function of some relevant variables: temperature, lattice distortions, magnetic field, and band filling. In the general formula of manganites, $Re_{1-x}D_xMnO_3$, n=1-x is the number of electrons in the twofold e_g band. Attempts to understand the physical behaviour of manganites have traditionally taken as a reference the undoped compounds $ReMnO_3$. For this reson, x, which is the number of holes with respect to the half-filled e_g band, and thus is normally used to characterize band filling. Either if we think in terms of electrons or holes, doping is a crucial parameter determining Manganites properties.

Optimal doping, x≈0.35 is particularly interesting. As the temperature is raised, the materials undergo a ferromagnetic-paramagnetic transition. The Curie temperature, T_C(x), is maximum for aproximately this doping, although normally lower that room temperature. In $La_{0.7}Ca_{0.3}MnO_3$, T_C is around 230 K.

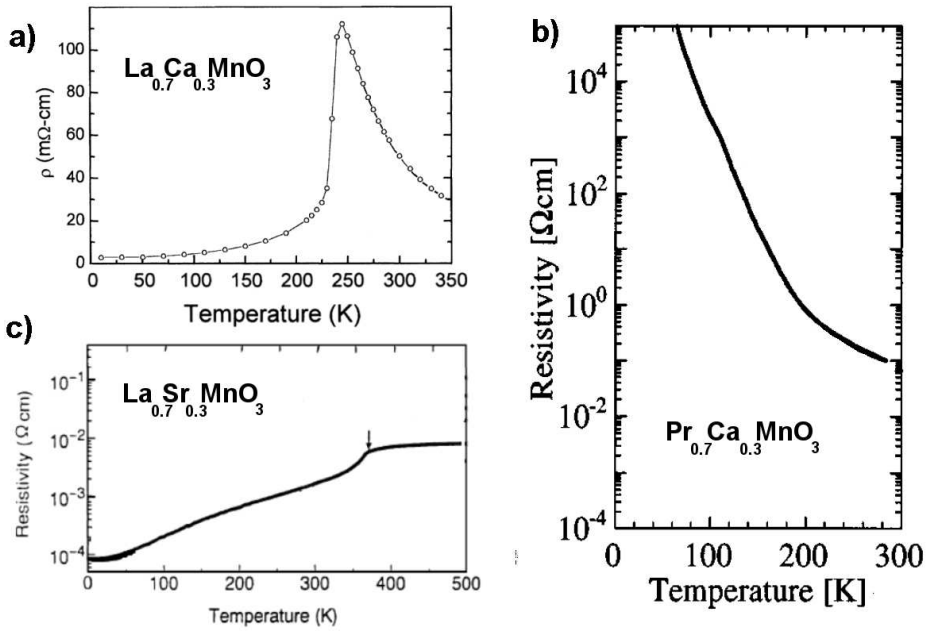

Figure 2.1: Resistivity as a function of temperature for different compunds: a) $La_{0.7}Sr_{0.3}MnO_3$, taken from [A.Urushibara 95] b) $La_{0.7}Ca_{0.3}MnO_3$, from [P.Schiffer 95] and c) $Pr_{0.7}Ca_{0.3}MnO_3$, from [Tomioka 96]. For manganites with the same ration of divalent to trivalent cations, the ionic sizes detrmine the bandwidth and the magnetic and electronic properties.

The magnetic transition is accompanied by a metal to insulator transition (Fig. 2.1 a)). That is, below T_C, resistivity is relatively low and increases with temperature, and above it is relatively high and decreases with temperature. The range of x where we find the metal-insulator transition depends on the nature of the cations. It is narrower in $La_{1-x}Sr_xMnO_3$ (which for x=0.3 is metallic at both sides of the transition, seee Fig. 2.1 b)).A few compounds do not display a metallic phase, not even at optimal doping where the resisitivity is typically lower (Fig. 2.1 c)).

As pointed out by Millis [Millis 98] there is a close relation between the metal-insulator transition and the famous CMR, the spectacular change in resistivity with an applied magnetic field. Since ferromagnetic-paramagnetic transitions are very sensitive to an applied field is natural to expect that the conductivity depends strongly on the magnetic field, specially around T_C, where susceptibility is larger. The work presented here supports the standard view [Dagotto 02, Millis 96] that the behavior of the conductivity is determined by the relation of kinetic energy, (sometimes measured as band width) and electron phonon coupling. In metallic materials kinetic energy dominates, in insulating materials the most important energy scale is the electron phonon coupling, and in materials with a metal-insulator transition, the two interactions have comparable strength conferring a crucial role to other parameters like temperature. However, we shall also show that temperature alone is not enough to produce a sharp metal-insulator transition.

The interactions needed to reproduce a metal insulator transition is a subject of controversy. It is well-known that spin disorder alone is not strong enough to explain the temperature induced insulating phases at arbitrary carrier densities [Calderón 99b]. In a recent work [Vergés 02], it was proved that the coupling of electrons to the lattice distortion was enough to localize particles on individual Mn positions giving rise to an insulating phase. Just because the double exchange mechanism needs hopping of the electrons through the lattice, localization also implies the depression of ferromagnetism. This mechanism nicely works below a ten percent of band filling but fails for higher carrier densities because direct hopping between polarons quickly broadens the band of localized electrons that become easily extended and give rise again to a (paramagnetic) metallic behavior.

The model is here extended to include the Mn d-orbital degeneracy which also implies the coupling to more detailed lattice distortions (just the breathing mode was considered in the previous study of spherical electron orbitals[Vergés 02]). Our aim was that a broader band structure will allow a higher number of localized carriers. Moreover, being the lattice distortion possibilities much richer, it was expected that the localization mechanism would work better than before. As an additional ingredient favoring the insulating phase a direct superexchange term has also been considered. All the calculations have been carried out in three dimensions. The metal insulator transition is a consequence of the close competition between localization effects (here found to arise from electron phonon interaction) and the kinetic energy tending to delocalize the carriers. Since this last effect depends strongly on dimensionality, we choose to study the

realistic three dimensional case.

We have succeeded in extending these ideas to the two orbitals model that is more realistic and describes better the phenomenology of manganites. Our results indicate that with these ingredients a temperature driven metal-insulator transition is found in the few carriers limit. This transition does show some features found in the experiments such as the accompanying magnetic transition and the increase of lattice distortions at the critical temperature [Teresa 97]. However, this transition does not survive the inclusion of superexchange interaction (needed to explain the antiferromagnetic phases of undoped manganites [Salafranca 06a]) and is not found at the doping range relevant for the experiments. Actually, neither the two-band extension nor direct superexchange allow to extend the range of dopings for which temperature induced localization, and consequently insulating behavior, is expected. Although the relevant phases are present for different ranges of parameters, a clear metal-insulator transition is not found. Our results add arguments to the extended idea that other effects such as electron-electron interaction or disorder [S.Kumar 03, Sen 06a] should be included to fully understand the colossal magnetoresistance effect of manganites.

2.2. Theoretical background

2.2.1. Two-band model

The standard double-exchange two-orbital model for manganites has been thoroughly used in our study. Since the model has been widely described in previous investigations[J.Kanamori Dagotto 02], just a brief summary will be given here. The two d-orbitals of the model come from the e_g states that are active at the Mn ions in Mn-oxides. This simplified band structure model has been extensively discussed before[Dagotto 02, Dagotto 05]. For just half electron per site of a square or cubic lattice, that is, for an electronic density of n=0.5 a CE state of manganites is experimentally known to be stable. Here, we will work at dopings away from commensurate values, that is, away from particular spin and orbital textures producing the insulator behavior. More specifically, we will try to find an upper limit for the formation of a polaronic incommensurate phase.

In more detail, the Hamiltonian for the two-orbital model is

$$\hat{H} = \sum_{\gamma,\gamma',i,\alpha} t^{\alpha}_{\gamma\gamma'} DE(\mathbf{S}_i, \mathbf{S}_{i+\alpha}) \hat{c}^{\dagger}_{i,\gamma} \hat{c}_{i+\alpha,\gamma'}$$

$$+ \frac{1}{2} \sum_i (\beta Q^2_{1i} + Q^2_{2i} + Q^2_{3i})$$

$$+ \lambda \sum_i (Q_{1i}\hat{\rho}_i + Q_{2i}\hat{\tau}_{xi} + Q_{3i}\hat{\tau}_{zi})$$

$$+ J_{\mathrm{AF}} \sum_{i,\alpha} \mathbf{S}_i \cdot \mathbf{S}_{i+\alpha}, \tag{2.1}$$

being $\hat{c}^{\dagger}_{i,\gamma}$ the creation operators of electrons in 3d Mn states $|a\rangle = 3\mathrm{d}_{x^2-y^2}(\gamma = 1)$ and $|b\rangle = 3\mathrm{d}_{3z^2-r^2}(\gamma = 2)$ of site i,

$$DE(\mathbf{S}_i, \mathbf{S}_j) =$$
$$\cos(\frac{\theta_i}{2})\cos(\frac{\theta_j}{2}) + \sin(\frac{\theta_i}{2})\sin(\frac{\theta_j}{2})e^{-i(\phi_i-\phi_j)}$$

where angles (θ_i, ϕ_i) describe the classical spin $\mathbf{S_i}$ of $t_{2\mathrm{g}}$ electrons of site i. The parameters $t^{\alpha}_{\gamma\gamma'}$ are the hopping amplitudes between the orbitals γ and γ' in the direction α. Since d-d hopping is mediated by the oxygen p-orbitals lying midway, symmetry considerations dictate the following relations: $t^x_{aa} = -\sqrt{3}t^x_{ab} = -\sqrt{3}t^x_{ba} = 3t^x_{bb} = 1$, $t^y_{aa} = \sqrt{3}t^y_{ab} = \sqrt{3}t^y_{ba} = 3t^y_{bb} = 1$, $t^z_{aa} = t^z_{ab} = t^z_{ba} = 0$, and $t^z_{bb} = 4/3$.

The second term of the Hamiltonian measures the phononic stiffness of the relevant octahedra deformations. Normal modes of vibration Q_{1i}, Q_{2i} and Q_{3i} of the oxygen atoms around any manganese ion can be expressed in terms of the oxygen coordinates $u_{i,\alpha}$ as:

$$\begin{aligned}
Q_{1i} &= \frac{1}{\sqrt{3}}[(u_{i,z} - u_{i-z,z}) + (u_{i,x} - u_{i-x,x}) \\
&+ (u_{i,y} - u_{i-y,y})], \\
Q_{2i} &= \frac{1}{\sqrt{2}}(u_{i,x} - u_{i-x,x}), \\
Q_{3i} &= \frac{2}{\sqrt{6}}(u_{i,z} - u_{i-z,z}) - \frac{1}{\sqrt{6}}(u_{i,x} - u_{i-x,x}) \\
&- \frac{1}{\sqrt{6}}(u_{i,y} - u_{i-y,y}).
\end{aligned}$$

We will take $\beta = 2$ in order to reduce local volume variations as discussed in previous literature[Aliaga 03].

The third term of the Hamiltonian gives the precise form of the coupling between manganese d-electrons and Jahn-Teller distortions of the MnO_6 octahedra. It is also dictated by symmetry considerations: $\hat{\tau}_{xi} = \hat{c}^{\dagger}_{ia}\hat{c}_{ib} + \hat{c}^{\dagger}_{ib}\hat{c}_{ia}$, $\hat{\tau}_{zi} = \hat{c}^{\dagger}_{ia}\hat{c}_{ia} - \hat{c}^{\dagger}_{ib}\hat{c}_{ib}$, and $\hat{\rho}_i = \hat{c}^{\dagger}_{ia}\hat{c}_{ia} + \hat{c}^{\dagger}_{ib}\hat{c}_{ib}$. The constant λ measures the strength of the electron-phonon coupling[Dagotto 02]. Finally, a superexchange term with coupling J_{AF} is also included.

The model Hamiltonian (2.1) used in this paper has been previously studied for some particular dopings in manganites, although most of the times the analysis has been restricted to two-dimensional systems assuming that the extension to three-dimensional cases would not change the main trends observed in 2D. On the contrary, we have preferred a consistent 3D analysis is spite of the great computational effort in order to accurately describe the kinetic energy of the carriers and preserve the cubic symmetry

2.2.2. Monte Carlo simulation

The behavior of a material described by Hamiltonian (2.1) as a function of temperature has been studied by means of a standard Monte Carlo simulation. Both core spins $\{S_i\}$ and phonon degrees of freedom $\{Q_{\alpha i}\}$ are treated as static, that is, no quantum dynamics for these variables is allowed. Then, for each core spin and phonon configuration, the quantum energy of the electrons is obtained diagonalizing a finite cluster described by model (2.1) and occupying electronic levels according to the doping of the material. Fermi distribution is assumed since the Fermi temperature $T_{\rm F}$ is much greater than any other energy scale in the system. Configurations are accepted or rejected according to the value of $\exp(\Delta E/(k_B T))$ being ΔE the energy change of the total energy (electronic plus deformation plus magnetic). Classical degrees of freedom are successively modified in a way that allows acceptance of about half the moves. Experience shows that this is the most efficient way of getting approximate thermodynamic averages using the Monte Carlo algorithm. Typically, 500 steps are needed to allow the system equilibration. About 5000 additional steps are necessary to get the averages and fluctuations of the physical magnitudes. The whole procedure should be repeated for each value of λ, $J_{\rm AF}$, and T before having some idea about the phase diagram of the material. All of the simulations described in this paper have been carried for a $N \times N \times N$ cluster with periodic boundary conditions. The rapid increase of the diagonalization time (which grows as N^9) has limited our numerical efforts to $N = 4$, that is, 128 electronic states in the simulated sample. At this point, it is interesting to mention an alternative numerical approach based in the study of the density of states that is not so direct as diagonalization to get the electronic energy but allows parallel calculation and, therefore, smaller wall times for the whole calculation[Furukawa 01, Alvarez 05, Sen 06b].

The analysis of the manganite phases that will be presented in this work relies on the values of several thermal averages that have been obtained by Monte Carlo simulation. They are: the overall magnetization M of the core spins, the mean gap of the electronic spectrum, Δ, the Fermi energy E_F of the system (remember that we work at a fixed number of carriers which implies that the Fermi energy at one point of the Monte Carlo simulation defined as the average of the last occupied state and the first unoccupied level is a fluctuating physical magnitude), the variance of the phonon normal modes σQ^2, the spin structure factor and the conductivity along different directions G_α.

2.2.3. Conductance calculation

Conductance has been calculated in previous works after attaching metallic leads to opposite faces of the simulated cube. Faces can be selected in three ways. This procedure has some inconvenients that have been improved in our work. Firstly, one has to carefully choice the metal in order to have good overlap between the sample levels and the metal bands. This becomes harder as the sample model becomes more involved as in the present case (more than one band, lattice deformations shifting the manganite levels,

etc.). Secondly, one calculates conductance through a small connected sample whereas experiment measures an intrinsic property of the material. Both deficiencies can be avoided if the cube is periodically repeated in any of the x, y or z directions. In this way the use of the standard Kubo formula for transport gives the precise number of bands at the studied energy and 0 if the energy lies at a gap. Notice that interactions among atoms in opposite cell faces (periodic boundary conditions are used within the Monte Carlo procedure) give rise to the inter-cell connections. The Green function of the quasi one-dimensional system has been obtained by a decimation technique [Guinea 00] whereas Kubo calculation follows a standard way [Vergés 99a]. In this way, we sensibly improve the calculation of an intrinsic value of the conductivity minimizing finite size effects.

2.3. Electron-Phonon Double Exchange results

2.3.1. Few carriers limit

As shown in a previous work [Vergés 02] for a one orbital model, electron-phonon coupling can produce a metal to insulator transition (MIT), at least in the few carriers limit. Present work confirms that this mechanism also works when both the degeneracy of the e_g orbitals and their spatial symmetry are taken into account.

The results obtained are summarized in Fig. 2.2. Three regimes have been found that appear for different values of the relevant model parameters (a similar behavior was shown in Ref.([Vergés 02]). For small λ (≤ 2.0) the system is metallic for the whole range of T, displaying therefore a Ferromagnetic-metal (FM) to Paramagnetic-metal transition. A change in the magnitude of the slope of the $G - T$ curve around the critical temperature T_C is observed (although the sign remains negative), as it is in the experiments for the so called wide band materials [Dagotto 02]. It is remarkable that the crystal is undistorted at $T = 0$ and, nevertheless, that some thermal active distortions take place afterwards. On the contrary, for high enough values of λ (≥ 2.7), we find a Ferromagnetic Insulator (FI) to Paramagnetic Insulator (PI) transition. The slope of G versus T is always positive while the values of G are much lower than the Mott limit. There is also an important reduction of the conductivity at the lowest studied temperature that we will ignore since quantum effects of phonons invalidate in any case the classical approximation near zero temperature. A strongly distorted crystal appears in this high coupling regime even at low temperatures. The more interesting region appears for e-ph coupling values between above commented limit values. Here the FM-PI transition is recovered. The steep change both in M and G suggest a first order transition. The elastic energy (Fig. 2.2c) shows clearly how the lattice distortion is responsible for the localization of the carriers, so that this results support the idea of an insulator state in manganites formed by polarons (polaron being an electron self-trapped in lattice distortion). The elastic energy also presents a jump from the low-λ to high-λ

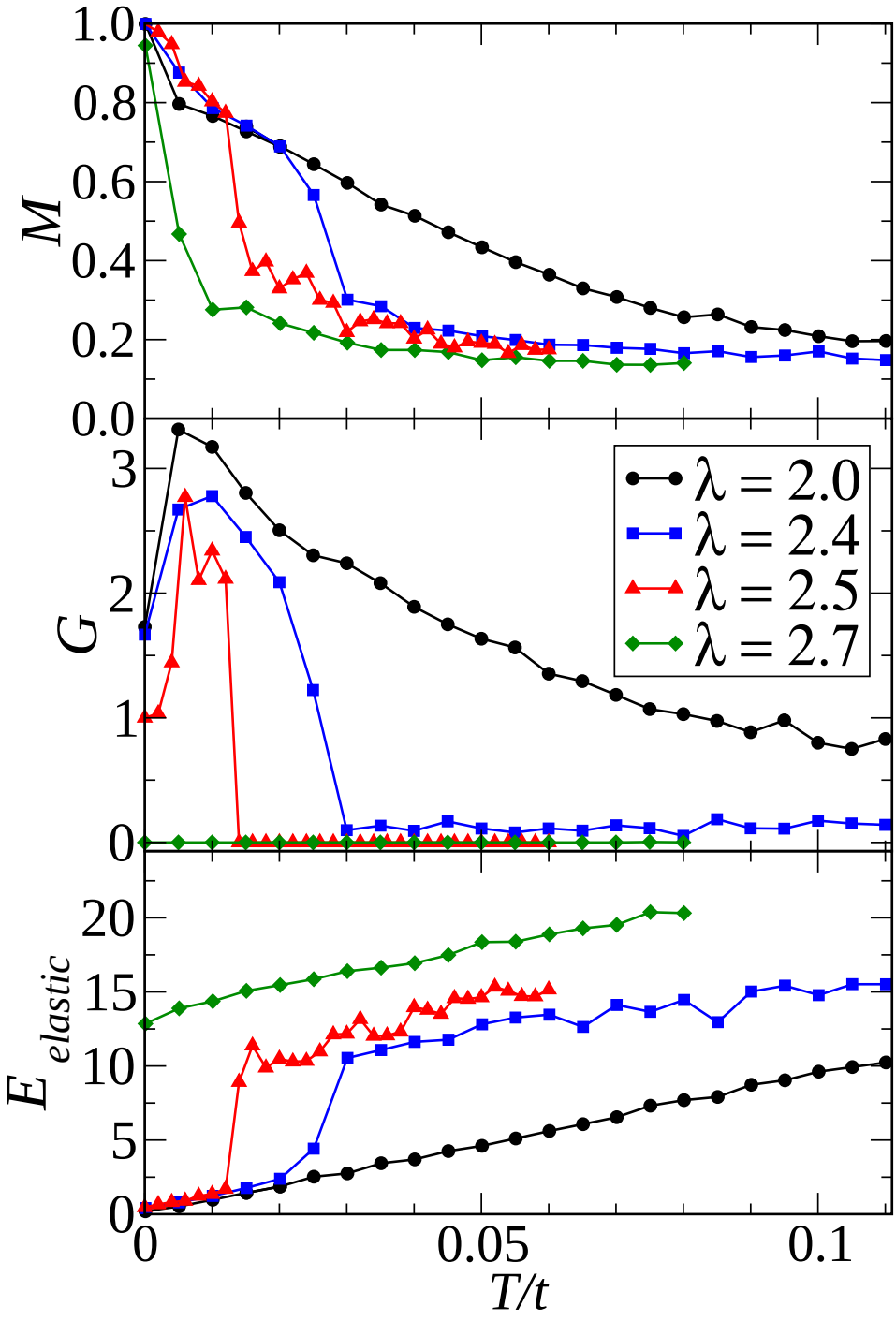

Figure 2.2: Results of Monte Carlo simulations in a $4 \times 4 \times 4$ cluster for the two orbital double exchange model (2.1). Magnetization M (a), conductance G (b), and elastic energy E_{elastic} (c) as a function of temperature are shown. Results are given for several values of the e-ph coupling strength λ in order to show the change of the physical magnitudes when a phase change takes place.

like behavior. As in [Vergés 02], there is a finite range of λ, for which the change in the electronic properties is accompanied by a magnetic transition.

2.3.2. Higher dopings

The behavior of the system is different for a higher number of carriers. For $n = 0.3$ we obtain a smooth change from metallic to insulator behavior as a function of the e-ph coupling strength λ, but both phases are stable with temperature (see Fig. 2.3). Simulations done at the experimentally optimal doping which is around $n = 0.7$ electrons per site show a quite similar behavior (see Fig. 2.4). For large values of λ (those that produce a MIT in the few carriers and low T limit), the system is insulator and the charge is localized. For lower values of λ (between 1.8 and 2.0) which produce an undistorted metal when filling is $n = 0.08$, we now observe a bad metal with a distorted lattice. So, when the conduction band is filled beyond the bottom, an insulator is obtained for high values of λ while for smaller values of e-ph coupling the slope of the conductivity versus temperature, dG/dT, decreases but remains positive everywhere. Finally, for small enough values of the coupling strength λ (≈ 2.0) the system is metallic ($dG/dT < 0$) in the whole temperature range.

From these results, two main conclusions can be extracted: (i) Electron-phonon coupling is important to understand the Metal-Insulator transition in manganites, as it is now widely accepted. For a Double Exchange model it explains the MIT for few carriers in the system, where the self-trapped electrons (polarons) are well separated. Both ferromagnetic-insulator and paramagnetic-insulator phases can be understood in terms of this polaron formation. (ii) When the electron density of the system increases, polaron formation still occurs, but the temperature effects are not as dramatic as observed in the experiments.

The model has to be improved if experiments in this doping regime should be explained. Obviously electron-electron interaction will be increasingly important as the number of polarons that is present in the system rises. It has been argued[Dagotto 02] that a high value of β in Eq. (2.1), which prevents double occupancy sites, can mimic Coulomb interaction. Although this argument seems quite plausible for localized electrons, it is not so clear for overlapping polarons.

If the interaction between neighboring polarons is preventing the appearance of a MIT at moderate λ, one would naively guess that MIT would be observable up to a doping of $n \approx 1/7 \approx 0.14$. This value corresponds to non-overlapping polarons assuming that a polaron occupies a lattice site and its nearest neighbors.

We have shown that the electron-phonon coupling cannot account for a MIT transition at dopings relevant to the experimental results. Although a polaronic band seems to appear it is wide enough to overlap with the conduction band. Some other mechanism that can account for a reduction of the band width must be taken into account. In this spirit we have investigated the effect of antiferromagnetic superexchange interaction between

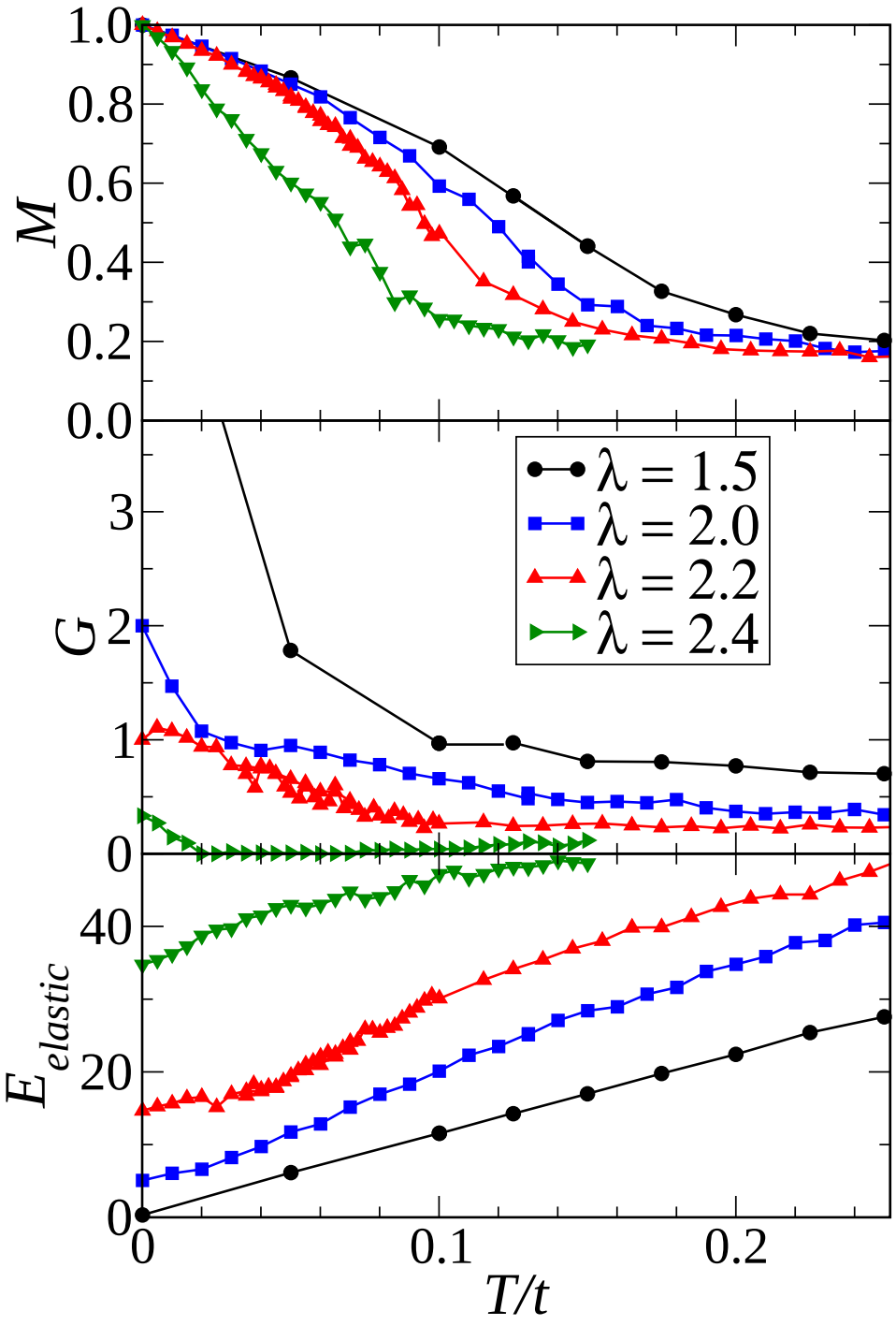

Figure 2.3: Same as Fig 2.2 for a higher electron doping $n = 0.3$ (lower hole density x). Again results are given for several values of the e-ph coupling strength λ.

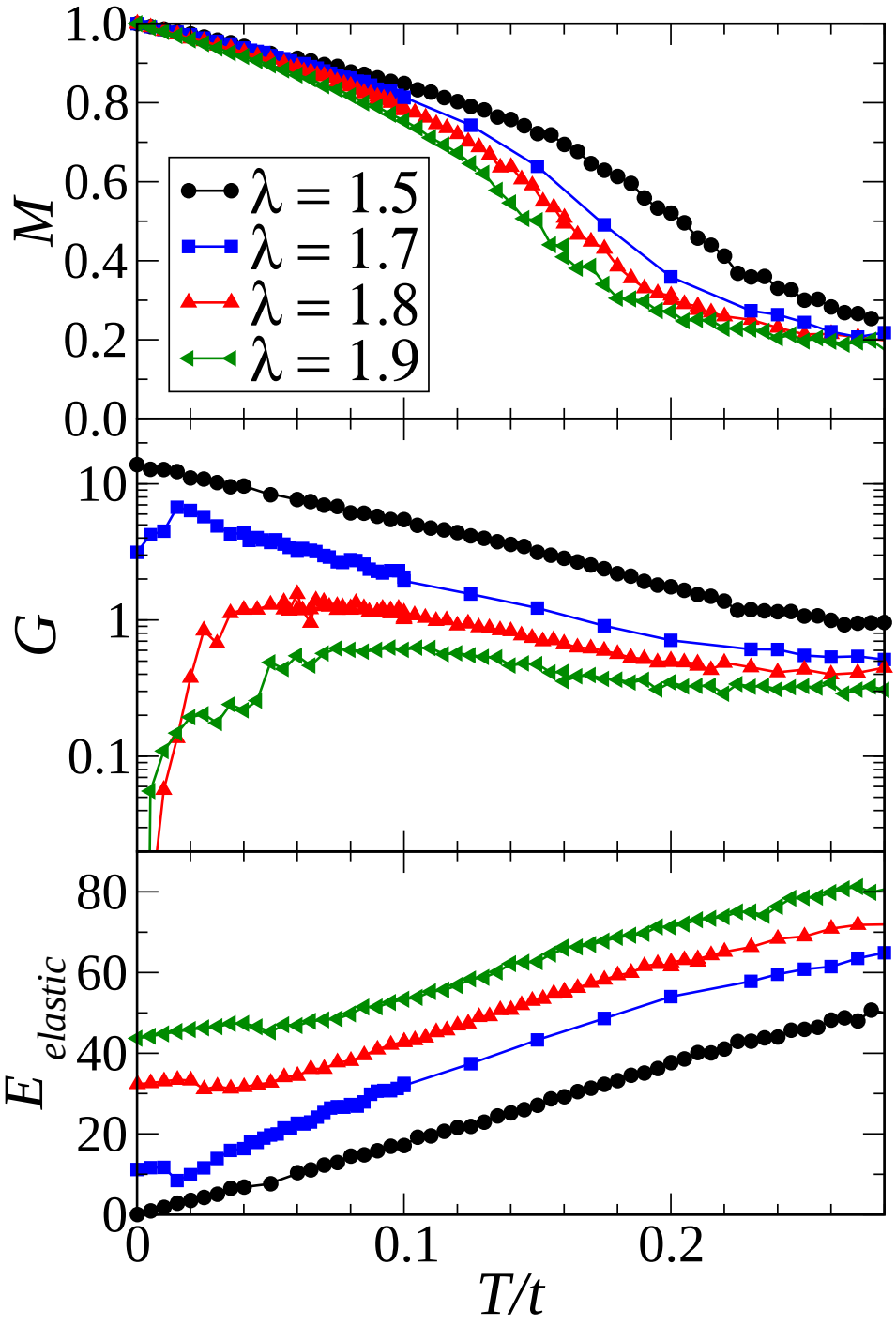

Figure 2.4: Results of Monte Carlo simulations for a larger electron density $n = 0.7$. Magnetization M (a), conductance G (b), and elastic energy E_{elastic} (c) as a function of temperature for several values of the e-ph coupling strength λ.

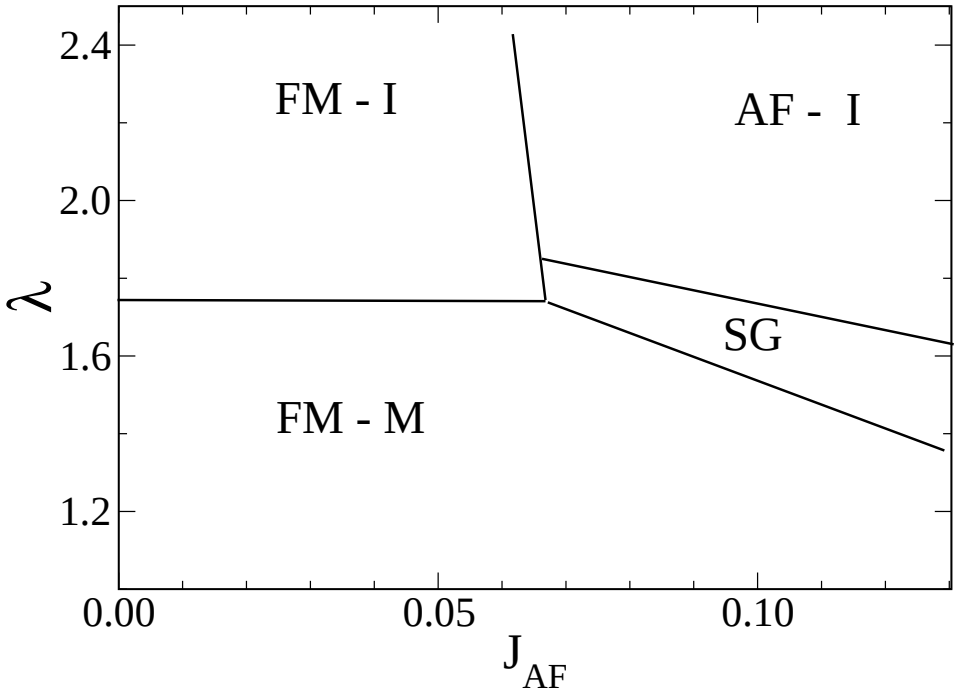

Figure 2.5: Electron-phonon coupling constant λ versus superexchange coupling J phase diagram. Phases are labeled according to their magnetic ordering and transport properties FMM *ferromagnetic metal*, FMI *ferromagnetic insulator*, SG possible *Spin-glass* phase which appears in the simulations as a state with both types of ferromagnetic and antiferromagnetic correlations and showing some tendency to become trapped in some regions of the phase space and AFI *antiferromagnetic insulator*. See text for an explanation of the high temperature behavior.

Mn ions. The importance of this interaction is widely accepted [Alonso 01c, Alonso 01a, Alonso 01b, Arovas 98], and the competition between the ferromagnetic double exchange and the antiferromagnetic superexchange lies at the heart of the rich magnetic phase diagram of manganites.

2.4. Effect of Superexchange

It is clear now that superexchange interaction plays an important role in the physics of manganites. Since the t_2g electrons are the ones that mediate the interaction, it is usually described by a Heisenberg-like term in Hamiltonian (2.1). This term increases the complexity and richness of the phase diagram (Fig. 2.5). Since the electron-phonon coupling has proved to be the main interaction to explain the MIT for a small number of carriers, in this section we study Hamiltonian for filling $n = 0.7$ ($x = 0.3$) where colossal magnetoresistance phenomena have been observed experimentally [Dagotto 02]. In the

diagram zone that we have explored, around the λ induced MIT, we have found some different behaviors.

For small values of J_{AF} rising λ implies a change in the system from a well known [Calderón 99b] ferromagnetic metal to a ferromagnetic insulator at $\lambda_c \approx 1.75$. Since the competing states have the same magnetic order, the λ_c, characterizing the transition between these states is J_{AF} independent. Nevertheless, for stronger antiferromagnetic coupling, $J_{\mathrm{AF}} \geq 0.07t$, the state competing with the ferromagnetic metal at low T is antiferromagnetic. Actually, both ferromagnetic and antiferromagnetic correlations are found. This magnetic order could eventually change if larger cells could be simulated, but it already appears for the relatively small $4\times4\times4$ cells. Doubtless, the appearance of a magnetic state with no net magnetization indicates, once again, the close competition between double exchange ferromagnetic and superexchange ferromagnetic interactions. It is an indication that colossal effects should be expected just close to these parameter values. The existence of such a phase even in the clean limit is quite remarkable, but the effect of disorder and other interactions should be studied. At higher values of either λ or J_{AF} the ground state is G-antiferromagnetically ordered, and therefore, shows a clear insulating behavior.

Let us finish discussing the effect of temperature on the different phases.

2.4.1. Ferromagnetic Phases

For the ferromagnetic metallic phase, the situation is quite similar to the one discussed in the last section. We find a transition to a paramagnetic metallic phase. The change in the slope of G versus T is more pronounced that it was for no antiferromagnetic coupling. Actually, the behavior is closer to the experimental results. Configurations with antiferromagnetic correlations now have a higher Boltzmann factor, and also the thermal average of G has decreased, especially for $T > T_C$. However, we do not find a metal-insulator transition.

The ferromagnetic insulator phase also presents a transition to a paramagnetic phase, the electron phonon coupling reduces the expectation value of the hopping and consequently, the Curie temperature. Both cases are illustrated in Fig. 2.6.

2.4.2. Antiferromagnetic phases

In the region of high values of λ and J_{AF} a G antiferromagnetic phase is found. Hopping is forbidden by the double exchange factor. Therefore, electrons are localized at random sites preventing the appearance of electrical currents at low temperatures. Consequently, this phase simply describes an insulator. This phase has not been observed experimentally at this doping, probably because the values of the parameters needed to stabilized it are beyond plausible values.

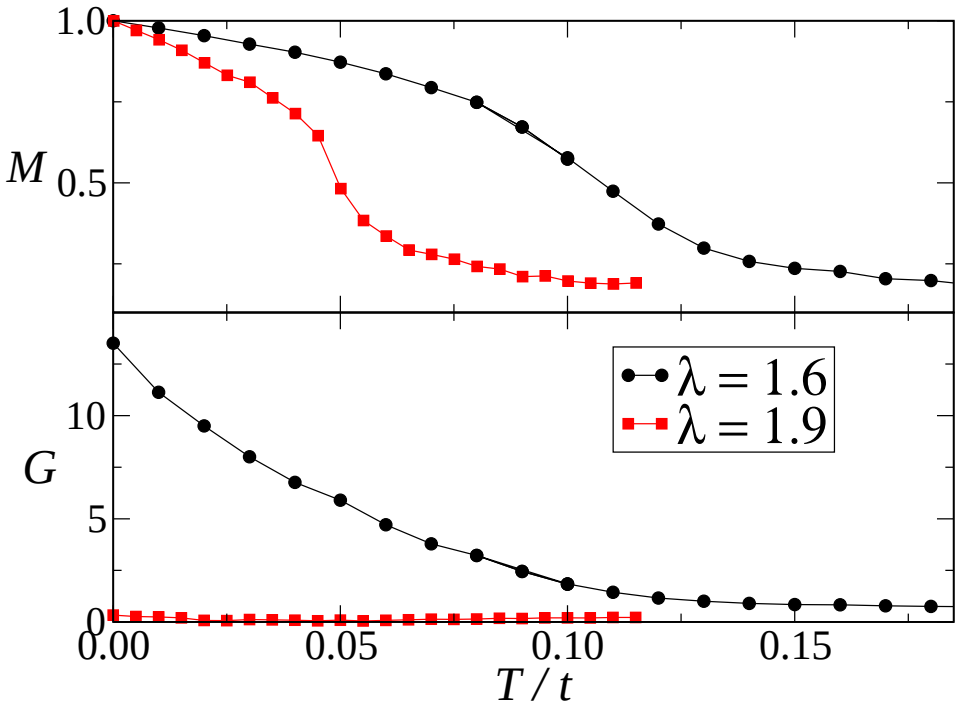

Figure 2.6: Magnetization and conductance versus temperature results at moderate superexchange interaction $J_{\mathrm{AF}} = 0.6$. Two values of the electron-phonon coupling constant λ are shown.

For smaller values of λ, another phase with no net magnetization is found. We have labeled it *SG* in figure 2.5. We are aware that the simulations carried out and the system size used are insufficient to conclude the existence of Spin Glass phase in the model. However the experimental observations and some features observed in the simulations suggest that this might be the case. In particular, simulations in this regime show very slow exploration rates of the phase space, and not even the limited cluster sizes with periodic boundary conditions (which tend to overestimate correlations) are enough to stabilize either a ferromagnetic or antiferromagnetic state. Anyhow, the appearance of this phase in our calculations, shows that the close competition between ferromagnetic and antiferromagnetic tendencies is present in the model. This strong competition has been argued to be responsible to colossal of effects in manganites[Dagotto 02].

2.5. Summary

We have studied a realistic double exchange model in three dimensions including superexchange interactions. By means of Monte Carlo simulations, we have sketched the phase diagram. An improved implementation of the Kubo formula that minimizes finite-size effects has allowed a detailed study of the intrinsic conductance G of the different phases and its variation with temperature. Overall behavior strongly depends on doping. For small carriers density ($n = 0.08$), the previously reported FM-PI transition is recovered: changes in G cover several orders of magnitude. The transport regime is strongly affected by the electron-phonon coupling λ. For small λ, the system always shows a metallic behavior whereas for large λ an insulating behavior is always found. Only for intermediate values, a transition appears in accordance with experimental evidence. For intermediate ($n = 0.3$) and high ($n = 0.7$) carriers density, the same phases are found, but the range in which temperature induces a FM-PI is reduced to become unobservable. Nevertheless, results closely reproduce the experimental behavior of the so called wide band materials (such us $La_{0.7}Ca_{0.3}MnO_3$). These materials present a paramagnetic-ferromagnetic transition accompanied by a pronounced change in the slope of the $G-T$ curve. The inclusion of a direct superexchange interaction improves these resemblance but fails to recover the FM-PI transition. On the other hand, superexchange induces the appearance of antiferromagnetic phases and phases with a strong competition between ferromagnetic and antiferromagnetic correlations.

Chapter 3

Phase Diagram and Incommensurate Phases in Undoped Manganites

3.1. Undoped Manganites.

3.1.1. Weak versus strong coupling in Manganites

The renaissance of Manganites research in the late 80's and early 90's was due to the discovery of Colossal Magnetoresistance (CMR, see introductory chapter), and thus most of the attention has been devoted to optimally or near optimally doped Manganites. The corresponding chemical formula is $Re_{1-x}D_xMnO_3$ where Re stands for a rare earth element, D is a divalent element, and $x \approx 1/3$. Many properties of manganites depend on the competition between the kinetic energy, tending to delocalize the carriers, and localization effects such as the Jahn-Teller (JT) coupling and the antiferromagnetic (AFM) coupling between Mn core spins. The properties of manganites at these intermediate dopings, in which metallic and ferromagnetic tendencies dominate, can be described within a band structure picture, where the itinerant e_g carriers have a strong ferromagnetic interaction with the core t_{2g} Mn spins, and are coupled to the Jahn-Teller distortions of the oxygen octahedra surrounding the Mn ions[Dagotto 02, L.Brey 05].

A natural questions to ask is what are the physical properties, and how can they be understood, at the two end members of the series, $ReMnO_3$ and $AMnO_3$. The traditional answer to this question is that $AMnO_3$ compounds, such as $CaMnO_3$, are antiferromagnetic insulators, G type in the Wollan-Koehler notation ([E.O.Wollan 55] and Appendix B). This can be explained, within the picture sketched in the introduction, as band insulating behavior, since the e_g band is empty. As explained there, it is Hund's rule what induces the polarization of the t_{2g} triplet. The antiferromagnetism comes from the inter site superexchange interactions between electrons in the t_{2g} symmetry orbitals. The other end of the series is much more interesting and is the subject of this chapter.

The e_g band in these undoped compounds is half filled. $LaMnO_3$, for example, is antiferromagnetic, A type, and presents a cooperative Jahn-Teller [Rodríguez-Carvajal 98] distortion. As a matter offact, $LaMnO_3$ was one of the compounds analyzed by Kanamori

in his pioneer work [J.Kanamori 60] where he established the model for degenerate e_g electrons coupled to lattice distortions used in this thesis and in most works about Manganites. The classical interpretation for this material's properties has been given in terms of the strong coupling limit. $LaMnO_3$ and isoelectronicmanganites are, in this scheme, Mott insulators, and therefore antiferromagnetic.

The degeneracy of the e_g orbitals is lifted by the cooperative Jahn-Teller distortion. The orbital order is then responsible for the peculiar A ($(\pi, 0, 0)$ wave vector) AF order, instead of the classical G (π, π, π) of a 's orbital' Mott insulator (notice that T_N the temperature of the antiferromagnetic phase transition, is lower that the temperature at which the orbital order sets in $< T_{OO}$). Calculations in terms of superexchange arguments [Millis 97], again in an strong coupling scheme, seem to support this view. However, as it was pointed out by Kanamori [J.Kanamori 60], severaltypes of orbital ordering and Jahn Teller distortions are degenerated, even in the presence of anharmonic terms in the electron phonon coupling. Kinetic energy arguments, taking into account the symmetry of the involved orbitals, were invoked in ref.[Popovic 00] to account for the further lifting of this degeneracy, paying attention to the importance of the band structure,

As it has often been the case in manganites, new physical behavior was unexpectedly unveiled; new experimental results on other undoped manganites were published challenging this classical understanding. In 2001 a work by several Spanish groups reported a new magnetic order in a similar compound, $HoMnO_3$ [Muñoz 01]. This was the E magnetic order described below (see also the appendix). This new magnetic phase in manganites, is not easy to account for in the strong coupling limit. A model which included the formation of a band by the e_g electrons, by means of a double exchange tight binding term in the Hamiltonian, does predict this phase [Hotta 03, T.Hotta 03].

New incommensurate phases were found afterwards in different experiments and presented in several works. A fairly complete picture and a comprehensive overview of the literature was drawn in Refs. [Kimura 03, Zhou 06]. The present chapter is an attempt to reach a coherent understanding, and a derivation from a microscopic model of the results presented in the cited references.

An important issue that has not been address in our work is the appearance of ferroelectricity in a few of this compounds. This is a mostinteresting problem on its own and as such has called the attention of many researchers. However, our results indicate that ferroelectricity is not crucial to determine the electronic and magnetic phase diagram in undoped manganites.

3.1.2. Incommensurate phases

In ref.[Kimura 03] (see Fig 3.1) the authors examine the magnetic and orbital order in a series of $ReMnO_3$ as a function of the ionic radius (r_{Re}) of the rare earth ion Re. For

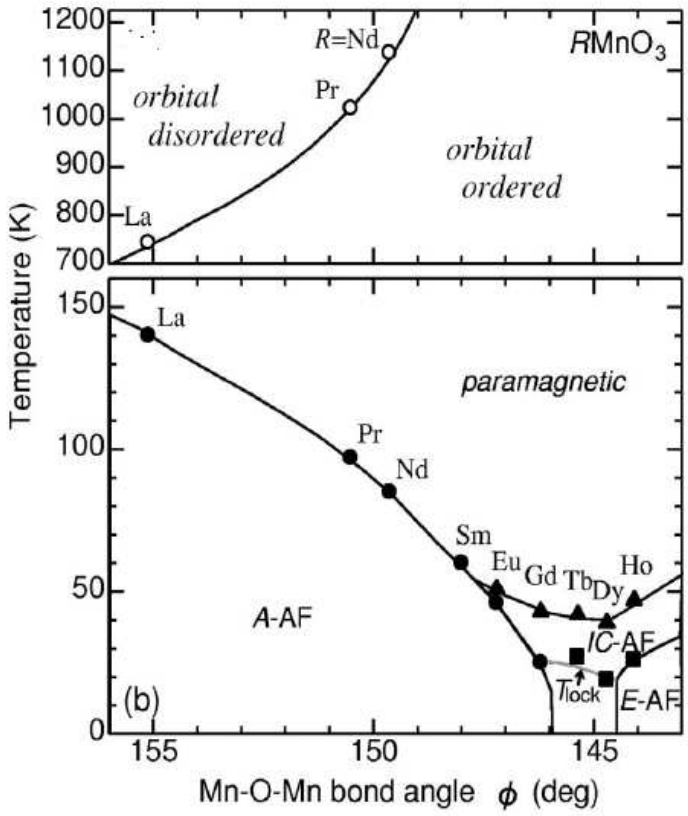

Figure 3.1: Experimental phase diagram of undoped manganites. Magnetic order, extracted from neutron or X ray diffraction patterns, and orbital order, inferred from resistivity measurements, are shown. Ionic radius of the rare earth cations, as the presented Mn-O-Mn angle, decreases from left to right. Taken from reference [Kimura 03]

big ionic radius (Mn-O-Mn angle ϕ close to 180^o), undoped manganites have a antiferromagnetic spin order of type A coexisting with a $(\pi, \pi, 0)$ orbital ordering, whereas for smaller values of r_{Re} (smaller ϕ), the magnetic order is of type E. In the A phase, a Mn spin is ferromagnetically coupled with the Mn spins located in the same plane $(x-y)$, and antiferromagnetically with the Mn spins belonging to different planes. In the E phase, the $x-y$ layers are antiferromagnetically coupled, but the magnetic structure within the planes is that of ferromagnetic zigzag chains antiferromagnetically aligned. The horizontal (x) and vertical (y) steps of the zigzag chains contain two Mn ions. For values of r_{Re} close to the critical value where the magnetic order changes from A-type to E-type ($\phi \approx 148^o$ in Fig 3.1), manganites develop different magnetic incommensurate phases whith increasing temperature. In this reference, assuming perfect orbital order, the problem was mapped into the anisotropic next-nearest-neighbor Ising or ANNNI model [P.Bak 80]. Although it provides a phenomenological explanation to the observed experimental results, this approach does not clarify the microscopic origin of the different phases.

These incommensurate phases, as the E phase, are difficult to understand in the picture of strongly correlated Mott localized d-electrons. This is surprising, since as the Mn-O-Mn angle gets smaller, away from the 180deg of the ideal perovskite structure, the overlap between the Mn d orbitals mediated by the oxygens gets smaller. It should be expected then that undoped manganites with smaller cations, such as $HoMnO_3$ should behave more like Mott insulators than the ones with bigger cations, $LaMnO_3$ or $PrMnO_3$. In Fig 3.1, more Mott insulator like behavior is expected as one goes to the right along the x axis.

It has been suggested recently[Hotta 03, T.Hotta 03, D.V.Efremov], that the complete nesting between the two e_g bands that occurs in the A structure produces a spin-orbital ordering and opens a gap in the energy spectrum of undoped $RMnO_3$. Quoting ref.[D.V.Efremov], we do not claim that the real $RMnO_3$ systems can be fully described by a weak coupling approach as correlation effects can be important, although a treatment based in band structure calculation may be very useful to understand some properties of these materials. In particular, in ref.[Hotta 03], using a two orbital double exchange model, it was obtained that the experimental observed E-phase exits in a wide region of parameter space, and it is adjacent to the A-type phase. Coulomb intraorbital interactions might be significant. However, some works [Brey 04, Dagotto 02] were moderate interorbital coulomb interaction has been taken into account, indicate that it renormalizes the different critical parameters, but the topology of the phase diagram is not altered.

Our work clarifies the microscopic origin of the incommensurate phases appearing near the A-type to E-type magnetic transition. Our aim is to explain these phases using a realistic microscopic model. The Hamiltonian we study describes electrons moving in two e_g bands, that are ferromagnetically strongly coupled to the Mn core spins as well to the Jahn-Teller phonons. In addition, we also consider a direct superexchange interaction between the core Mn spins. Starting from this Hamiltonian we derive a functional that

describes a temperature induced commensurate-incommensurate transition similar to that observed experimentally.

The main result presented in this chapter is that near the A to E phase transition, the competition between the nearest neighbor antiferromagnetic superexchange interaction and the double exchange induced long range ferromagnetic interaction, results in the appearance of incommensurate phases. These phases consist of a periodic array of domain walls.

The rest of the chapter is organized as follows. In Sec.II we describe the microscopic model and we present the zero temperature phase diagram. In Sec.III we outline the method for obtaining the critical temperatures and we present the phase diagram composed of the different uniform phases. In Sec.IV we develop the functional for describing spatially modulated phases. Also in Sec.IV we study how the phase diagram of manganites at x=0 is altered when soliton incommensurate phases are taken into account. We finish in Section V with a brief summary.

3.2. Microscopic Hamiltonian and zero temperature phase diagram.

We are interested in the transition between A and E phases. In these phases the $x-y$ planes are coupled antiferromagnetically. In the approximation of infinte Hunds coupling, double exchange precludes the motion in the z direction, therefore we can analyze the properties of these phases and the transition between them by studying a Hamiltonian which describes electrons moving in the $x-y$ plane. Although the Hamiltonian does not explicitly include Coulomb interactions, some effects are implicitly taken into account. The crystal field splits the Mn d levels into an occupied t_{2g} triplet and a doublet of e_g symmetry, half filled for undoped manganites. Coulomb interactions, responsible for Hund's rules, align the spin of the t_{2g} electrons among them and with the spin of the eg electrons. This is described by the Double Exchange term in the Hamiltonian, 1.1 in which the usual double exchange factor, f, modulates the hopping of the e_g electrons depending on the relative orientation of the neighboring t_{2g} spins. The degeneracy of the e_g orbitals is also included in the model (see Introduction chapter). Finally, the electron-phonon interaction is modelled through a Kanamori-like term [J.Kanamori 60], with coupling constant λ. The hopping amplitude is taken as the energy unit.

We therefore study a double exchange model coupled to Jahn-Teller (JT) phonons, the direct antiferromagnetic coupling between the Mn core spins J_{AF} is also included:

$$H = H_{DE} + H_{e-ph} + J_{AF} \sum_{<i,j>} \mathbf{S}_i \mathbf{S}_j \tag{3.1}$$

In the perovskite structures the oxygens are shared by neighboring MnO_6 octahedra and the Q's distortions are not independent, cooperative effects being very important[Vergés 02].

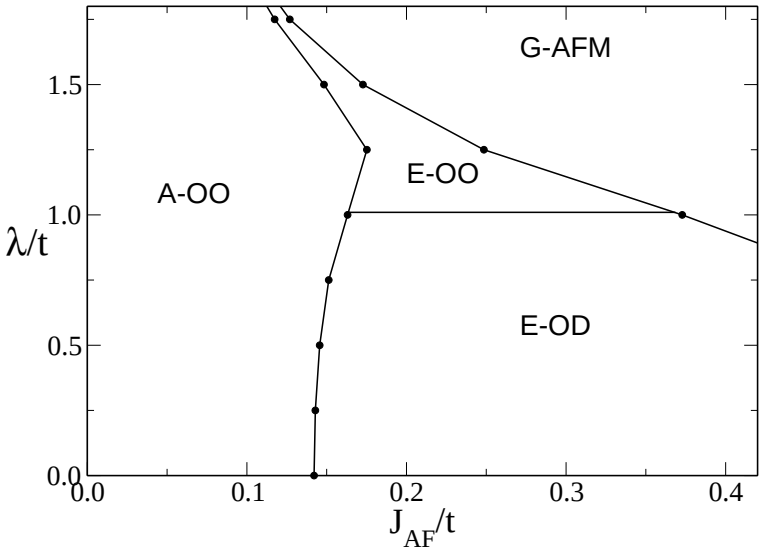

Figure 3.2: Zero temperature phase diagram for x=0 for the two-dimensional DE two orbital model with cooperative Jahn Teller phonons. The symbols OO and OD stand for orbital ordered and disordered respectively. A, E and G name the different magnetic orders defined in the text.

In order to consider these collective effects, we consider the position of the oxygen atoms as the independent variables of the JT distortions.

For given values of the parameters λ and J_{AF}, and a texture of core spins $\{\mathbf{S}_i\}$, we solve self-consistently the mean field version of Hamiltonian (3.1) and obtain the energy, the local charges $\{\rho_i\}$, the orbital pseudospin order $\{\tau_{xi}, \tau_{zi}\}$ and the oxygen octahedra distortions $Q_{\alpha,i}$. These quantities are better described by their Fourier transforms, that are represented by the same symbol with a hat: $\hat{\rho}(\mathbf{G})$, $\hat{Q}_1(\mathbf{G})$, ...

Fig.1 presents the phase diagram obtained by solving self-consistently Eq.3.1 for the parent compound $RMnO_3$. For the range of parameters studied, we do not find any solution showing charge modulation. In all the phases there is an electron located on each Mn ion, therefore in our model any gap in the energy spectrum is due to the spatial modulation of any other physical quantity.

For small values of J_{AF} the ground state is ferromagnetic, A-order. In the absence of Jahn-Teller coupling this phase is metallic, however, for $\lambda \neq 0$, and due to the perfect nesting between the e_g bands, the A phase develops a gap at the Fermi energy. The Jahn-Teller coupling produces and orbital order characterized by a finite Fourier component of the x-component of the pseudospin $\hat{\tau_x}(\pi,\pi) = \hat{\tau_x}(-\pi,-\pi) \neq 0$, see Fig. 3.3 a). The orbital order (OO) is produced by an ordered distribution of the oxygen octahedra distortions $\hat{Q}_2(\pi,\pi) = \hat{Q}_2(-\pi,-\pi) \neq 0$, that depends on the value of λ. The amplitude of the distortions are modulated in order to minimize the elastic energy of the cooperative Jahn-Teller distortions, and the signs arise from cooperative effects. In this phase the

(π, π) orbital modulation opens a gap at the Fermi energy and the x=0 manganite is an insulator, being the energy gap proportional to the value of the Jahn-Teller coupling.

For large value of J_{AF} and λ the system presents a G-type antiferromagnetic ground state and an orbital order characterized by a Fourier component of the pseudospin $\hat{\tau_x}(\pi, \pi) = \hat{\tau_x}(-\pi, -\pi) \neq 0$. Each Mn ion is coupled antiferromagnetically with its next neighbors and the double exchange mechanism precludes the motion of the carriers, being this phase an insulator. The minimal value of J_{AF} for the occurrence of this phase depends on λ, but in general is very large, so that this phase is rather unlike to occur in manganites.

For intermediates values of J_{AF} the system develops a magnetic order of E-type; the E phase consists of ferromagnetic zigzag chains coupled antiferromagnetically among them. The horizontal and vertical steps of the chain contain two Mn ions. For large enough values of the Jahn-Teller coupling the E magnetic order coexists with an orbital order similar to the one occurring in the A and G phases; this order opens a gap at the Fermi energy. In the E-OO phase the magnetic order is characterized by a periodicity $(2a, 2a)$, being a the lattice parameter of the square lattice. For small values of λ the E phase does not present orbital order, although it has a gap at the Fermi energy. In the orbital disorder (OD) E-phase, the dispersion energy for the e_g electrons along the FM zigzag chain is given by[Hotta 03], $\varepsilon_k = (2/3)(\pm \cos k \pm \sqrt{\cos^2 k + 3})$, indicating the existence of a large band gap at occupancies corresponding to x=0. The physical origin of this gap is the dependence of the tunneling probability on the spatial direction, $t^x_{\mu,\nu} = -t^y_{\mu,\nu}$ for $\mu \neq \nu$. It produces a periodicity in the hopping amplitude along the zigzag chain, leading to a periodic potential for the e_g electrons. It is important to note that, contrary to what happends in the x=1/2 case[Brey 04, L.Brey 05], this modulation in the hopping amplitude does not produce an orbital order. *The E-OD phase is stable due to the spatial modulation of the coherence between next neighbors Mn ions along the zigzag chain*, $< C^+_{i,\mu} C_{i+1,\nu} >= - < C^+_{i+1,\mu} C_{i+2,\nu} >$ for $\mu \neq \nu$. The phases E-OO and E-OD have different symmetry and therefore the transition between them that occurs at finite values of λ is a discontinuous transition.

3.3. Finite Temperature Magnetic Phase Diagram.

The simplest way of obtaining information on the phase diagram corresponding to a given microscopic Hamiltonian is by means of the mean field approximation. This approximation is insufficient for describing second order transitions, but it is successful in describing the phases away from the transition and in predicting the topology of the phase diagram. Therefore we compute the magnetic critical temperature of the different phases in this approach.

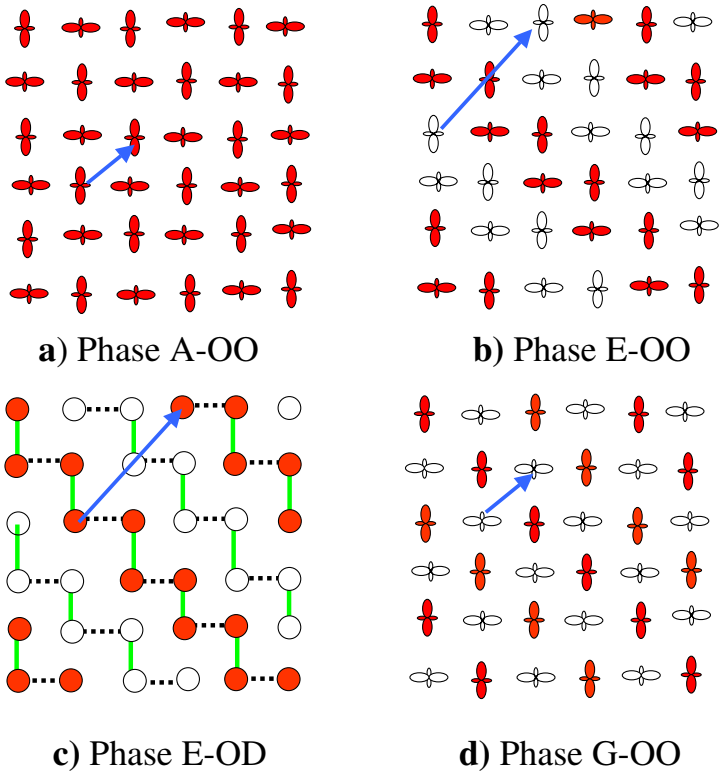

Figure 3.3: Orbital and spin order of x=0 manganites in the x-y plane. Elongated orbitals along the x (y) directions represent $d_{3x^2-r^2}$ ($d_{3y^2-r^2}$) orbitals. Circles represent the Mn ions in an orbital disordered phase. **a**) Orbital order presents in the ferromagnetic *A-OO* phase. **b**) Same than **a** but for the *E-OO* phase. **c**) Spin order in the *E-OD* phase. The solid and the dashed lines joining the Mn ions indicate the modulation of the electronic coherence along the zigzag chains. **d**) Same than **a** but for the *G-OO* phase. In all the phases there is not modulation of the electric charge and there is exacltly one electron located at each Mn ion. The vectors in the different schemes, represent the spatial periodicity in the different phases, (a, a) in the *A-OO* and *G-OO* phases and $(2a, 2a)$ in the *E-OO* and *E-OD* phases. In all the figures open and close symbols represent up and down spins.

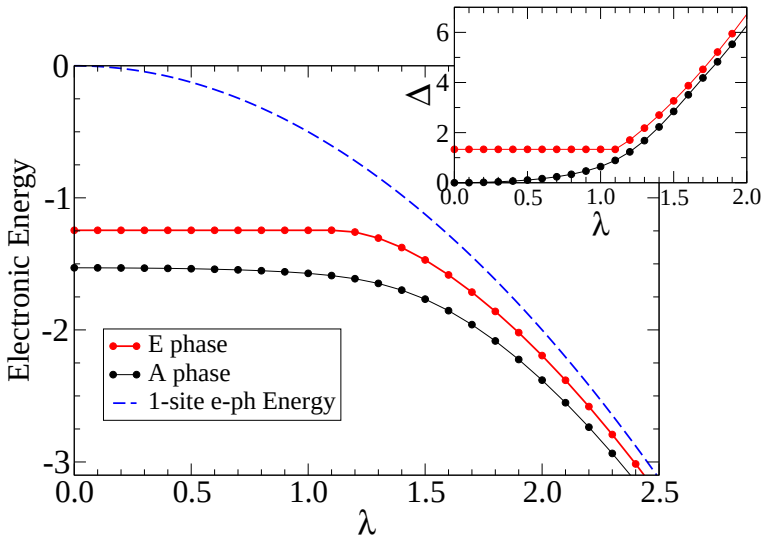

Figure 3.4: Energy and electronic Gap dependence on the electron-phonon coupling λ for the A (a)) and E (b)) phases. Notice how the A phase is distorted for an arbitrarily small value of λ due to perfect nesting of the Fermi surface for this filling of the band. Notice also the two, different origins of the E phase gap (see text)

3.3.1. Ferromagnetic (A) phase

In this phase all the Mn spins point, on average, in a particular direction, and there is a finite relative magnetization $<m>$. Using a virtual crystal approximation, we consider a unique value for the spin reduction factor $f_{i,j}$ that corresponds to its expectation value[D.Arovas 99, L.Brey 05],

$$f_{ij} \simeq <\sqrt{\frac{1+\cos\theta_{ij}}{2}} > \simeq \sqrt{\frac{1+<\cos\theta_{ij}>}{2}} = \sqrt{\frac{1+<m>^2}{2}}. \tag{3.2}$$

A reduction of $<m>$ produces a decrease in $f_{i,j}$ and therefore in the kinetic energy. In this way the importance of the Jahn-Teller coupling increases as the temperature decreases. The internal energy per Mn ion of this phase can be written as

$$E^A = \varepsilon_A(\lambda, <m>) + 2J_{AF} <m>^2 \quad . \tag{3.3}$$

where the electronic energy per Mn ion, $\varepsilon_A(\lambda, <m>)$, depends in a complicated way on λ and $<m>$ and has to be obtained numerically by solving Eq.(3.1).

In order to describe thermal effects it is necessary to compute the free energy. As the entropy of the carriers is very small[Brey 04] only the entropy of the classical Mn spins is included. We use a mean field approximation that neglects spatial correlations and assume for each individual spin a statistical distribution corresponding to an effective

magnetic field[de Gennes 60, Brey 04]. In this molecular field approximation, the entropy of the Mn spins takes the form:

$$S(<m>) = \frac{\log 2}{2} - \frac{3}{2} <m>^2 - \frac{9}{20} <m>^4 + ... \ . \tag{3.4}$$

Using this expression for the Mn spins entropy the total free energy of the system for small values of $<m>$ takes the form

$$F(<m>) = E^A - TS(<m>)$$

The Curie temperature of the A phase is given by:

$$T_C = -\frac{2}{3} \left. \frac{\partial \varepsilon^A(\lambda, <m>)}{\partial <m>^2} \right|_{<m>=0} - \frac{4}{3} J_{AF} \ . \tag{3.5}$$

The derivative for finite λ has to be calculated numerically. Higher derivatives of the internal energy with respect to the magnetization indicate that the transition is second order. Notice from Eq.3.5 that for a given value of the Jahn-Teller coupling the Curie temperature decreases linearly with the superexchange antiferromagnetic coupling J_{AF}.

3.3.2. Antiferromagnetic E phase.

The magnetization of the E phase is described by the relative amount of saturation in each zigzag chain $<m_s>$. In the virtual crystal approximation fluctuations are neglected and the hopping is modulated by the spin reduction factor that is different along the zigzag FM chain (f^{FM}) than between the AFM coupled chains, (f^{AF}) [de Gennes 60, L.Brey 05],

$$\begin{aligned} f^{FM}(<m_S>) &= \sqrt{\frac{1+ <m_S>^2}{2}} \\ f^{AF}(<m_S>) &= \sqrt{\frac{1- <m_S>^2}{2}} \ . \end{aligned} \tag{3.6}$$

The internal energy of this phase depends on λ, and $<m_S>$, and can be written as,

$$E^E = \varepsilon_E(\lambda, <m_S>) \ . \tag{3.7}$$

As each Mn spin core is surrounded by two Mn spins FM coupled and other two AFM coupled, the superexchange energy is zero.

In order to compute the Neel temperature of the E phases, we introduce an effective field for each spin sublattice. Taking into account that both, the magnetization and the effective magnetic field, have different sign in each sublattice, we end up with the

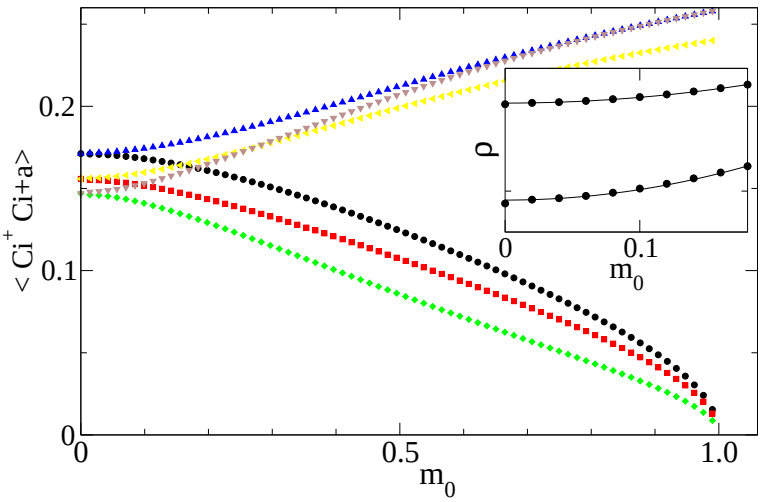

Figure 3.5: Intersite coherence within the $x-y$ plane as a function of the average magnetization of the two sublattices in the E phase. m_0=0 corresponds to the paramagnetic phase, intersite coherence in this limit depends only on the orbitals involved and not in the sublattice. In this limit, it is maximum for the coherence between x^2-y^2 orbitals, minimum between $3z^2-r^2$ and intermediate for coherence between both different orbitals. For $m_0>0$ increses for rbitals within the same chain (ferromagnetic aligned neighbourging sites) and decreases for orbitals in different chains (antiferromagnetic aligned neighbourging sites). The inset shows how the intersite coherence grows as m_0^2 (lines are parabolic fits) as explained in the text.

same expression for the entropy than in the A phase, but just changing $< m >$ by $<m_S>$[L.Brey 05]. With this the free energy takes the form,

$$\begin{aligned} F(<m_S>,\lambda) &= E^E - TS(<m_S>) \\ &\simeq F(0,\lambda) + <m_S>^2 \left(\frac{3}{2}T + a\right) \\ &+ <m_S>^4 \left(\frac{9}{20}T + b\right) + \\ &+ <m_S>^6 \left(\frac{99}{350}T + c\right) + ... \ , \end{aligned} \tag{3.8}$$

where

$$E^E \approx cte + a <m_S>^2 + b <m_S>^4 + c <m_S>^6 + ... \ . \tag{3.9}$$

Due to the symmetry of the E phase the coefficient a is zero, and the Neel temperature depends on the coefficients b and c. Numerically, the coefficient b is negative and the transition from the E to the paramagnetic (PM) phase is a first order phase transition.

It is interesting to analyze the origin of the negative sign of the quartic term. In the OD-case the Jahn-Teller coupling is not large enough to produce orbital order. In this situation the electronic energy is just kinetic energy. Therefore near $<m_S>=0$ we would expect that the electronic energy could be obtained perturbatively from the paramagnetic energy as, $E^E_{\lambda=0} \approx \frac{1}{\sqrt{2}} \left(f^{FM}(<m_S>) + f^{AF}(<m_S>) \right) \varepsilon^0_E$. Here $\varepsilon^0_E \equiv \varepsilon_E(0,0)$ is the paramagnetic energy per Mn ion. Expanding the spin reduction factors near $<m_S>$ we find $E^E_{\lambda=0} \approx \left(1 - \frac{1}{8} <m_S>^4 - \frac{5}{128} <m_S>^8 - ...\right) \varepsilon^0_E$. As the electronic energy of the paramagnetic phase is negative, the last expression suggests that the Neel temperature should be zero. However, numerically, we find a finite Neel temperature even for λ=0. This discrepancy occurs because, as commented above, in the E-OD phase the minimization of the kinetic energy produces a modulation of the electron coherence along the zigzag chain, $< C^+_{i,\mu} C_{i+1,\nu} >= - < C^+_{i+1,\mu} C_{i+2,\nu} >$ for $\mu \neq \nu$. We describe this modulation by an order parameter ξ that represents the $(\frac{\pi}{2}, \frac{\pi}{2})$ Fourier component of the electron coherence. This order parameter is coupled with the staggered magnetization and the functional describing the electronic energy has the general form:

$$\begin{aligned} E^E_{\lambda=0} &\approx \frac{1}{\sqrt{2}} \left(f^{FM}(<m_S>) + f^{AF}(<m_S>) \right) \varepsilon^0_E \\ &+ \alpha\xi^2 + \beta\xi <m_S>^2 + ... \ . \end{aligned} \tag{3.10}$$

This expression includes the elastic energy associated with the electron coherence and the minimal coupling between the staggered magnetization and the electron coherence. Minimizing this energy with respect the coherence parameter ξ, we find $\xi = -\frac{\beta}{2\alpha} < m_S >^2$. Introducing this value in the expression of the electronic energy, Eq.(3.10), the electronic energy can be expresed in terms of $<m_S>$ and the coupling constants:

$$E^E_{\lambda=0} \approx \left(1 - \frac{1}{8} <m_S>^4\right) \varepsilon^0_E - \frac{\beta^2}{4\alpha} <m_S>^4 + ... \ . \tag{3.11}$$

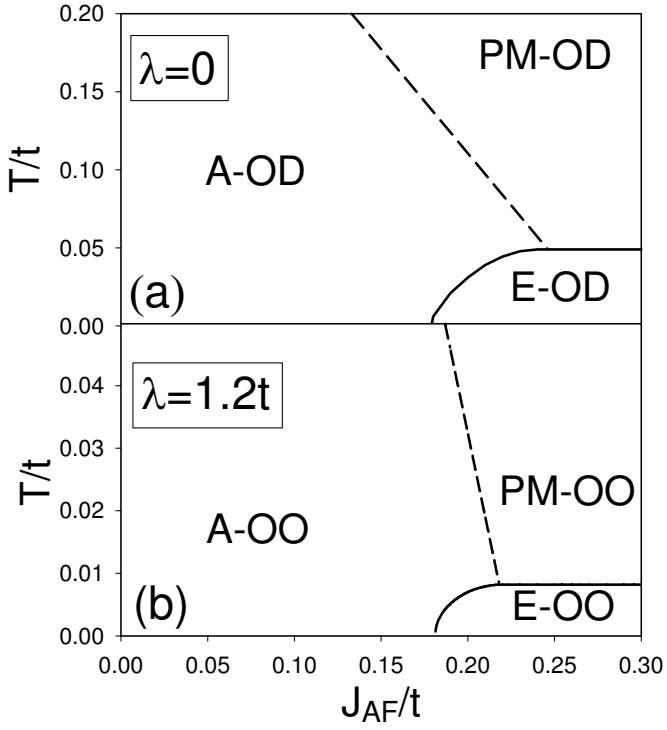

Figure 3.6: Phase diagrams T-J_{AF} for the two dimensional DE two orbital model with cooperative Jahn-Teller phonons and x=1. In a) we plot the $\lambda = 0$ case and in b) the $\lambda = 1.2t$ case. Continuous lines represent first order transitions whereas dashed lines indicate second order transitions. The abbreviations naming the different phases are explained in the text.

Showing thatr for strong enough coupling between $< m_S >$ and the orbital coherence, the quartic term is negative and a finite Neel temperature is expected. Therefore, the coupling between electron coherence and the staggered magnetization is responsible for the occurrence of a finite Neel temperature.

In the OO-case there exists a finite orbital order parameter $\hat{\tau_x}(\pi, \pi)$, that is coupled to the staggered distortion and it is the responsible for the existence of finite Neel temperature.

3.3.3. Temperature-J_{AF} magnetic phase diagram

In Fig.3, we plot the T-J_{AF} magnetic phase diagrams for λ=0 (a) and λ=1.2t (b). These phase diagrams have been obtained by minimizing and comparing the free energies of the A, E and paramagnetic phases. While for λ=0, all the phases are disordered in the

orbital sector, for large enough values of λ, E and A phases present orbital order. In the latercase, λ=1.2t, we find that the critical temperature associated with the orbital order is much larger than the magnetic critical temperatures and, therefore, in Fig.3b the paramagnetic phase presents orbital order. In any case, it is important to note that, from the magnetic point of view, both phase diagrams are topologically equivalent. At large temperatures the systems are always paramagnetic, for small J_{AF} and small temperature the systems present ferromagnetic order, whereas for small temperature and moderates values of J_{AF} an antiferromagnetic order of type E appears. For very large values of the AFM coupling, not shown in Fig.3, antiferromagnetic order of type G would appear. The Curie temperature corresponding to the paramagnetic-A phase transition decreases linearly with J_{AF}, Eq.6, until it reaches the, J_{AF} independent, Neel temperature corresponding to the paramagnetic-E transition. As discussed in the previous subsection the A-paramagnetic transition is second order while, because of the coupling between different order parameters, the E-paramagnetic transition is first order.

The phase diagrams present a Lifshitz point where the uniform ferromagnetic A phase, the modulated ordered E phase and the paramagnetic disordered phase meet. Near the Lifshitz point there is a range of values of J_{AF} where, by increasing the temperature, the system undergoes an E-A transition followed by an A-PM transition. The topology of this phase diagram is similar to that of a Ising model with competing interactions. In that model, near the Lifshitz point, solitons, spatially modulated phases and commensurate incommensurate transitions appear when the temperatures varies[P.Bak 80]. In the next section we explore the possible existence of solitons and incommensurate phases in the model described by the Hamiltonian Eq.3.1 at x=1 and near the Lifshitz point that appears in the T-J_{AF} phase diagram, Fig.3.6.

3.4. Soliton theory and spatially modulated phases.

3.4.1. Landau functional

The magnetic order of the phases described in the previous sections only differs in the direction perpendicular to the chains, see Fig.3.3. In the mean field approximation the E phase is described by a spin density wave of the form $<S>=\sqrt{2}\,m_0\,\cos(q_0 z+\pi/4)$, with $q_0=\pi/2$. Here z is the position of the atoms along the direction perpendicular to the chains. We are taking the distance between first neighbors diagonal lines of atoms, $\sqrt{2}a/2$, as the unit of length. In general the expression

$$<S>=\sqrt{2}\,m_0\,\cos\left(q_0 z+\frac{\pi}{4}+\theta(z)\right) \tag{3.12}$$

describes different spatially modulated magnetic phases. With $\theta(z)$=0 it describes the E phase, whereas with $\theta(z)$=$-q_0 z$, it represents the average magnetization in the position independent ferromagnetic A phase. The case m_0=0 corresponds to the paramagnetic

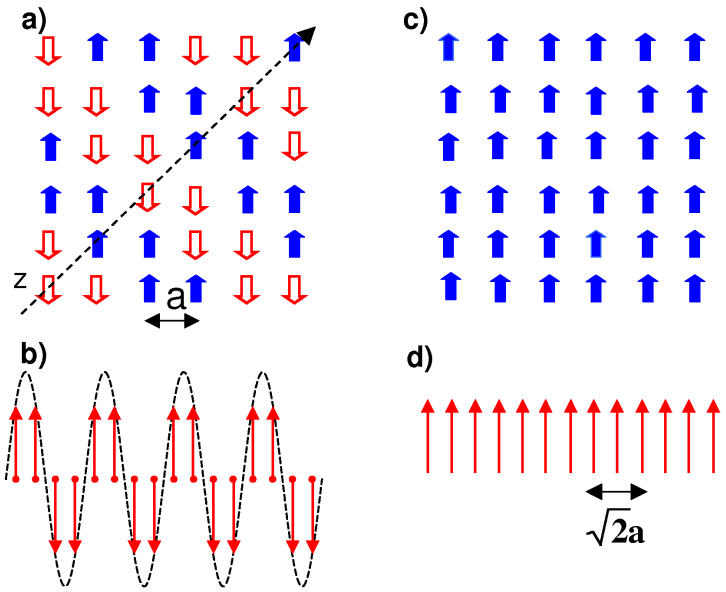

Figure 3.7: Spin order of x=1 manganites in the x-y plane. (a) Corresponds to the E phase whereas (c) represents the A phase. The direction perpendicular to the zigzag chains is shown in (a). The averaged magnetization along the z direction for the E and A phases are plotted in (c) and (d) respectively.

case. In general $\theta(z)$ describes phases where the average magnetization changes along the direction perpendicular to the chains.

While both E and A phases are commensurate with the underlying lattice, the existence of solitons and incommensurate phases in the system will be considered in this study. Solitons are static domain walls between commensurate domains. In this section, we present a formalism which makes contact with phenomenological theories and provides the basis for the calculation of the nature of the phase diagram at finite temperature.

We want to build a Landau theory functional where the order parameter is the modulation of the average spin along the diagonal direction. Following references [W.L.McMillan 76, W.L.McMillan 77], in Eq.3.12 we consider the amplitude of the magnetization, m_0, as constant in the space.

In order to set up a Landau theory we need to calculate the different contributions to the free energy. For a magnetization given by Eq.3.12, and near the order-disorder magnetic transition, the entropic contribution to the free energy can be estimated as described in Sec.III,

$$\begin{aligned} -TS \simeq k_B T \int \Big[& -\log 2 + \frac{3}{2} m_0^2 + \frac{27}{40} m_0^4 + \frac{99}{140} m_0^6 \\ & - \left(\frac{9}{40} m_0^4 + \frac{297}{700} m_0^6 \right) \cos 4\theta(z) \Big] \, dz \quad . \end{aligned} \tag{3.13}$$

The superexchange antiferromagnetic interaction takes the form

$$E_{AF} \simeq 2 J_{AF} \, m_0^2 \int \sin \left(\nabla \theta(z) \right) dz \ . \tag{3.14}$$

being $\nabla\theta(z)$ the derivate of $\theta(z)$ with respect z. In the previous expression we have treated the position z as a continuous variable and we have discarded second and higher spatial derivatives of θ.

Concerning the electronic contribution to the internal energy, E_e, we assume that it is local an can be written as $E_e = \int dz \, \mathcal{E}(z)$, being $\mathcal{E}(z)$ the electronic energy density. We expect that it can be expanded in powers of the order parameter $< S >$ and its derivatives,

$$\begin{aligned} \mathcal{E}(z) = \mathcal{E}^0 \ & + \ \tilde{a}_l(z) < S(z) >^l + \tilde{b}_l(z) \left(\nabla < S(z) > \right)^l \\ & + \ \tilde{c}_{l,m}(z) < S(z) >^l \ \left(\nabla < S(z) > \right)^m \ ... \end{aligned} \tag{3.15}$$

Here the sum over repeated indices is assumed, and because the symmetry of the system only even powers of $<S>$ and $\nabla <S(z)>$ contribute. The coefficients $\tilde{a}_l$, $\tilde{b}_l$ and $\tilde{c}_{l,m}$ are periodic in z with the periodicity of the crystal lattice and for a magnetization of the form Eq.3.12, the density of electronic energy can be written as,

$$\begin{aligned} \mathcal{E}(z) = \mathcal{E}^0 \ & + \ a_2 m_0^2 + a_4 m_0^4 + a_6 m_0^6 \\ & + \ (b_4 m_0^4 + b_6 m_0^6) \cos 4\theta(z) \\ & + \ (c_2 m_0^2 + c_4 m_0^4 + c_6 m_0^6) \left(\nabla \theta(z) + q_0 \right)^2 . \end{aligned} \tag{3.16}$$

Here we have neglected higher terms in the derivatives of the phase θ and, as there are first order phase transitions in some part of the phase diagram, we keep terms up to the sixth power in m_0. The second term in Eq.3.16 is the *umklapp* term that favors the modulated commensurate solutions, $\theta(z)$=0, $\frac{\pi}{2}$, π, $3\frac{\pi}{2}$, corresponding to the E phase. The last term is an elastic energy which favors the occurrence of the ferromagnetic A-phase, $\theta(z)=-q_0 z$. The competition between the elastic and the *umklapp* contributions will produce the existence of solitons and incommensurate phases.

From the expression of the electronic energy of the E-phase as function of the order parameter m_0, we notice $a_2=-c_2\, q_0^2$. Analyzing the dependence of the electronic energy on a constant phase ($\theta(r)=\theta_0$), we find $b_4=a_4+c_4\, q_0^4$ and $b_6=a_6+c_6\, q_0^6$. In this way only two subsets of parameters (for instance b's and c's) are independent. Finally, for each value of λ, we perform microscopic calculations of the electronic energy of the A and E phases and obtain the numerical values of the coefficients b's and c's respectively.

Adding the entropy, Eq.3.13, the antiferromagnetic energy, Eq.3.14 and the electronic internal energy, Eq.3.16, we obtain the following expression for the free energy of the system,

$$\begin{aligned} F &= F_0(T,m_0) \\ &+ C\int\left[\frac{1}{2}\left(\nabla\theta(z)+q_0\right)^2 + w\left(1+\cos 4\theta(z)\right)\right] dz \end{aligned} \tag{3.17}$$

with,

$$\begin{aligned} F_0(T,m_0) &= \left(-\log 2 + \frac{3}{2}m_0^2 + \frac{9}{10}m_0^4 + \frac{198}{175}m_0^6\right) T \\ &- 2J_{AF}m_0^2 + \varepsilon_e^0 - c_2 m_0^2 q_0^2 \ , \end{aligned} \tag{3.18}$$

$$C = \left(2c_2 + 4\frac{J_{AF}}{q_0^2}\right) m_0^2 + 2c_4 m_0^4 + 2c_6 m_0^6 \ , \tag{3.19}$$

and

$$w = \frac{\left(b_4 - \frac{9}{40}\right) m_0^4 + \left(b_6 - \frac{297}{700}T\right) m_0^6}{C} \ . \tag{3.20}$$

In the limit $w \to 0$, the elastic contribution is the more important term and the phase $\theta(z)$ tends to be $\theta(z) = -q_0\, z$. On the contrary, for large values of w, the *umklapp* term is dominant and θ wants to get a constant value, θ=0, $\frac{\pi}{2}$, π, $3\frac{\pi}{2}$. A transition between the commensurate phase, $\theta = 0$ and the uniform ferromagnetic phase takes place because of the competition between these two terms; by tuning the values of J_{AF} and T we are going to see that a soliton incommensurate phase appears between these two limits.

For a given temperature and a particular value of J_{AF}, the constant amplitude m_0 and the phase function $\theta(z)$ that characterize the solution are obtained by minimizing the functional Eq.3.17. The function that makes F extremal is given by the corresponding Euler equation, which reads:

$$\frac{1}{2}\frac{d^2\theta}{dz^2} + 4w\frac{\partial}{\partial\theta}(1+\cos 4\theta) \tag{3.21}$$

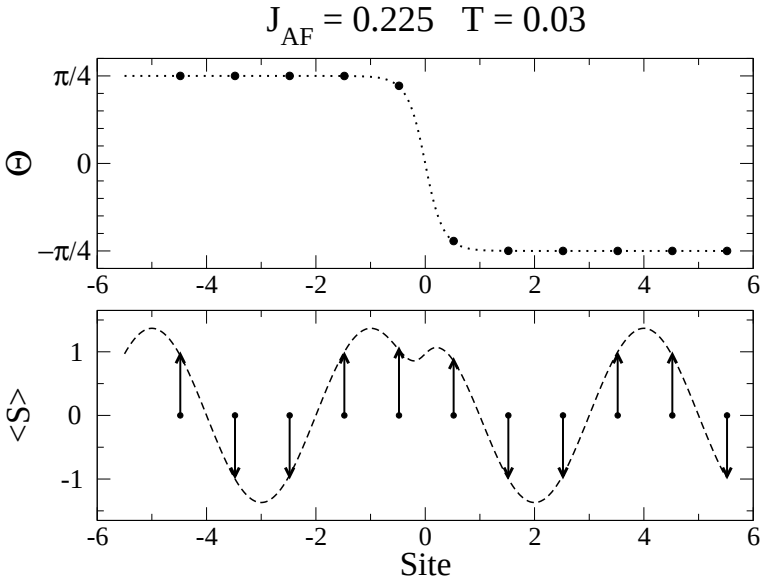

Figure 3.8: a) Anti-soliton solution to Eq. 3.22 for spatial variation of θ corresponding to Eq. 3.23. It can be understood as a domain wall between two essentially commensurate regions. The actual thermal average of the spins is shown in b). The most general solution is an array of solitons with very similar shape. The separation among them gives the periodicity of the system, and is calculated as explained in the text

It turns out to be the Sine-Gordon equation:

$$\frac{1}{2}\frac{d^2\theta}{dz^2} + 4w \sin 4\theta = 0 \tag{3.22}$$

The phase has to satisfy this equation for each value of m_0. The equation has been extensively studied in soliton theory, in fact one solution is the anti-soliton :

$$\theta(z) = \tan^{-1} \exp\left(4\sqrt{w}z\right) \quad . \tag{3.23}$$

This solution is a domain wall which separates two almost commensurate z regions.

A general solution of Eq.3.17 is a soliton lattice formed by a regular array of domain walls, each of length L.

At each soliton the phase θ tumbles $\frac{\pi}{2}$. The deviation of the average wave vector $\bar{q}$ from q_0 is inversely proportional to the distance between the domain walls,

$$\bar{q} = \frac{\pi}{2L} \quad . \tag{3.24}$$

The value of $\bar{q}$ is proportional to the soliton density, it can be calculated by minimizing the free energy following the procedure outlined in references [P.Bak 80, W.L.McMillan 76, W.L.McMillan 77, G.DeGennes 68] and detailed below for our particular case.

The temperature at which solitons appear in the system can be calculated by the condition that the condensation energy of the first soliton is negative . It can be shown that this corresponds to

$$w_c = \left(\frac{\pi}{4}\right)^2 q_0^2 \tag{3.25}$$

The total length L of a soliton corresponds to a change of $\frac{\pi}{2}$ in θ, therefore:

$$L = \int_{\frac{\pi}{2}}^{0} d\theta \frac{dz}{d\theta} \tag{3.26}$$

One can easily integrate once the Sine-Gordon Eq. 3.22, the periodicity of the system is then related to the integration constant. Substituting the general solution in Eq. 3.26 it is found that the distance between solitons can be expressed as:

$$L = \frac{\tilde{k}}{2\sqrt{w}} \int_0^{\frac{\pi}{2}} \frac{d\tilde{\theta}}{\sqrt{1+\tilde{k}^2 \sin^2\theta}} = \frac{\tilde{k}}{2\sqrt{w}} K(\tilde{k}) \tag{3.27}$$

where $\tilde{k}^2 = 4wk^2 = 2w/C$ C being the integration constant. $\tilde{\theta} = \frac{\pi}{2} - \theta$, and K(k) is the elliptic integral of the first kind. Without explicity knowing the expression for $\theta(x)$ we can minimize Eq. 3.18 with respect to the constant k, and therefore find L as a function of m_0, and T.

The minimization condition can be expressed as a function of the elliptic integral of the second class $E(k)$:

$$\frac{E(\tilde{k})}{\tilde{k}} = \frac{\pi |q_0|}{4\sqrt{w}} \tag{3.28}$$

The free energy for the soliton phase is on the form:

$$F = F_0 + \frac{q_0^2}{2} - \frac{2w}{k^2} \tag{3.29}$$

We can recover the commensurate phases in the proper limits. As k goes to one we recover the E phase with free energy $F = F_0 + \frac{\delta^2}{2} - 2w$ and as both k and w go to zero we approximate to the ferromagnetic phase (with vanishing m) and $F \approx F_0$

In the soliton lattice phase the magnetic periodicity along the z-direction is characterized by the wave vector

$$q = \frac{\pi}{2} - \frac{\pi}{2L} \quad . \tag{3.30}$$

In the E-phase there are not solitons in the system, L=∞ and $\bar{q}$=0, and the wave vector of the magnetic modulation is q=$\frac{\pi}{2}$. In the continuous approximation the ferromagnetic A-phase corresponds to a extremely dense lattice soliton, L=1. In this limit, θ is too quickly varying, the continuous approximation is not valid and we take the criterium that for $L \leq 1.1$, the soliton lattice is the ferromagnetic A-phase.

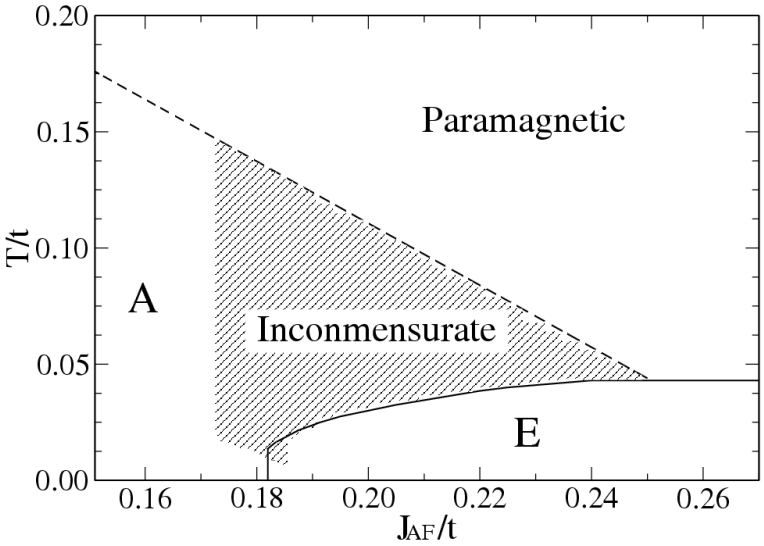

Figure 3.9: Phase diagram $T - J_{AF}$ as obtained by minimizing the free energy Eq.3.17. The parameters of entering in the free energy are obtained by minimizing the microscopic Hamiltonian Eq.3.1 for λ=0 and x=1. Continuous lines represent first order transitions whereas dashed lines indicate second order transitions. The shadow region indicates the region where the incommensurate phase exits.

3.4.2. Results

In order to find inhomogeneous phases in manganites at x=1, we have minimized the free energy Eq.3.17 with the coefficients a's, b's and c's obtained from the microscopic model described in Section II. The solutions are characterized by the value of the magnetization m_0 and the density of solitons $\bar{q}$. We present results for the case λ=0, but similar results are obtained for finite Jahn-Teller coupling.

If we consider only the uniform solutions, E and A phases, the minimization of the free energy results in the phase diagrams already presented in Sec. III, Fig.3.6. When inhomogeneous solutions are considered, we obtain the phase diagram shown in Fig.3.9. Several comments on this phase diagram are in order, (i) There are not solitons for values of J_{AF} larger than the antiferromagnetic coupling corresponding to the Lifshitz point. The paramagnetic-E phase transition is first order, with a large jump in the value of m_S, and therefore in the value of w. In this situation, large values of w, the *umklapp* term is much stronger than the elastic term and the system prefers to be commensurate with the lattice. Note than in the paradigmatic Ising model with competing interactions[P.Bak 80] all the transitions are second order and incommensurate phases appear at both sides of the Lifshitz point. (ii) For small values of J_{AF} the elastic term is very strong and the solution corresponds to a dense soliton phase. For small values of J_{AF} the distance between solitons is smaller than the cutoff and we consider that this commensurate phase is actually, in the discrete real crystal, the ferromagnetic A-phase.

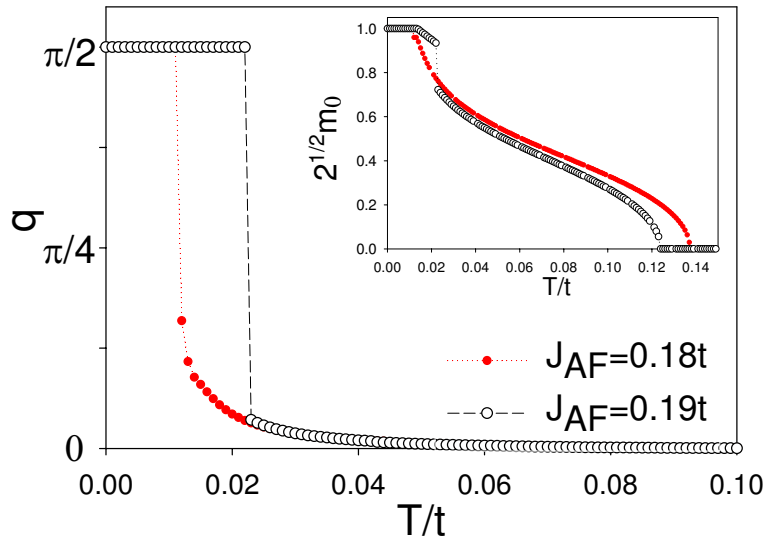

Figure 3.10: Temperature dependence of the magnetic wave vector, q, and of the order parameter amplitude, m_0 (inset), for two values of J_{AF}. The wave vector $q{=}\frac{\pi}{2}$ corresponds to the E-phase and $q{=}0$ to the A-phase. The results are obtained by minimizing the free energy (Eq. 3.17).

(iii) For intermediate values of J_{AF}, the competition between the elastic and the *umklapp* term results in the appearance of incommensurate solitonic phases.

In Fig.3.9, the shadow region indicates the incommensurate phase. The frontier of this phase with the ferromagnetic A-phase is diffuse because, as we have already discussed, to distinguish between a dense soliton phase and the ferromagnetic A-phase we take a criterion based on the distance between solitons. Within our approximation, we do not find solitons at $T{=}0$. Experiments show lock-in transition for Tb and and Dy compounds at low temperatures, with values of q between $\frac{\pi}{2}$ and zero [Kimura 03]. Neither the expansion of the entropy (equation 3.4) nor the ignorance of higher order umklapp terms are accurate in this limit, so we can not expect our model to explain this behavior. A recent work [Sergienko] might clarify this issue. Typical temperature dependence of the magnetic wave vector and magnetization amplitude near the incommensurate phase is illustrated in Fig.3.10. For low temperature the system is in the commensurate E-phase, corresponding to a wave vector $q{=}\frac{\pi}{2}$. At low temperatures the spins are highly polarized and that makes the magnetic modulation too *rigid* to allow solitons. As temperature increases, the amplitude of the spin-modulation, m_0 decreases and, at a J_{AF} dependent temperature, a jump to the solitonic phase takes place. For values of J_{AF} closer to the Lifshitz point, the incommensurate phase appears at temperatures near the A-paramagnetic critical temperature. In that case the amplitude of the magnetization m_0 is small and hence the magnetic wave vector of the incommensurate phase is also

very small. Therefore, in this part of the phase diagram the incommensurate phase is similar to the A-phase.

For values of J_{AF} near the zero temperature A to E phase transition, there is a small portion of the phase diagram where, by decreasing the temperature, the system evolves first from a paramagnetic, $q = 0$, phase to a incommensurate phase characterized by a finite q, and then to a ferromagnetic A phase without magnetic modulation, $q = 0$.

The magnetic phase diagram shown in Fig.3.9 contains the essence of the magnetic properties experimentally observed in undoped manganites[Kimura 03]. Systems with large hopping amplitude, (J_{AF}/t small) as $LaMnO_3$ have a ground state with a magnetic order of type A and a relatively large Neel temperature. The relative value of the AFM coupling increases when the ionic radius of the rare earth in the manganite increases. Therefore we understand the experimental decrease of the Neel temperature in the series of $RMnO_3$ (R=La, Pr, Nd, Sm) as the diminution of the A-paramagnetic critical temperature when J_{AF} increases, see Fig.3.6 and Fig.3.9. Experimentally it is observed that for large enough ionic radius, $HoMnO_3$, the ground state of the undoped manganite has a magnetic order of type E, and present incommensurate phases when temperature increases. We claim that this situation corresponds in the phase diagram Fig.3.9 to values J_{AF}/t in the range 0.18-0.20. Experimentally it is also observed that in some compounds as $TbMnO_3$ and $GdMnO_3$, when the temperature increases, the system undergoes two phase transitions, first a a ferromagnetic-incommensurate transition and, at higher temperatures, a incommensurate -paramagnetic transition. In the phase diagram presented in Fig.3.9 similar behavior occurs for values of J_{AF} near $0.18t$.

3.5. Summary

By starting from a microscopic Hamiltonian we have derived an expression for the free energy of undoped manganites. We have considered first the commensurate A and E phases. For them, we have confirmed the previously reported phase diagram and established the nature of the gap in these phases, and found the physical origin of the finite T_N the E phase.

We have quantified the competition between the short range superexchange antiferromagnetic interaction, and the long range double exchange ferromagnetic interaction, using a realistic model. We find that the competition between these interactions, inducing correlation with opposite sign and their different nature, results in the existence of magnetic incommensurate phases as the recently experimentally observed in undoped manganites. The incommensurate phases can be described as arrays of domain walls separating commensurate phases by a distance that depends on temperature. We have established a phase diagram and calculated the temperature dependence of the periodicity of the system as a function of the relative strength of the interactions. The

results presented in Fig.3.9 explain qualitatively the experimental results published in Ref.[Kimura 03]

Chapter 4

Disorder effects in the Magnetic Properties of Manganites

4.1. Introduction

Manganites are very sensitive to disorder - disorder understood as inhomogeneities in the materials, or more rigorously, as departures from crystallinity - . The long held discussion to elucidate which aspects of manganites physics were intrinsic and which ones were spurious is a most visible reflection of this property. It is common to find articles in which several paragraphs are devoted to demonstrate the correct stoichiometry of the samples and the crystal structure. We already discussed in the introduction chapter the interrelation between the (possibly disorder induced) phase separation and colossal magnetoresistance (CMR), and the relevance of the Griffiths phase, which is intrinsically related to disorder, to the physical properties of manganites.

Other important examples of the effects of disorder that have attracted much attention are the influence of Oxygen vacancies [Hossain 99, Ritter 97], which were surely present in most of the early samples, and of the grain boundaries of polycrystals in the transport properties of manganites [Rivas 00, de Andrés 99] In other works, disorder has been introduced on purpose, to test its effects, for instance substituting Manganese cations with Gallium or Aluminum [Sawaki 00a, Blasco 03, MARTIN 96] All these issues can be understood as manifestations of the sensitiveness of Manganese oxide perovskites to perturbations in general, and to different kinds of disorder in particular [Millis 03].

But there exist more subtle sources of disorder. Even in monocrystalline samples, some degree of disorder is always present. Suppose we had a perfect perovskite where all the sites corresponding to MnO_6 octahedra were occupied by the correct species. To introduce charge carriers we would need to dope the perovskite's A site with cations of different valence. This doping would be a source of disorder. When doping, the position of the different cations is, in principle, random, they make up a solid solution. Only very recently this more subtle kind of disorder could be controlled in experiments. We devote this chapter to study the very notable effects that even this *lighter* disorder has on the properties of manganites.

When studying the effects of disorder in materials, two aspects are crucial. One is to have a good control of the amount of disorder in the samples. Disorder is anyhow a vague concept and it is sometimes difficult to determine what kind of disorder is relevant and what is not. Attfield and coworkers [Williams 03, Rodriguez-Martinez 96] found that in FM perovskites of the form $AMnO_3$, the variation of Curie temperature (T_C) with disorder is related to the distribution of the A cations radius, r_A, and there is no significant dependence on the A site charge variance. How well the A sitting cations fit in the perovskite structure is characterized by the tolerance factor (See the introduction chap. determined by the mean size of the cations. This was soon identified as crucial for the properties of manganites. What the work of Attfield and collaborators shows is that not only the tolerance factor is important, but also the differences in sizes between the different cations, a source of structural disorder, plays a very important role. They identify the cations size variance as an adequate measure of the size differences.

The other crucial aspect is to obtain clean enough samples. By clean enough we understand samples where the effect of whatever kind of disorder present does not obscure the intrinsic behavior of the material. The obtention of highly ordered samples, have been allowed by the advances in the synthesis, allowing careful and enlighten experiments. Recently, some groups [Akahoshi 03, Millange 98] have been able to synthesize cation ordered perovskites. The chemical formula of these samples is $Ln_{0.5}Ba_{0.5}MnO_3$. Ln is a rare earth, and LnO and BaO planes alternate along the c axis. These half-doped manganites may give a good benchmark to test theories of the influence of disorder on the electronic and magnetic properties of manganites.

Interestingly enough, as the different A site doping cations are placed in planes, they break the isotropy of the material, and the unit cell is doubled only in one direction. Although the environment *seen* by the Manganese ions might not be exactly cubic, however, we assume that this is a minor effect.

In manganites the ferromagnetic order is driven by the motion of the carriers. Therefore, their properties depend on the competition between kinetic energy, tending to delocalize the carriers, and localization effects, such as antiferromagnetic coupling between the Mn core spins and Jahn-Teller coupling. Disorder also reduces the carriers mobility, and, thus, it strongly affects the stability of the ferromagnetic (FM) phases.

Experimental work in FM $La_{0.5}Ba_{0.5}MnO_3$ [1] shows[T.J.Sato 04] that disorder strongly reduces the transition temperature and changes the character of the transition, from continuous to weakly first order.

In the light of the experiments by Rodriguez-Martinez and Attfield, [Rodriguez-Martinez 96], we expect that the observed[T.J.Sato 04] difference in T_C between the ordered and disordered $La_{0.5}Ba_{0.5}MnO_3$ perovskites is related to the different distributions of r_A's. Note that standard ionic radii values are $r_A = 1.21$ for La^{3+} and $r_A = 1.47$ for Ba^{2+}[Rodriguez-Martinez 96]. In the ordered $La_{0.5}Ba_{0.5}MnO_3$ perovskite, Fig. 4.1(a),

[1] In practice, the authors of Ref. [T.J.Sato 04] chossed to work with $La_{0.46}Ba_{0.54}$. At this doping the compound does not show any sign of charge or antiferromagnetic order.

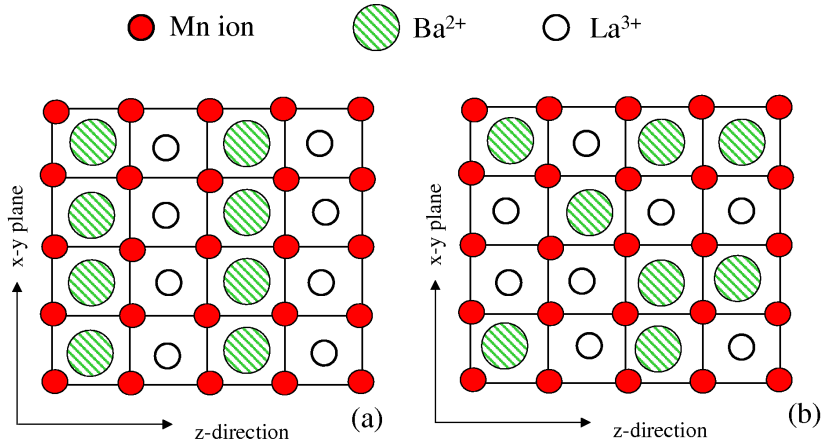

Figure 4.1: Schematic representation of an ordered (a) and disordered (b) $La_{0.5}Ba_{0.5}MnO_3$ perovskite. In the ordered case planes containing La and Ba cations alternate along the z-direction. In the disorder case the cations are randomly distributed.

alternating planes of LaO and BaO separate MnO_2 sheets in such a way that each Mn ion has four La^{3+} neighbors in one direction and four Ba^{2+} neighbors in the opposite direction, being all the Mn ions equivalent. In the disordered perovskites, Fig.4.1(b), La and Ba cations are randomly distributed and Mn's are surrounded by different combinations of divalent and trivalent cations. Similar experiments by Tokura's group [Akahoshi 03] extended the analysis to other rare earth manganites. Their results confirm this view, as the the Rare Earth cations size is decreased, the depression in T_C of the different compounds, with respect to their ordered analogous increases. The picture is, then, that environments of Mn consisting in cations with different sizes affect the physical properties of these materials. In the example above, the bigger the difference in size between the cations (Lanthanoids elements with respect to Barium) the most drastic the change in the environment that different Manganese ions of each material *feel*. In the ordered materials with the same composition, as they are half doped, all manganese are equivalent to each other and no disorder due to A-site doping is present.

In the present chapter we combine Ginzburg-Landau formalism with realistic two orbital DE microscopic calculations, to study the effect that the disorder in the position of the trivalent and divalent cations has on the magnetic properties of FM manganites. We model the difference in Mn environments as a source of disorder in the electronically active Mn levels. The experimentally observations about the marked reduction of the Curie temperature and the change in the order of the transition are recovered. Our analytical results provide a framework for understanding the dependence of T_C on disorder, both, in experiments and in Monte Carlo simulations of simplified

models[Motome 03, S.Kumar 03, C.Sen 04, S.Kumar 06, Trukhanov 02]. Different disorder distributions are studied in order to confirm the variance of disorder strength as the relevant parameter to characterize the change in the magnetic properties.

4.2. Model.

As explained in the introduction chapter, in a manganite of formula $R_{1-x}A_xMnO_3$, there are $4-x$ electrons per Mn ion. The crystal field splits the Mn d levels into an occupied strongly localized t_{2g} triplet an a doublet of e_g symmetry. Furthermore, the Hund's coupling in Mn ions is very large and aligns the spins of the d orbitals. The low lying t_{2g} triplet is thus polarized and it is commonly consider as a *core spin*. Effectively, there are $1-x$ electrons per Mn ions hoping between the empty e_g Mn states.

The large Hund's coupling forces each electron spin to align locally with the core spin texture. The spin of the carriers is conserved in the hoping between Mn ions, being the tunneling amplitude maximum (minimum kinetic energy) when the spins of the Mn ions are parallel and the system is ferromagnetic. This is basically the so called double exchange (DE) mechanism proposed fifty years ago [C.Zener 51, Anderson 55, de Gennes 60] to explain FM order in manganites. When temperature increases the kinetic energy minimized by the FM order competes with the orientational entropy of the Mn core spins and, at T_C, the system becomes paramagnetic (PM)[Calderón 98]. In the PM phase the reduction of the kinetic energy could favor that localization effects become more effective and a metal insulator transition could occur near the FM-PM transition[Vergés 02]. In the case of $La_{0.54}Ba_{0.46}MnO_3$, localization effects are rather weak and the material is metallic at both sizes of the FM-PM transition. Therefore, in our model we do not consider coupling with the lattice, however as the DE mechanism depends strongly in the kinetic energy gain, we treat the motion of the carriers in a realistic way by including the two e_g orbitals.

We shall therefore derive an expression for the energy of the DE model in the presence of the disorder arising form cation size mismatch, and an approximate expression for the entropy near the FM-PM transition. With these two pieces, we build up our Ginzburg-Landau functional.

Hamiltonian. With the above considerations, the two orbital DE Hamiltonian takes the following form,

$$H = \sum_{<i,j>,a,b} f_{i,j}\ t^u_{a,b}\ c^+_{i,a}c_{j,b} + \sum_{i,a} \epsilon_i\ \hat{n}_{i,a}\ \ , \tag{4.1}$$

here $c^+_{i,a}$ creates an electron in the Mn ion located at site i in the e_g orbital a (a=1,2 1=$|x^2-y^2>$ and 2=$|3z^2-r^2>$). In the limit of infinite Hund's coupling, the spin of the carrier should be parallel to the Mn core spin $\mathbf{S}_i$, and the tunneling amplitude is

modulated by the spin reduction factor:

$$f_{i,j} = \cos\frac{\vartheta_i}{2}\cos\frac{\vartheta_j}{2} + e^{i(\phi_i-\phi_j)}\sin\frac{\vartheta_i}{2}\sin\frac{\vartheta_j}{2} \tag{4.2}$$

where $\{\vartheta_i, \phi_i\}$ are the polar angles of the Mn core spins. The hopping amplitude depends both on the direction u between sites i and j and the orbitals involved; $t_{1,1}^{x(y)} = \pm\sqrt{3}t_{1,2}^{x(y)} = \pm\sqrt{3}t_{2,1}^{x(y)} = 3t_{2,2}^{x(y)} = t$. In the z direction the only nonzero term is $t_{2,2}^{z} = 4/3t$ [Dagotto 02]. Hereafter t is taken as the energy unit.

The last term describes the diagonal disorder. $\hat{n}_{i,a} = c_{i,a}^{+}c_{i,a}$ is the occupation operator of orbital a at site i and ϵ_i is the energy shift produced by the *chemical pressure* on the Mn ion at site i. This shift affects equally both e_g orbitals. As discussed above, the *chemical pressure* at site i depends on the ionic radii of the cations surrounding the Mn ion. We assume that the total shift at site i is the sum of the shifts produced by the eight next neighbors cations. Cations with big ionic radius induce a positive energy shift Δ, whereas cations with small ionic radius induce a negative energy shift $-\Delta$. With this, election a Mn ion surrounded by equal number of small and large cations has zero energy shift. The diagonal shift takes values in the range $-8\Delta < \epsilon_i < 8\Delta$. In this description of the cationic disorder the strength of the disorder is defined by the value of Δ.

Entropy and free energy. In order to describe thermal effects we have to compute the free energy. In manganites the Fermi energy of the carriers is much greater than the typical Curie temperature and we only consider the entropy of the classical Mn core spins.

We need to compute the entropy of an isolated spin, J in a magnetic field, h. We know the energy corresponding to each state, so statistical mechanics equations can be directly applied [N.W.Ashcroft 76]:

$$\exp\left(-\beta F\right) = \sum exp(-\beta\gamma h J_z) \tag{4.3}$$

γ is the gyromagnetic ratio, relating angular momentum and magnetic dipole moment, the rest of the notation is well known. Equation 4.3 is just a geometric series which can be easily summed [N.W.Ashcroft 76]:

We go on by applying the thermodynamic definition of magnetization, $m = -(1/\beta)\frac{\partial F}{\partial h}$, and expanding it for small h and m, thus obtaining:

$$m = \frac{1}{3}J(J+1)\beta h + \frac{1}{45}((2J+1)^4 - 1)(\beta h)^3 + O(\beta h)^5 \tag{4.4}$$

This series can be inverted to give h as a function of m. We can then substitute in the result of the sum of equation 4.3, and apply the definition of Free energy:

$$-TS(m) = F(m, h(m)) + mh(m) \tag{4.5}$$

In particular, for $J = 3/2$ the entropy per Mn takes the form,

$$S(m) = \frac{\log 2}{2} - \frac{3}{2}m^2 - \frac{9}{20}m^4 + ... \tag{4.6}$$

where m is the thermal average of the relative magnetization of the Mn core spins.

At finite temperatures the magnetization is not saturated and the spin reduction factor, Eq. (4.2) is smaller than unity. Treating spin fluctuations in the virtual crystal approximation, the spin reduction factor is substituted by its expectation value, which for small magnetization has the form[de Gennes 60],

$$f_{i,j} \simeq f_m = \frac{2}{3} + \frac{2}{5}m^2 - \frac{6}{175}m^4 + ... \tag{4.7}$$

With this the thermal average of the internal energy per Mn ion can be written as,

$$E \;\; = \tfrac{f_m}{N}\left(\sum t^u_{a,b} < c^+_{i,a}c_{j,b} > + \tfrac{1}{f_m}\sum \epsilon_i < \hat{n}_{i,a} >\right) \tag{4.8}$$

being N the number of Mn ions in the system. In Eq. (4.8), it is evident that the relative importance of the disorder term increases when the magnetization, and thus the spin reduction factor, decreases. For small values of Δ, the internal energy can be expanded in powers of the disorder strength. As the mean value of ϵ_i is zero, the first finite term is proportional to the variance, $\sigma^2(\epsilon_i)$, of the diagonal disorder distribution,

$$E = f_m\left(E_0 + a\frac{\sigma^2(\epsilon_i)}{f_m^2}\right) \;\; , \tag{4.9}$$

where $E_0 < 0$ is the kinetic energy per Mn ion in the disorder free FM phase, and

$$\sigma^2(\epsilon_i) = \frac{1}{N}\sum_i {\epsilon_i}^2 \;\; . \tag{4.10}$$

In Eq. (4.9), the coefficient a is negative as electrons prefer to place on sites with negative values of ϵ_i.

Combining Eq. (4.6-4.10), the dependence of the free energy, $F = E - TS$, on the magnetization, can be written as

$$\begin{aligned} F \;\; &= F_0 + \frac{3}{2}Tm^2 + \frac{2}{5}\left(E_0 - \frac{9}{4}\,a\,\sigma^2(\epsilon_i)\right)\, m^2 \\ &+ \frac{9}{20}Tm^4 - \frac{6}{175}\left(E_0 - 18\,a\,\sigma^2(\epsilon_i)\right)\, m^4 \, + ... \end{aligned} \tag{4.11}$$

and the Curie temperature takes the form

$$T_C = -\frac{4}{15}\left(E_0 - \frac{9}{4}\,a\,\sigma^2(\epsilon_i)\right) \;\; , \tag{4.12}$$

where is clear that T_C decreases when the disorder strength increases. The order of the transition can be inferred from the sign of the quartic term in Eq. (4.11). If the quartic term is positive the transition is second order, while a negative quartic term implies the existence of a first order phase transition. Using the previous expression for T_C, a first order transition takes place if,

$$\sigma^2(\epsilon_i) > \frac{1}{18}\frac{E_0}{a}\left(\frac{1+\frac{7}{2}}{1+\frac{7}{16}}\right) \quad . \tag{4.13}$$

Equations (4.12) and (4.13) are the main results of this chapter, they show that the Curie temperature decreases when the strength of the disorder increases, and that for strong enough disorder the FM-PM transition changes from second to first order. Comparing Eq. (4.12) and Eq.(4.13) it results that for changes in the Curie temperature between 30 and 40 per cent, the FM-PM transition transforms from second to first order.

4.3. Numerical results.

In order to check the approximations we have done, and the validity of the results obtained, we diagonalize numerically the FM two orbital DE Hamiltonian, in the presence of diagonal disorder, Eq. (4.1). We consider the case of disorder in the ionic radii of the cations surrounding the Mn ions. As discussed above, this disorder produces a distribution of diagonal energy shifts in the range $-8\Delta < \epsilon_i < 8\Delta$. For a random distribution of the two type of cations, the variance of the diagonal disorder distribution is $\sigma^2(\epsilon_i) = 8\Delta^2$. We have diagonalized the Hamiltonian for different disorder realizations and different values of the disorder strength Δ. In this way we are also taking into account spatial correlations of disorder strength among sites.

We work with a cluster containing 12×12×12 atoms and with periodic boundary conditions. By studying smaller clusters we have checked that our results are free of finite size effects.

In Fig.4.2a we plot, for the full polarized FM phase, the internal energy per Mn ion as function of the disorder strength Δ. As expected[G.D.Mahan 00], for small values of the disorder the internal energy decreases quadratically with Δ. Taking into account the dependence of the internal energy on the spin reduction factor, in mean field approximation the Curie temperature gets the form

$$T_C = -\frac{2}{3}\frac{\partial E}{\partial m^2} \quad . \tag{4.14}$$

In Fig.4.2b, we plot T_C, obtained numerically from the internal energy, as function of Δ. In the disorder free case, $T_C \sim 0.4t$ that compared with the Curie temperature of the ordered $La_{0.5}Ba_{0.5}MnO_3$, T_C=350K, [T.J.Sato 04], implies a value of the hopping amplitude of $t \sim 0.076eV$. For changes up to 30 per cent, we find that the decrease of

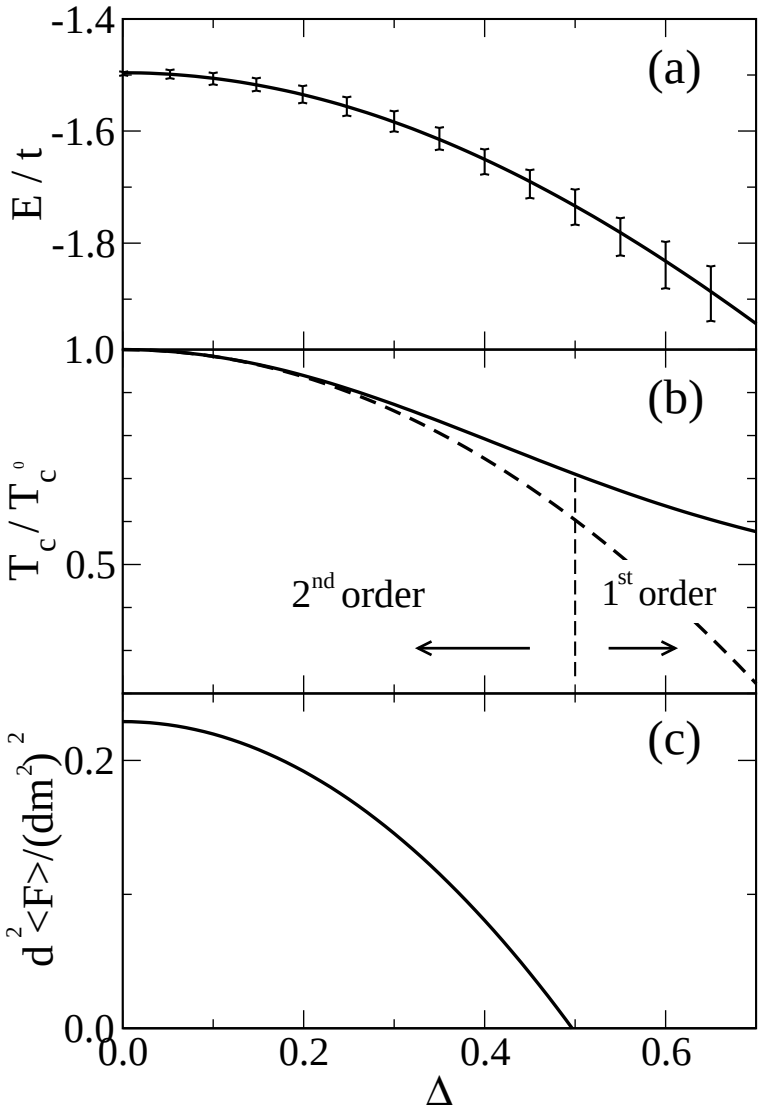

Figure 4.2: Polynomial fit to a) internal energy (Eq. 4.8) and b) Curie temperature as obtained from numerical simulations. Bars in a) indicate the typical indetermination in the numerical calculations. In b) the dashed line corresponds to the quadratic approximation to T_C (Eq. (4.12)). The vertical dashed lines separates regions with first and second order FM-PM transition. c) Shows the quartic coefficient in the expansion of the free energy (Eq. (4.11)) evaluated at the Curie Temperature.

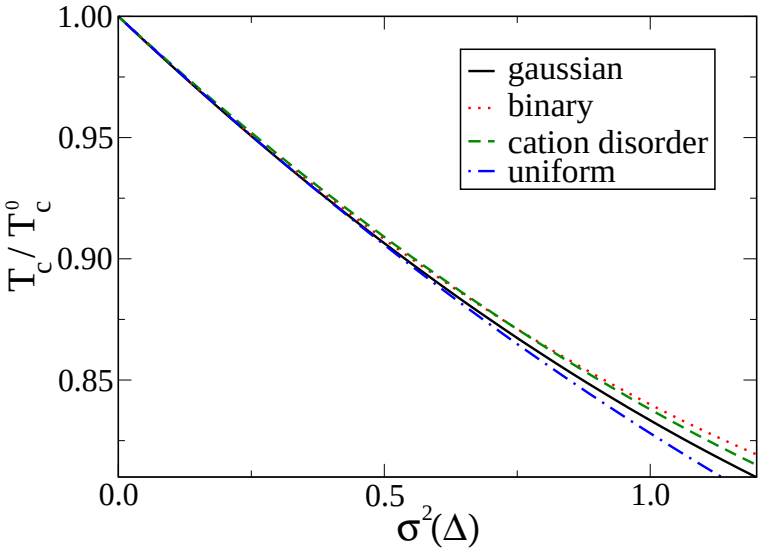

Figure 4.3: Curie temperature versus variance of diagonal disorder for different models of disorder. The different kinds of disorder are explained in the text

T_C with Δ can be fitted very accurately with a quadratic dependence. Experimentally differences in T_C between the ordered and disordered samples in $La_{0.5}Ba_{0.5}MnO_3$ range between 14 per cent [T.J.Sato 04] and 33 per cent [dabrowski 02], therefore we expect that for manganites with atomic radii size disorder, the expressions obtained analytically for T_C, Eq. (4.12), and the order of the transition, Eq. (4.13) should be valid.

In fig.4.2b, we also indicate the disorder strength for which the magnetic transition changes from second to first order. As discussed above, the transition becomes first order for changes in T_C larger than 30-40 per cent. In the case of $La_{0.5}Ba_{0.5}MnO_3$, disorder produces changes in T_C of 15-30 per cent and therefore our results could explain quantitatively the experimentally observed change in the order of the magnetic transition[T.J.Sato 04]. As the critical disorder is close to that found in $La_{0.5}Ba_{0.5}MnO_3$, we expect that in FM manganites with smaller differences in the atomic radii, for example $La_{0.5}Sr_{0.5}MnO_3$ ($r_A = 1.21$ for La^{3+} and $r_A = 1.31$ for Sr^{2+}[Rodriguez-Martinez 96]) the effect of disorder in T_C should be smaller and the magnetic transition should be second order independently of the order in the position of the cations.

Finally we want to check that, as proposed by Rodríguez-Martínez and Attfield[Rodriguez-Martinez 96], the relevant figure for quantifying the disorder is the variance of the disorder distribution. We have repeated the numerical calculation of T_C for different distribution of diagonal disorder. Apart from the *cation disorder* distribution , we have also analyzed a *uniform* distribution of the diagonal energy shift between two values, a *binary* distribution and a *gaussian* distribution of the diagonal disorder.

The results are plotted in Fig.4.3. For all models studied, we find that for moderate disorder strength, the Curie temperature decreases linearly with the variance of the disorder. There are deviations from this dependence in the limit of strong disorder. In

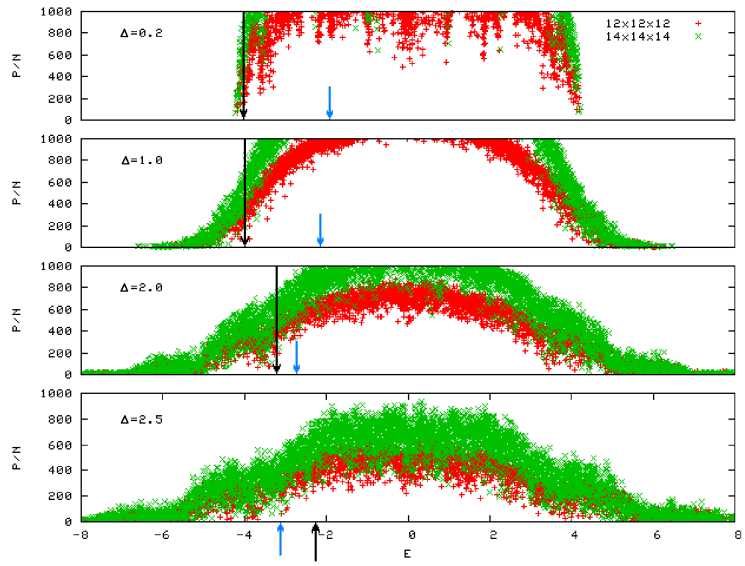

Figure 4.4: Participation number for the different eigen functions of the system as a function of the eigen energies. The position of the Fermi energy (blue arrows) and the approximate position of the mobility edge (black arrows) are shown.

this limit the carriers start to localize in the sites with smaller energy and perturbation theory becomes not valid. This regime is not the relevant one in FM manganites, and the results shown in Fig. 4.3 agree with the experimental results obtained by Rodríguez-Martínez and Attfield[Rodriguez-Martinez 96].

****

In fact, the calculation of the participation number [not] shows that much higher disorder strengths are needed in order to produce an insulator (at half doping) that the ones producing a change in the order of the magnetic transition. Although our calculations are not well refined (a more detailed finite size scaling its needed to find the exact position of the mobility edge), they are sufficient to make a brief quantitative analysis. In fig 4.4 it is shown that a disorder strength of $\Delta \gtrsim 2$ is needed to turn the system into insulator. For the PM phase this would mean $\sigma^2 \approx 75 t_{eff}$. This results are for a two orbitals DE model with *cation* disorder. From the numerical data of Li *et al.* [Li 97] we find that a similar value for a one orbital model with uniform distribution of disorder. We conclude that the influence of disorder in the magnetic properties of FM manganites is not necessarily related to the proximity to the insulating phase, To reproduce this insulating it is needed to consider electron-phonon coupling [Vergés 02, Calderón 99b], that does not play a key role on the materials which present metallic behavior at both sides of the FM-PM transition.

****

The numerical results support our analytic findings. For moderate disorder strength

the variation of the Curie temperature and the order of the transition depend on the variance of the distribution of the diagonal energy shifts in the electronic Hamiltonian.

4.4. Summary

In summary, we have studied a realistic model of manganites by means of exact microscopic calculations and Landau Theory formalism. The different sizes of cations surrounding a manganese ion are included in the model as an energy shift in that manganese site. This model reproduces the experimental results. It explains the observed strong reduction of T_C in disordered samples with respect to ordered ones[T.J.Sato 04]. Moreover, it demonstrates, in agreement with experiments[T.J.Sato 04], that disorder makes the FM-PM transition more abrupt and, for a big enough disorder strength, this transition becomes first order. Finally our formalism identifies in a natural way the variance of the distribution of the diagonal energy shifts as the relevant parameter to characterize changes in the magnetic properties, independently of the model of disorder[Rodriguez-Martinez 96, Fontcuberta 98, Collado 05].

Chapter 5

Heterostructures of Manganites

5.1. Motivation

In previous chapters, we have focused on intrinsic properties of manganites. Even disorder introduced by the random positions of some cations, studied in chapter 4, might be classified as an intrinsic effect. However, not only intrinsic properties of bulk materials are interesting; mutual influence of different compounds and physical behavior at the reduced length scales typical in electronic devices, or interfacial effects are important subjects in applied and basic condensed matter physics. In this chapter we study an example of manganite heterostructure paying close attention to all these issues.

Our aim is encouraged by recent advances in some related systems. New electronic phases appear at the interfaces of strongly correlated systems heterostructures (electronic reconstruction). A high mobility two-dimensional electron gas forms at the interface between a correlated Mott insulator and a band insulator [Okamoto 04, Huijben 06, Kancharla 06]. At the interfaces between ferromagnetic (FM) metallic manganites and insulators, charge, orbital and spin ordered phases [Lin 06, Brey 07] appear. Manganese perovskites are specially important because of their potential application in spintronics [Zutic 04]: in the ferromagnetic phase they are half-metals [Pickett 96, Park 98b] and, therefore, very efficient spin injectors and detectors [Bowen 03, Yamada 04, Bibes 07].

The rest of the chapter is divided as follows. In section 5.2 we discuss recent experiments on manganite heterostructures relevant for our calculations. In Section 5.3 an effective model is discussed; it is also shown that it correctly reproduces the essential features of manganites' phase diagram. The application of this model to heterostructures is the subject of sections 5.4 and 5.5. Section 5.4 is devoted to explore the phase diagram of $La_{2/3}Sr_{1/3}MnO_3$ (LSMO) and $Pr_{2/3}Ca_{1/3}MnO_3$ (PCMO) multilayers of equal thickness. Magnetic and Transport properties of a spin valve are studied in section 5.5. It is also composed of LSMO, which makes up the FM metallic leads, and a thin insulating barrier of PCMO, which turns metallic under certain conditions.

5.2. Experiments In Manganite Heterostructures

Because manganites present a strong coupling between the electric and magnetic properties, these materials are ideal candidates for spintronics applications. The most popular existing spintronic devices are spin valves. A spin valve is a three layered device, with a first FM lead that is used as a spin polarizer, a non-ferromagnetic spacer, and a second FM lead used as spin analyzer. These devices are based in the fact that the electrical resistance of a material connected to spin polarized source and drain, strongly depends on their relative orientation. The efficiency of a spin valve is given by tunneling magnetoresistance (TMR) [Jullière 75], defined as the difference in resistance R between parallel (P) and antiparallel (AP) relative orientations of the magnetization in the FM metallic electrodes [TMR= $(R_{\mathrm{AP}} - R_{\mathrm{P}})/R_{\mathrm{AP}}$].

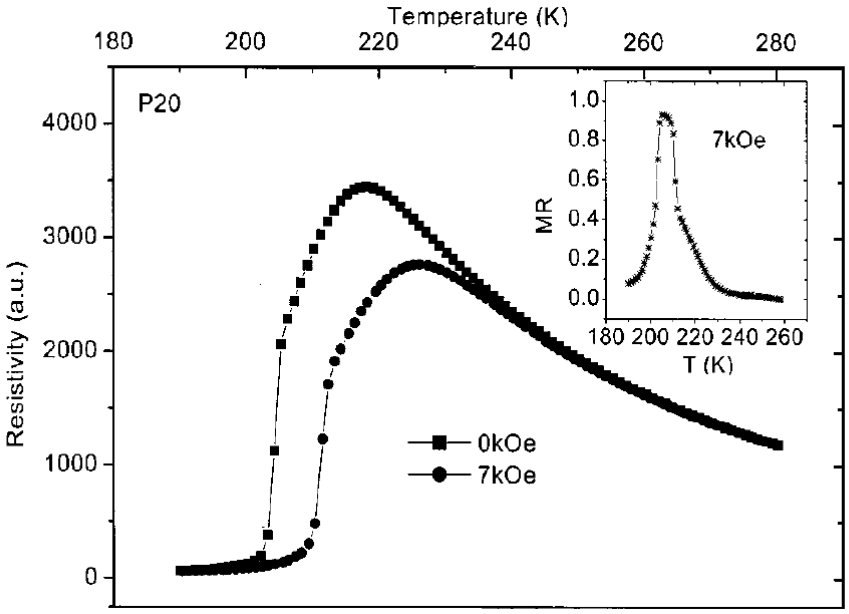

Figure 5.1: Resistivity as a function of temperature for an all-manganite multilayer, according to [Li 02]. The multilayer is composed of alternate layers of 100Å thick LCMO and 20Å thick PCMO. The inset shows MR in a field of 7 kOe as a function of temperature for the same multilayer.

Manganite surfaces are known to behave differently from the bulk, the typical example being the striking suppression of the spin polarization of a free surface at temperatures much lower than the bulk FM T_C [Park 98a, Calderón 99a]. This could have a very negative effect on the efficiency of spin valves because TMR depends very strongly on the properties of the electrode/barrier interface [LeClair 00]. Indeed, early reports of TMR in manganite heterostructures showed a very strong decrease with increasing temperature [Lu 96]. The reduction of the spin polarization at the interface occurs because the

lack of carriers at the interface attenuates the double exchange FM coupling between the Mn ions [Brey 07]. Also strain at the interfaces might lead to a depression of the magnetic properties of the manganite FM layer [Infante 07]. The optimization of structural matching and the use of nonpolar interfaces make possible to achieve spin polarization close to that of the bulk up to higher temperatures [Yamada 04, Garcia 04, Ishii 06], with the concomitant enhancement of TMR. Alternatively, the use of an insulating manganite as a spacer in the spin valve would provide a very good match to the lattice structure of the electrodes and a smoother variation of the carriers density.

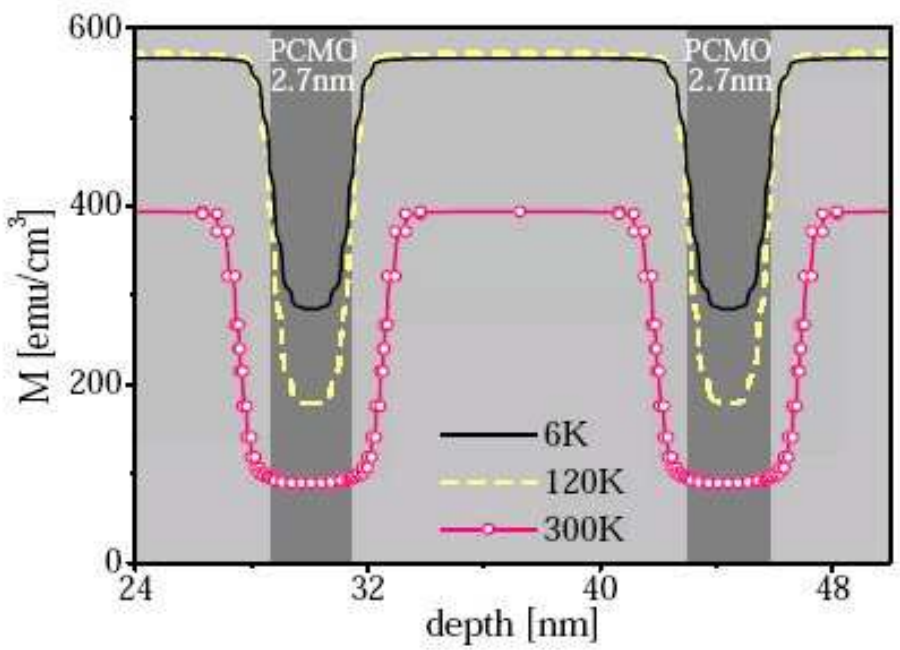

Figure 5.2: Magnetization profile for a multilayer composed of 11.9 nm thick LSMO layers and 2.7 nm thick PCMO layers. The data is obtained by means of Polarized Neutron Reflectometry [Niebieskikwiat 07].

In manganite heterostructures the interfaces play a key role in determining the electric and magnetic properties. In Ref. [Li 02] the authors try to obtain high values of MR by growing multilayers of LCMO and PCMO. For very thin layers of PCMO ($\leq$20Å) separated by thicker layers of LCMO, transport properties present an interesting behavior as a function of temperature (Fig. 5.1). As temperature is lowered, two transitions are found. First, a paramagnetic-ferromagnetic transition takes place, it is accompanied by a change in the slope sign of the resistivity as a function of temperature. This behavior is also observed in pure LCMO, suggesting that LCMO layers order FM at this temperature. In a second transition, magnetization increases and resistivity suddenly drops ($\sim$50% decay in 1K). The authors attribute this drop to the onset of ferromagnetism in all the system. Similar results were obtained in Refs. [Venimadhav 01, Lian 99]. Notice that FM order can be induced in bulk PCMO, but a magnetic field

of 2 Tesla is needed [Dagotto 02]. In LSMO/LCMO based heterostructures, T_C and the range where large MR exists increase with respect to LCMO [Alldredge 04, Jain 06, Mukhopadhyay 06]. Finally, Niebieskikwiat and coworkers [Niebieskikwiat 07] studied, by means of Polarized Neutron Reflectometry, the magnetization profile along the growth direction in a LSMO/PCMO multilayer. They found that a FM moment is induced in the PCMO layers, Fig. 5.2.

5.3. Effective Model for Manganites

We have seen along this thesis that changing the hole doping and/or the size of the ions of the manganites, different electronic and magnetic phases arise (See Figs. 2.1 and 2.5 in chapter 2). In general, Double exchange favors FM correlations, while superexchange tends to produce antiferromagnetic (AF) order. Double exchange efficiency is directly related to the energy gained in the electron transfer among Mn ions (see Introduction), and this obviously depends on bandwidth and number of carriers. But the relative strength of this interactions is very sensitive to many parameters, (which often have subtle influences among themselves) that measure the effects of different degrees of freedom. Electron phonon coupling localizes carriers and makes the hoping of electrons less favorable, disorder produces local distortions which reduce the overlap of the relevant orbitals, again reducing hopping. Departures from the perfect perovskite structure produce a similar effect in the hole material. These factor also influence superexchange interactions.

Besides the issue of the relative strength of the interactions, there is the problem on how the compromise between the two opposite tendencies (FM and AF) leads to a ground state. e_g orbitals that build up the conduction band are anisotropic, with anisotropic overlaps, and their energy is sensitive to the geometry of the environment. This allows symmetry to be broken in many different ways. Here also bandwidth and filling play a crucial role, determining which orbitals are occupied.

Despite the complexity and the numerous parameters playing a role, one might think that once a material is synthesized, the number of carriers, and the ratio between bandwidth and the effective strength of antiferromagnetic interactions determine the magnetic properties of the material. In this spirit, the authors of Ref. [et al. 02] drew an schematic phase diagram (reproduced in Fig. 5.3 b)). A similar approach was used in recent theoretical works. A Double Exchange model with effective antiferromagnetic interactions reproduces the phase diagram of undoped manganites (Chapter 3 and [Salafranca 06b]) , including commensurate-incommensurate phase transitions. In [Brey 07], Brey studied an insulator/manganite heterostructure with analogous model.

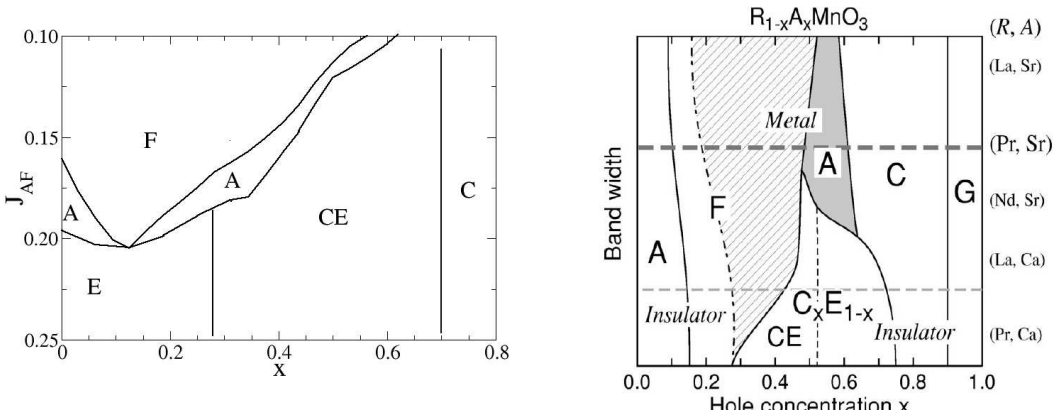

Figure 5.3: a) Phase diagram for homogeneous materials described by Hamiltonian 5.1. F is the ferromagnetic phase, A , E, C and CE antiferromagnetic phases are described in Appendix B. The G-antiferromagnetic phase ((π, π, π) wave vector) is not included. Equivalent phase diagram by Kajimoto and coworkers [et al. 02], it is representative of much experimental work and present understanding of manganites physics.

The Hamiltonian used in this chapter has the following terms.

$$\begin{aligned} H &= -\sum_{i,j,\gamma,\gamma'} f_{i,j} t^u_{\gamma,\gamma'} C^\dagger_{i,\gamma} C_{j,\gamma'} + \sum_{i,j} J^{ij}_{AF} \mathbf{S}_i \mathbf{S}_j \\ &+ U' \sum_i \sum_{\gamma \neq \gamma'} n_{i\gamma} n_{i\gamma'} + H_{\text{Coul}} \end{aligned} \tag{5.1}$$

where $C^\dagger_{i,\gamma}$ creates an electron on the Mn i-site, in the e_g orbital (see Chapter 1) . $\langle n_i \rangle = \sum_\gamma \langle C^\dagger_{i,\gamma} C_{i,\gamma} \rangle$ is the occupation number on the Mn i-site. The hopping amplitude depends on the Mn core spins orientation given by the angles θ and ψ via $f_{i,j} = \cos(\theta_i/2)\cos(\theta_j/2) + \exp[i(\psi_i - \psi_j)]\sin(\theta_i/2)\sin(\theta_j/2)$ (double-exchange mechanism), and on the orbitals involved $t^{\text{x(y)}}_{1,1} = \pm\sqrt{3}\, t^{\text{x(y)}}_{1,2} = \pm\sqrt{3}\, t^{\text{x(y)}}_{2,1} = 3\, t^{\text{x(y)}}_{2,2} = 3/4\, t^{\text{z}}_{2,2} = t$ where the super indices x,y, and z refer to the direction in the lattice. All the parameters are given in units of t which is estimated to be $\sim 0.2 - 0.5$ eV. J_{AF} is an effective antiferromagnetic coupling between first neighbor Mn core spins.

U' is a repulsive interaction between electrons on a site lying on different orbitals, and H_{Coul} is the long range Coulomb interaction between all the charges in the system, treated in the mean-field approximation. It can be ignored for bulk (homogeneous) phases but it is crucial for heterostructures.

$$H_{\text{Coul}} = \frac{e^2}{\epsilon} \sum_{i \neq j} \left(\frac{1}{2} \frac{\langle n_i \rangle \langle n_j \rangle}{|\mathbf{R}_i - \mathbf{R}_j|} + \frac{1}{2} \frac{Z_i Z_j}{|\mathbf{R}^A_i - \mathbf{R}^A_j|} - \frac{Z_i \langle n_j \rangle}{|\mathbf{R}^A_i - \mathbf{R}_j|} \right) \tag{5.2}$$

with $\mathbf{R}_i$ the position of the Mn ions, eZ_i the charge of the A-cation located at $\mathbf{R}_i^A$, and ϵ the dielectric constant of the material. The strength of the Coulomb interaction is given by the dimensionless parameter $\alpha = e^2/a\epsilon t$ [Lin 06].

The electron-lattice interaction has not been explicitely included in the Hamiltonian (5.1). However, the effect of this coupling on the ground state energies can be described using an effective J_{AF} [van den Brink 99b]. In particular, the ground state of Hamiltonian (5.1) for a bulk system with $J_{AF} \gtrsim 0.2t$ is the CE-type AF ordering associated to the lattice distortions that produce the charge and orbital ordering illustrated in Fig. 5.7. The values for J_{AF} that effectively include the electron-lattice coupling are therefore larger than the ones inferred from the magnetic ordering only (J_{AF}^S from superexchange between the t_{2g} electrons is $\sim 1 - 10$ meV) [Dagotto 02].

By choosing constant J_{AF}, we can calculate the energy of the different bulk phases. In fact, this model reproduces the phase diagram of [et al. 02] surprisingly well (see Fig. 5.3 b)). From the comparison of the two phase diagrams, it is possible to get an estimation of the appropriate values of the effective antiferromagnetic coupling for the different compounds.

We shall use this model to study magnetic and transport properties of heterostructures in this chapter. In order to simulate the different materials composing the heterostructures, different values of J_{AF} are used for the corresponding regions of the system. In order to make a realistic description of the interface, we consider an average J_{AF} for Mn ions at the interface. The Hamiltonian is solved self-consistently for the different heterostructures described below.

5.4. LSMO//PCMO Multilayers

Experiments discussed in section 5.2 demonstrate that the magnetic ordering of a material is strongly influenced by the boundary conditions: whether it is found in bulk, thin film, or in a multilayer under the influence of a neighboring material. Here we explore the phase diagram of multilayers composed of two manganites with similar composition and very different magnetic and electronic properties.

In particular, we study a multilayer system composed of layers of LSMO and PCMO of six unit cells thickness. The emphasis is made on relative stability of the FM and CE magnetic orders, that are found in these compounds in their bulk form. The main results of this section are: i) Charge transfer between compounds greatly influences the magnetic phase diagram. In order to obtain a realistic and physically coherent charge profile, Coulomb interaction must be taken into account. ii) Due to the particular density of states of the CE phase, Fig.5.4, the FM phase is more stable. For a significant range of parameters characterizing the two materials, FM correlations are induced in the PCMO layers close to the interfaces.

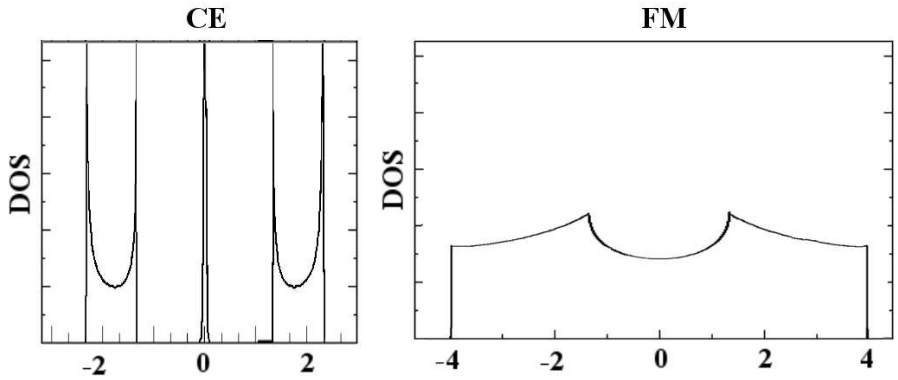

Figure 5.4: Density of states (DOS) for the FM and CE orderings considered. The lower energy gap in the CE phase corresponds to an x=0.5 filling, as shown in Fig. 5.3, experimentally, it is observed that the CE phase is most stable at this band filling.

These main results are summarized in Fig. 5.5. For simplicity only some particular configurations are included: the obvious magnetic configuration as inferred from bulk phase diagram, in which LSMO is in the FM state and PCMO presents CE order (labeled I in Fig. 5.5); and slight variations on this, configuration II where FM order extends to the Mn ions in PCMO next to the interface, and configuration III where all the Mn ions in PCMO and those in LSMO next to the interface are CE ordered. Other configurations in which all the system is in the FM or CE state are stable for some range of parameters but are not included in Fig. 5.5 for the sake of simplicity.

This way we investigate mutual influence of the two magnetic orderings, whether FM correlations are induced in PCMO, it is energetically more favorable to have CE ordering in the region of LSMO or none of these effects take place. Each material is described by an effective value of J_{AF} as explained in previous sections. J_{AF} for PCMO is labeled J_{PC}, and the corresponding values are in the vertical axis, while J_{LS} are the J_{AF} values for LSMO and are plotted on the horizontal axis in Fig. 5.5. Notice that the bulk phase diagram, Fig. 5.3, and the fact that bulk PCMO is CE ordered imply that J_{PC} is larger that the critical value separating CE and FM phase, $J_{PC} \gtrsim 0.18$, equivalently $J_{LS} < 0.18$. A slightly wider range of values have been included in Fig. 5.5 so that the correct limiting behaviours are included.

The phase diagram for a model with no long range Coulomb interaction is drawn in Fig 5.5 b). As one could naively expect, the larger region in of the phase diagram recovers the bulk ordering FM for LSMO and CE for PCMO (region I). FM correlations appear in PCMO (region II) only for very low values of J_{PC}, that are not appropiate to describe this material. A similar situation appears when looking for the range of parameters where CE ordering is induced in LSMO (region III), the values of J_{PC} are larger than expected for a FM metallic material. The magnetic ordering in the absence of long range Coulomb interaction is solid and corresponds to a configuration in which each

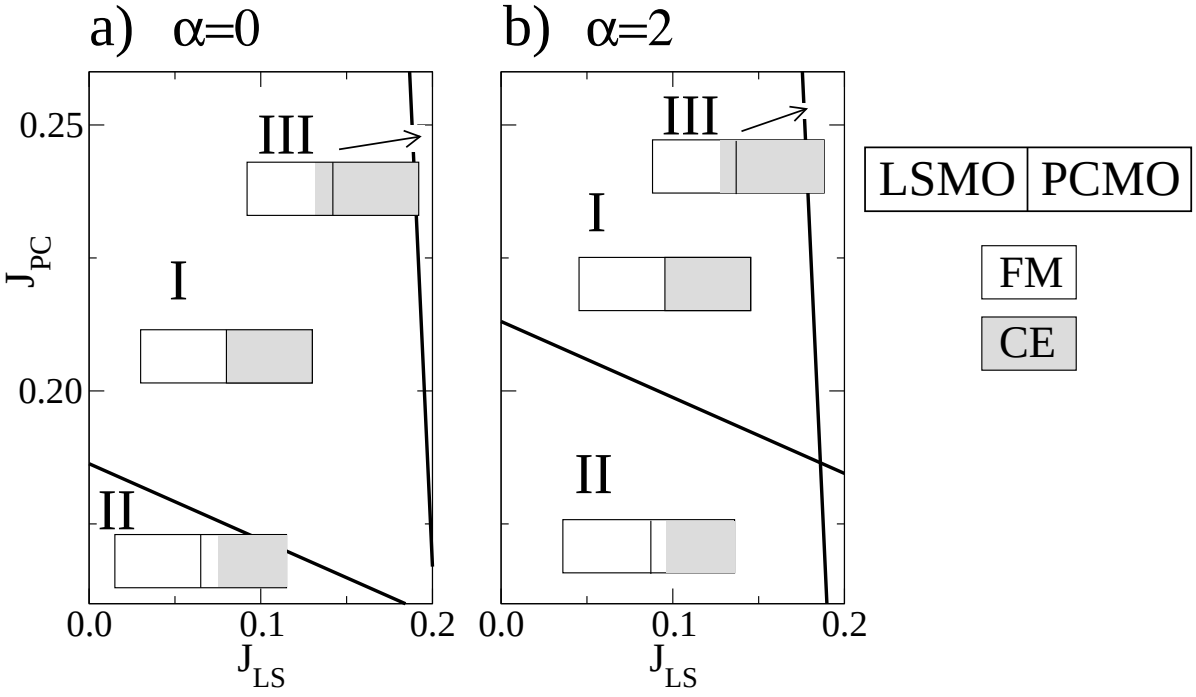

Figure 5.5: Phase Diagram of a manganite multilayer composed by LSMO and PCMO layers 6 unit cell thick. The horizontal and vertical axis correspond to the strength of the effective antiferomagnetic coupling in the layers. α measures the strength of the Coulomb interaction. a) Without considering Coulomb interaction, and b) for a realistic value of Coulomb interactions. An scheme of the different configurations considered in the phase diagram is shown, the shadowed area corresponds to CE order, while un-shadowed area corresponds to FM order. Configurtaion I therfore corressponds to LSMO and PCMO in their bulk magnetic ordering (6 u.c. FM and 6 u.c. CE), configuration II correponds to FM ordering in Mn ions of PCMO next to the interface (8 u.c. FM and 4 u.c. CE), and configuration III correponds to CE ordering in Mn ions of LSMO next to the interface (4 u.c. FM and 8 u.c. CE). Precise definitions of the parameters and the magnetic orderings are given in the text.

material is ordered with the same magnetic ordering it presents in bulk. However, a closer look at the charge density profile (top panel of Fig. 5.6, only the most relvant configurations, I and II, are included) reveals that the situation is similar to the phase separation discussed in Ref. [van den Brink 99b]. Due to the existance of a Gap at x=0.5 for the CE phase, (Fig. 5.4) there exists a phase separated state in the double exchange model for a wide range of dopings. This phase separtion includes a CE phase with electron density n=0.5 and a FM phase with a higher electron density. We see that the situation is quite similar in the multilayer. Top panel of Fig. 5.6 shows that charge in the CE region is actually 0.5 electrons per Mn except in the layers next to the interface.

In fact, the heterostructured nature of the system is providing an ideal framework for phase separation to take place, since we have regions (PCMO layers) more favorable for the CE phase and regions more favorable for the FM pahse.

It has been argued [Dagotto 02] that phase separation scenario does not survive the consideration of long range Coulomb interaction. For our particular problem, Coulomb significantly alters the magnetic phase diagram, Fig. 5.5, left panel. The relative stablility of Configuration II (FM correlations within PCMO) is greatly enhanced. Again, a physical interpretation can be made in terms of charge transfer. Charge profile in configuration I (Fig. 5.6, botton) shows that, although Coulomb repulsion greatly moderates charge transfer, electronic density in the FM phase is greater that in the CE phase. A charge dipole is created at the interface, some excess of (negative) charge exists in the FM region close to the interface, this excess decays to the bulk value with a decay lenth of around three unit cells. Equivalently the CE phase is electron deficient near the interfaces. Let us recall the different density of states of the two phases. The existence of a gap in the CE phases, implies that much energy is gained if electrons are transfered to the FM phase, while the energy of the FM phase depends little on the electronic density. When J_{Pc} is small enough (although still adecuate for PCMO) a better energy balance can be reached by switching from configuration I to configuration II. The spins of Mn in PCMO nest to the interface order ferromagnetically. The dipole then moves with the magnetic interface, and this way the proportions of Mn ions in the CE phase and *low chrage* increases (low charge means less than the bulk value of 2/3 and closer to the ideal value of 1/2). This effect is more important in thin layers because electron poor regions, of characteristic lenth of 3 or 4 lattice parameters, overlap, as it can be observed in Fig. 5.6 b). The aditional effect of the energy gain due to further delocalization of carriers in the bigger FM region of configuration II (as compared to confioguration I) is much smaller as it is unobservable in the absence of Coulomb interactions.

5.5. All Manganite Spin Valve

In this section we study a spin valve where the barrier is an AF insulating manganite and analyze the charge distribution, magnetic ordering, and the interplay of the different orders in the different layers. In particular, calculations are performed in the trilayer $La_{2/3}Sr_{1/3}MnO_3/Pr_{2/3}Ca_{1/3}MnO_3/La_{2/3}Sr_{1/3}MnO_3$ illustrated in Fig. 5.7 (multilayers with the same composition were experimentally studied in [Niebieskikwiat 07]). Our main results are: i) a FM moment is induced in the PCMO layer in accordance with [Niebieskikwiat 07], ii) the ground state configuration in the PCMO layer depends on the relative orientation of the magnetization in the LSMO layers and, as a consequence, the system shows a large TMR (see Fig. 5.5), iii) in the P configuration, the application of an external magnetic field affects the PCMO layer magnetic ordering giving rise to negative MR (see Fig. 5.5). In general, we find that the itinerant carriers in the leads try to minimize their kinetic energy penetrating into the insulating spacer. This enhances

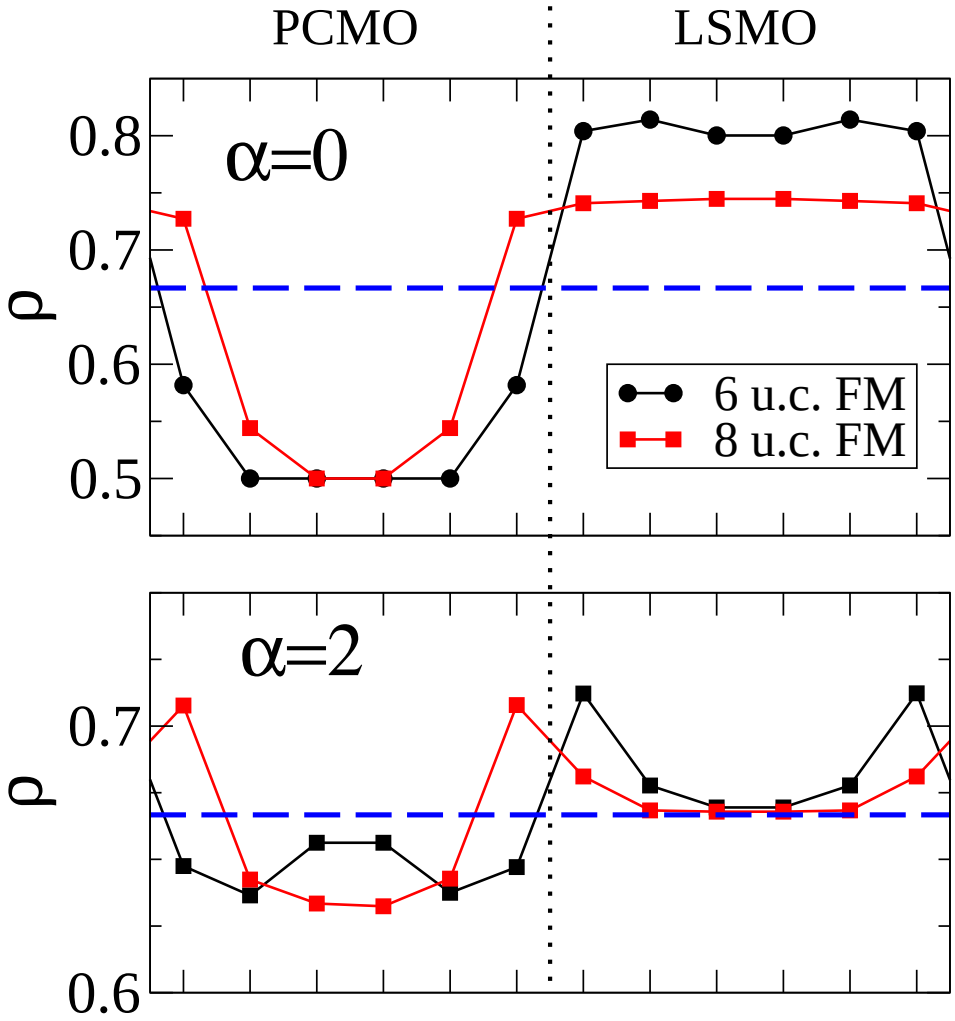

Figure 5.6: Charge distribution for the multilayer consisting in 6 u.c. thick LSMO layers and 6 u.c. thick PCMO layers. Average charge in the different Mn sheets is shown only for the two most stable phases of Fig. 5.5. In the absence (α=0, top panel), and with a realistic strentgth of Coulomb ionteraction (α=2, botton panel). The average electronic charge is shown with a dashed line, it coincides with the background charge arising from divalent and trivalent cations. Notice the different scale in the top and botton panels.

the FM double exchange mechanism in the first layers of the manganite barrier and produces an effectively thinner insulating barrier.

We address these issues by finding the minimal energy spin, charge and orbital configuration in a very thin PCMO spacer [two (PCMO-2) to three (PCMO-3) lattice parameters, a, wide] between two wider and perfectly ferromagnetic LSMO layers. The tight-binding Hamiltonian is described in section 5.3

In Fig. 5.8 we show the total energy versus J_{PCMO} for a pure FM, CE and an inter-

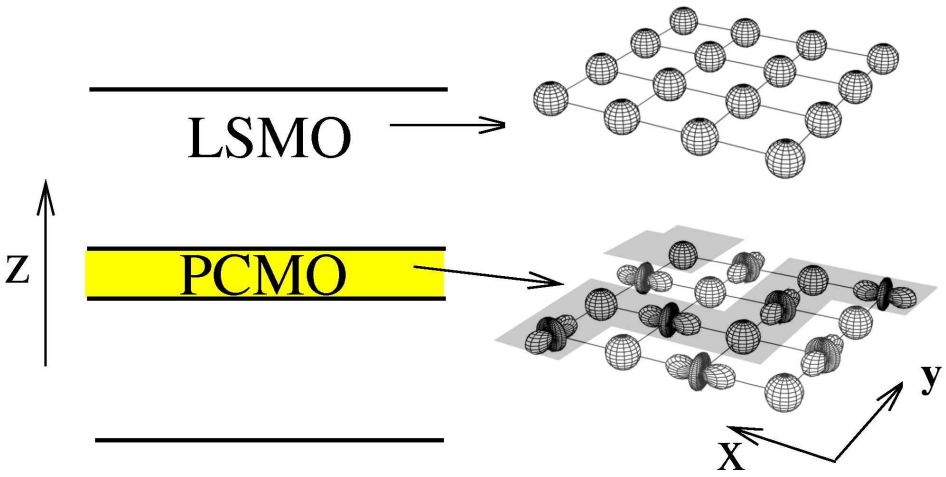

Figure 5.7: Schematic view of the heterostructure under consideration. LSMO stands for $La_{2/3}Sr_{1/3}MnO_3$ and PCMO for $Pr_{2/3}Ca_{1/3}MnO_3$. At this doping ($x = 1/3$), bulk LSMO is FM and metallic, and bulk PCMO is CE-type AF, with FM zig-zag chains in the xy-plane antiferromagnetically coupled to neighboring chains, orbital/charge-ordered and insulating.

mediate *canted* configuration of the PCMO-2 layer for P and AP configurations of the electrodes. All the other magnetic orderings considered were higher in energy in this range of parameters. For $0.17\,t < J_{\rm PCMO} < 0.3\,t$, the magnetic ground state configuration in the spacer is always canted with the canting angle depending on the value of $J_{\rm PCMO}$ and on the relative orientation of the magnetization in the LSMO layers. In the P configuration [Fig. 5.8(a)], PCMO tends to order more FM and collinearly with the electrodes, while for the AP case [Fig. 5.8(b)], the PCMO configuration corresponds to smaller magnetization and the spins lie perpendicular to the electrodes magnetization. The results for PCMO-3 (not shown) are qualitatively similar.

For PCMO-2 and $J_{\rm PCMO}$ relatively small ($\lesssim 0.24\,t$), the magnetic order at the barrier is canted, and the charge/orbital order is mostly suppressed due to charge transfer between the layers. FM correlations and, due to double exchange, conductance are larger in the P configuration than in the AP configuration. Therefore, this geometry could be used as a magnetic sensor. The conductance has been calculated numerically via Kubo formula [Mayr 01, Calderón 99b] for a trilayer with semi-infinite FM LSMO leads. The results for a PCMO-2 spacer are plotted in Fig. 5.5 (a) where a finite TMR for $J_{\rm PCMO} \lesssim 0.24\,t$ is shown. The superstructure in the curve is due to numerical inaccuracies except for the peak at $J_{\rm PCMO} \sim 0.17\,t$, which is quite robust (the TMR increases monotonically in the range $0.1\,t < J_{\rm PCMO} \lesssim 0.17\,t$). This peak appears because, below $\sim 0.17\,t$, the P ground state configuration is almost FM [Fig. 5.8 (a)] while the AP configuration is already canted [Fig. 5.8 (b)] and, as a consequence, $R_{\rm AP}$ increases faster with $J_{\rm PCMO}$ than $R_{\rm P}$.

For PCMO-3 there is a range of parameters, $0.22\,t \leq J_{\rm PCMO} \leq 0.24\,t$, for which the TMR

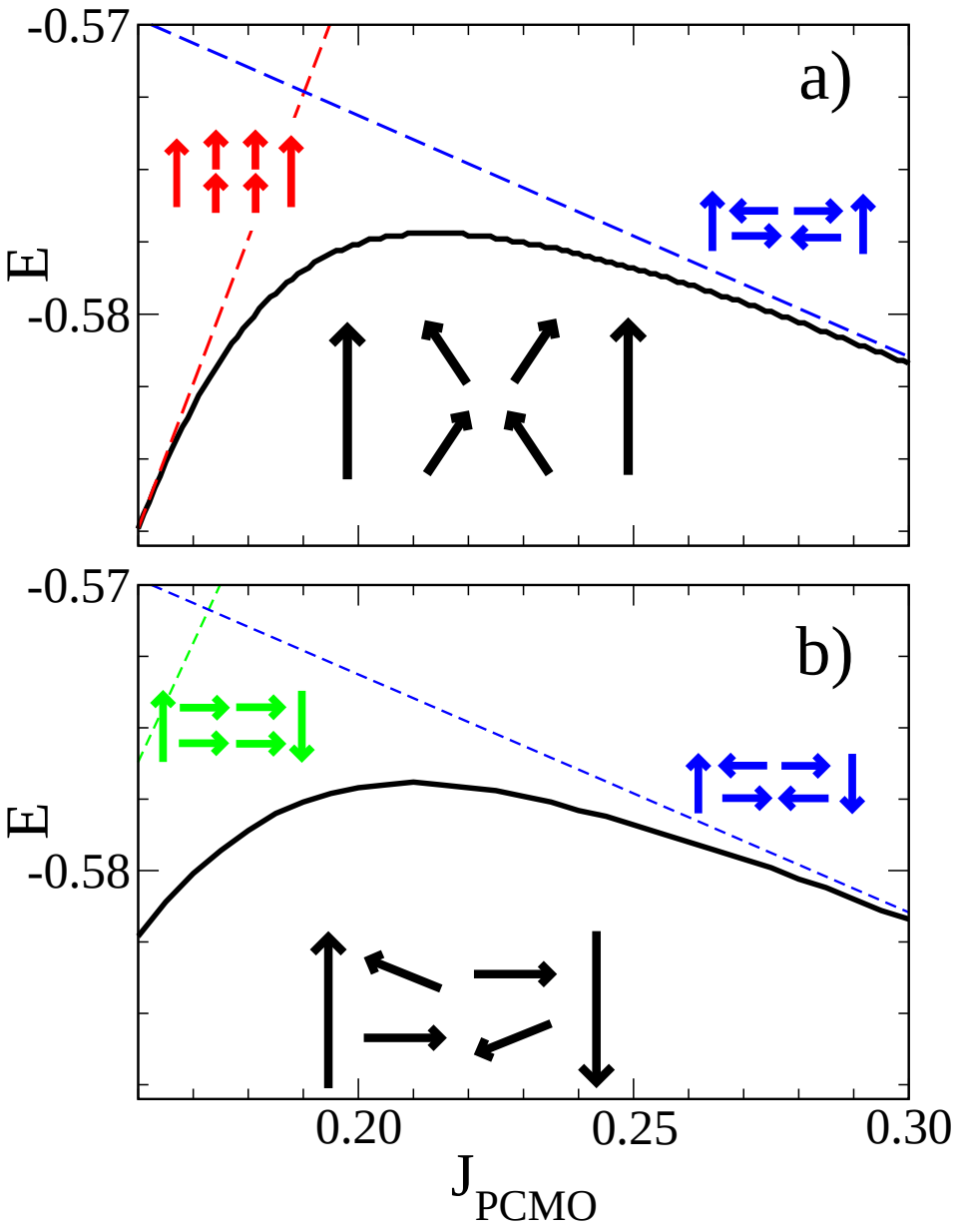

Figure 5.8: Energy versus J_{PCMO} for a parallel (a) and antiparallel (b) configuration of the LSMO layers, with PCMO thickness of two lattice parameters, PCMO-2. The dashed lines are the energy for the pure FM and pure CE configurations in the intermediate PCMO layer. The actual ground state (solid line) corresponds to canted intermediate configurations (illustrated in the insets). The big arrows represent the magnetization orientation in the FM layers and the small ones represent the order considered in the PCMO-2 layer. In the CE and canted phases each arrow in the PCMO layer represents a FM zig-zag chain (see Fig. 5.7).

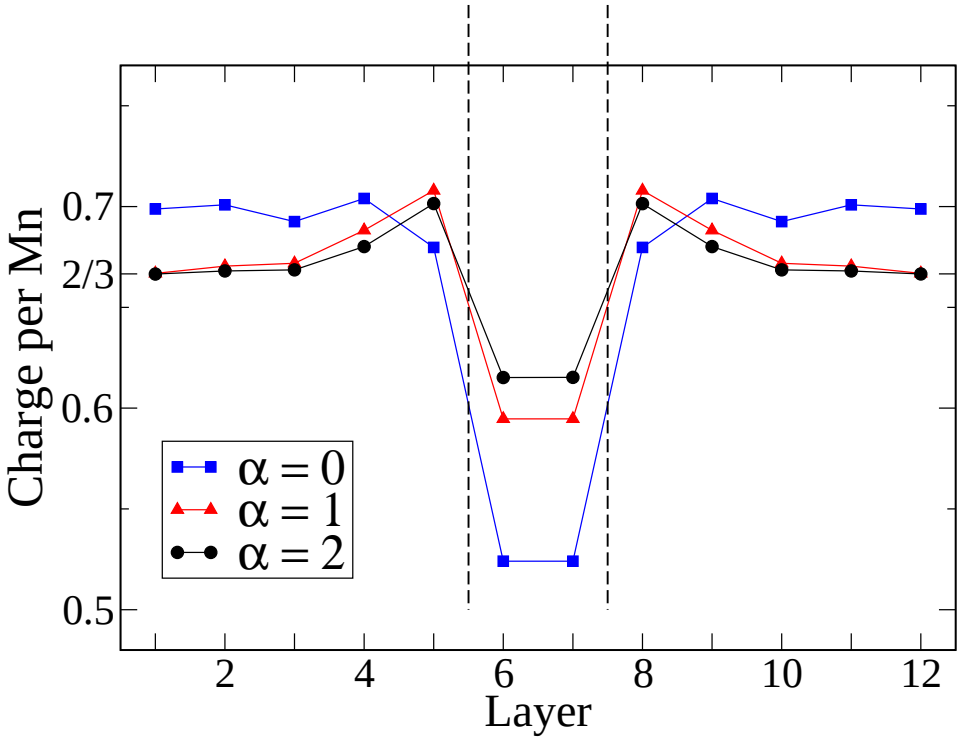

Figure 5.9: Charge distribution for a trilayer illustrated in Fig. 5.7 with a PCMO layer two unit cells thick for different strengths of the Coulomb interaction. Notice that charge prefers the ferromagnetic layer due to the lower chemical potential of this phase and how a surface dipole is formed when Coulomb interaction is taken into account. In this latter case, bulk charge density of 2/3 is recovered in LSMO after a decay length of about 3 unit cells

is close to its maximum possible value of 100%. In this range, the P configuration is metallic as it has a relatively large FM component in the three Mn planes that constitute the barrier, while the AP configuration is insulating and corresponds to perfect CE in the middle atomic plane and canted FM in the outer planes. For smaller values of $J_{\rm PCMO}$ ($\leq 0.2\,t$), for both the P and AP configurations, the middle plane is a perfect CE while the outer planes are essentially FM and parallel to the nearest electrode; this leads to $R_{\rm P} = R_{\rm AP}$ and, hence, TMR= 0. The negative TMR at $J_{\rm PCMO} \sim 0.22\,t$ is produced by the different dependence of the canting angle on $J_{\rm PCMO}$ for P and AP configurations. The different behavior of the TMR in PCMO-2 and PCMO-3 is due to the limited charge transfer in the middle Mn plane of the wider barrier. For large $J_{\rm PCMO}$ ($> 0.24\,t$), see Figs. 5.5 (a) and (b) the AF ordering in the barrier is preserved and the system does not show TMR at all: both $R_{\rm P}$ and $R_{\rm AP}$ are strictly 0. A systematic analysis for wider barriers is out of our computational capabilities. The calculations indicate that the penetration of the wave functions of the FM leads into the insulating barrier is always limited to the first two or three layers, and therefore these results suggest that significant values of TMR are either absent or appear in a narrow range of parameters for barriers

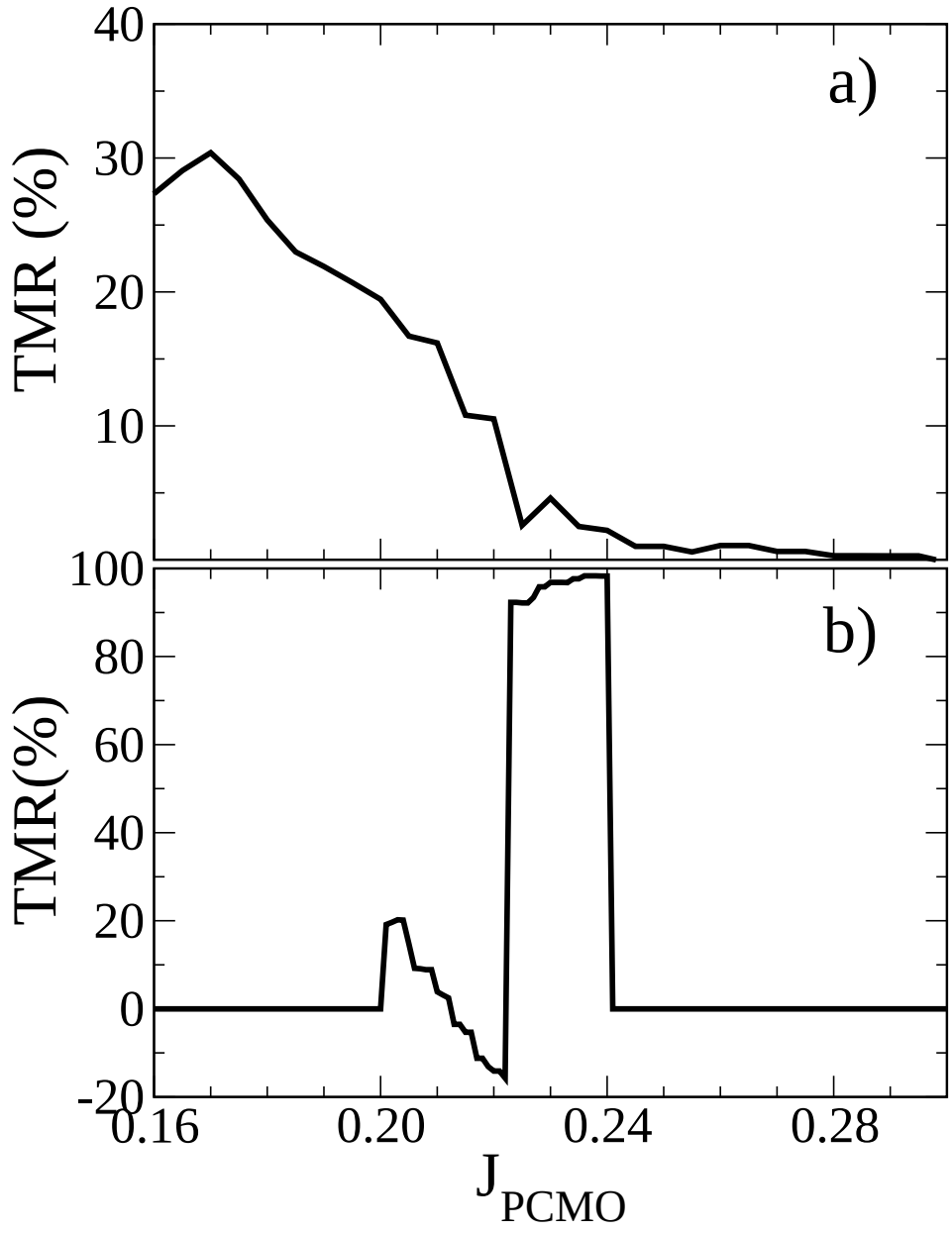

Figure 5.10: Tunneling magnetoresistance versus J_{PCMO} calculated for PCMO layer thicknesses of two (a) and three (b) lattice parameters. For large values of J_{PCMO}, the TMR is very small because the PCMO spacer is AF and insulating for both P and AP configurations. For $J_{\mathrm{PCMO}} < 0.24\,t$ (a) and (b) show different qualitative behaviors (see text for discussion). The maximum sensitivity to magnetization is reached in PCMO-3 for $0.22\,t < J_{\mathrm{PCMO}} < 0.24\,t$ where the system is metallic in the P configuration while insulating in the AP configuration.

thicker than three atomic layers.

We have also calculated the MR in the P configuration that results of applying an external magnetic field parallel to the magnetization in the electrodes. The results are shown for PCMO-2 and PCMO-3 in Fig. 5.5. We define MR= $(R(H) - R(0))/R(0) \times 100\%$ so its maximum possible absolute value is MR= 100%. The dots represent the numerical values and the steps are an artifice of the calculation that considers a discrete set of values of the canting angle. The lines are a fit to the data. When a magnetic field H is applied, the system is effectively moving towards smaller values of J_{PCMO} (see Fig. 5.8) and therefore towards less resistive configurations, hence the negative MR. This MR is produced by the alignment of the barrier spins with the applied field and is smaller than the CMR measured in bulk PCMO [Anane 99] which is probably related to inhomogeneities and phase separation. The real advantage of this heterostructure as a device is that its resistivity can be orders of magnitude smaller than the bulk PCMO's (mainly because there is no gap at the Fermi energy for the thin spacers in the P configuration). As a guideline, the resistivity of bulk LSMO at low T is $\sim 10^{-4}\,\Omega$.cm [A.Urushibara 95], much smaller than that of bulk PCMO $\gtrsim 10^{5}\,\Omega$.cm ($\sim 10^{-3}\,\Omega$.cm at 7 T) [Yoshizawa 96]. These results agree with the experimental work presented in ref [Li 02]. For LCMO(100Å)/PCMO(15Å) multilayers, they find that metalicity is induced in PCMO at low temperatures. The behavior of resistivity versus temperature also agrees with the results in Fig.5.8. As T is raised, spin disorder reduces the effective hopping, and the relative strength of the superexchange interaction, J_{PCMO}, increases. This explains the experimental observation that ferromagnetic correlations in PCMO are lost with increasing temperature [Li 02, Venimadhav 01].

It is well known that strain (produced by lattice mismatch between the substrate and the thin films) can affect the orbital ordering [Y.Tokura 00]. In heterostructures with an STO substrate [Niebieskikwiat 07] the in-plane lattice parameter is 3.90Å for all layers while the out-of-plane lattice parameters are 3.85Å (LSMO) and 3.76Å (PCMO), slightly smaller (less than a 2% in any case) than the bulk values. Our calculations are done in a cubic lattice but the variations in unit cell dimensions in actual heterostructures [Niebieskikwiat 07] are not expected to produce a dramatical change in the orbital ordering [Y.Tokura 00]. In any case it would emphasize the tendency to CE ordering in the PCMO barrier that can be included in our model simply by increasing the value of J_{PCMO}. Strain can also produce phase separation [Infante 07] and colossal magnetoresistance [K.H.Ahn 04]. The inclusion of phase separation in our model would lead to an increase of both TMR (Fig. 5.5) and MR (Fig. 5.5) with respect to the calculated values.

In conclusion, we study an all manganite trilayer. It is composed of two ferromagnetic metallic manganite electrodes ($La_{2/3}Sr_{1/3}MnO_3$) and a thin AF manganite barrier ($Pr_{2/3}Ca_{1/3}MnO_3$). Both materials have, *a priori*, suitable properties for an efficient spin valve device. LSMO is half metallic and it has relatively low resistivity. PCMO growths in the same crystal structure as LSMO, and with a very similar lattice parameter. We find that the spin valve presents high values of TMR. The ground state configuration in

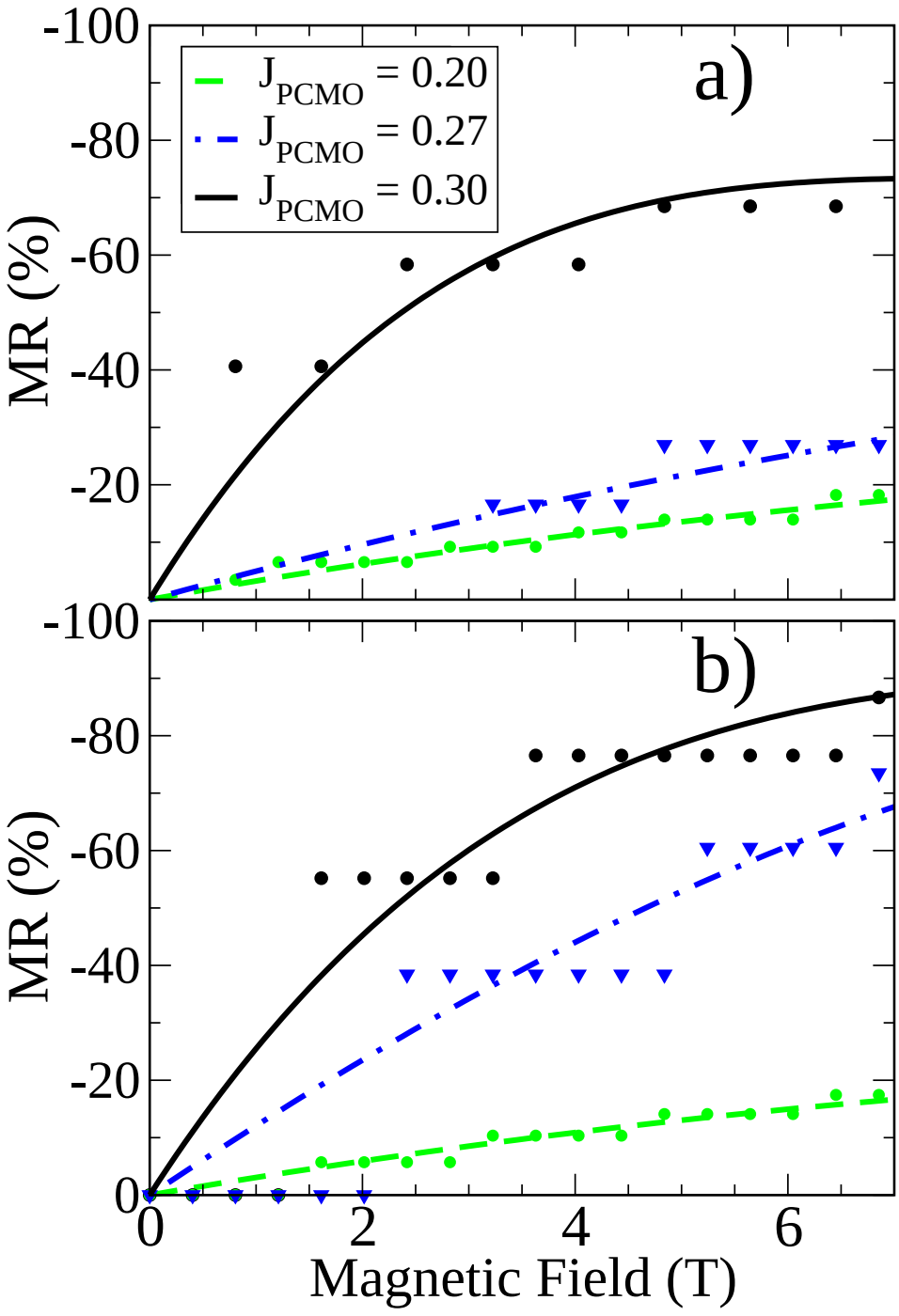

Figure 5.11: Magnetoresistance in the parallel configuration upon application of a small magnetic field in the x-direction for three different values of J_{PCMO} (a) PCMO-2 and (b) PCMO-3. $t = 0.25$ eV is used for the estimation of the magnetic field H. The lines are fits to the dots.

the PCMO layer depends on the relative orientation of the magnetization in the FM electrodes. For a relevant range of parameters the electronic state of the PCMO slab in the parallel configuration is metallic whereas it is insulating in the antiparallel arrangement. Therefore it might be possible to reversibly switch the system between a metallic and insulating state. We also find that, due to the coupling of the electrical and magnetic properties, the resistance of the heterostructure depends on an applied field, presenting large negative magnetoresistance. These effects are manifestations of the enhancement of double exchange effects in the AF slab due to the presence of the neighbors FM slabs. This mechanism explains some experimental observations in manganite multilayers: the onset of a metallic state [Li 02, Venimadhav 01], reduction of resistivity and increase of magnetoresistance [Lian 99, Alldredge 04, Jain 06, Mukhopadhyay 06].

In Fig. 5.8 we show the total energy versus J_{PCMO} for a pure FM, CE and an intermediate *canted* configuration of the PCMO-2 layer for P and AP configurations of the electrodes. All the other magnetic orderings considered were higher in energy in this range of parameters. For $0.17\,t < J_{\mathrm{PCMO}} < 0.3\,t$, the magnetic ground state configuration in the spacer is always canted with the canting angle depending on the value of J_{PCMO} and on the relative orientation of the magnetization in the LSMO layers. In the P configuration [Fig. 5.8(a)], PCMO tends to order more FM and collinearly with the electrodes, while for the AP case [Fig. 5.8(b)], the PCMO configuration corresponds to smaller magnetization and the spins lie perpendicular to the electrodes magnetization. The results for PCMO-3 (not shown) are qualitatively similar.

Appendix A

Conductance

The standard approach to calculate the conductance of microscopic systems is the Kubo formula:

$$G = -e^2 h\pi \lim_{\omega \to 0} \sum_{\alpha,\beta} | < \alpha|\hat{v}_x|\beta > |^2 \times \frac{f_\alpha - f_\beta}{\epsilon_\alpha - \epsilon_\beta} \delta\left(\epsilon_\beta - \epsilon_\alpha - \hbar\omega\right) \tag{A.1}$$

Kubo formula gives the coefficient of the linear system's response to an electric field. It can be obtained by first order perturbation theory. Details about the derivation can be found in [Datta 97]. As pointed out by Vergés [Vergés 99b], for finite size systems, numerical troubles arise with the use Eq.A.1 since the conductivity is obtained as a sum of delta functions. Avoiding them with different averaging procedures distorts the calculation of the static conductance. An alternative approach is a calculation based on the Green function of the system ($\widehat{G}$) [Fisher 68]. The equivalent to Eq. A.1 then reads [Datta 97, Vergés 99b]:

$$G = 2\left(\frac{e^2}{h}\right) \mathrm{Tr}\left[(i\hbar\hat{v}_x)\widehat{G}(E)(i\hbar\hat{v}_x)\widehat{G}(E)\right], \tag{A.2}$$

where the velocity operator is defined in terms of the current:

$$i\hbar\hat{I} = -ei\hbar\hat{v}_x. \tag{A.3}$$

A very similar problem was already addressed in Ref. [Vergés 99b]. In particular, the implementation there was restricted to a one orbital per site system in two dimensions within tight binding approximation. Here, we describe a straight-forward generalization for the case of any orbitals per site and three dimensions, and apply a more sophisticated and efficient method for the self-consistent calculation of the Green functions. For this last purpose we use a decimation technique like the one reported in [Guinea 83] in the context of surface physics.

The main computational problem is to calculate the Green function of the system at the Fermi energy. Normally, the system of interest can be described by a finite Hamiltonian. One might assume perfectly metallic leads and use an appropriate analytical expression for a one band metal [Vergés 99b]. However, when the nature of the leads, or the matching between leads and system, plays a role, it might be more convenient to obtain

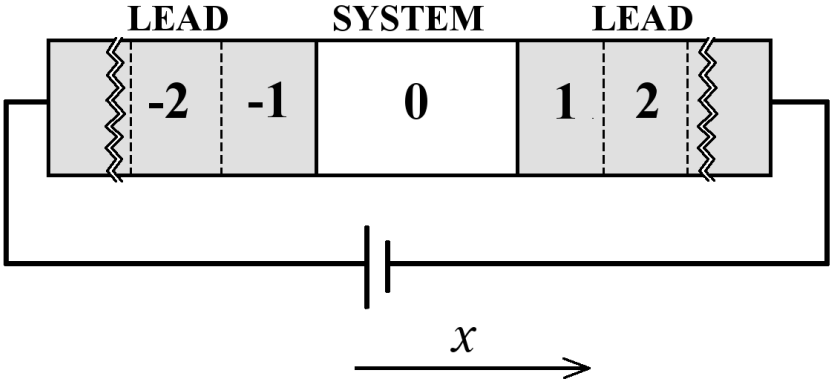

Figure A.1: Scheme illustrating the physical situation and notation. The conductance, G, of a finite system attached to semi infinity leads is calculated. The leads are assumed to be periodic in the direction of the current; they can be built up with some primitive cell labeled with positive numbers for the right lead and negative for the left lead.

the Green function numerically. This Appendix explains an efficient method to calculate the conductance of a physical system based on the Kubo formula and a rapid converging method to calculate the Green function. The rest of the calculation

We will go over this problem in a quite general way. A system, described by a finite Hamiltonian matrix, is attached to two leads (labeled left and right lead). The layers will be considered semi-infinite in a sense that will be clear below. It is worth to remark some particular cases, relevant for this thesis. In chapter 2, the interest is focused in the intrinsic conductivity of manganites, in particular, Kubo formula is utilized to calculate the conductance for a double exchange model with certain spin and octahedra distortions configurations. The algorithm explained here is applied with the peculiarity that the leads are built up with identical copies of the system (in Fig.A.1, $-1 \equiv 0 \equiv 1$). In chapter 5, we are interested in the conductance of a thin layer grown between two wider metallic layers, that act as electrodes. In principle the system there would be effectively infinite as the calculation includes the particular nature of the electrodes. We then redefine system as the insulating layer and some unit cells of the metallic layers , while other big enough portion of the metallic layers is repeated to build up what is called leads in Fig. A.1.

A typical situation is illustrated in Fig. A.1. x is taken as the direction of the current. The leads are in principle infinite in that direction. Therefore, they cannot be described by with a tight-binding approach. Assuming homogeneous and periodic leads, they can be constructed by repeating a primitive cell (each of the -1, -2... *boxes* in Fig. A.1 make up the left lead and 1, 2... make up the right lead). This situation is described by a Hamiltonian of the complete system (system + leads) which will have the following

structure :

$$\widehat{H} = \left(\begin{array}{c|c|c|c|c} \dots & \dots & 0 & & \\ \hline \dots & H_{-1\,-1} & H_{-1\,0} & 0 & \\ \hline 0 & H_{0\,-1} & H_{0\,0} & H_{0\,1} & 0 \\ \hline & 0 & H_{1\,0} & H_{1\,1} & \dots \\ \hline & & 0 & \dots & \dots \end{array}\right) \tag{A.4}$$

The notation is almost self explaining: H_{00} is the Hamiltonian describing the material which conductance we want to calculate, H_{11}=H_{22}... is the Hamiltonian corresponding to each of the primitive cells of the right lead, and, equivalently, H_{-1-1}=H_{-2-2}... refer to the left lead. H_{01} and H_{-10} describes the coupling of the material and the leads. Implicit assumptions (direct coupling between the leads is negligible, H_{01}=H_{12}...) can be fulfilled by a suitable redefinition of material and leads. For instance, in chapter **??**, H_{00} describes the antiferromagnetic layer **and** part of the ferromagnetic leads. This way, a Hamiltonian with a tridiagonal structure can be obtained. In terms of the Hamiltonian, the green function is defined as:

$$(\omega - \widehat{H})\widehat{G} = 1 \tag{A.5}$$

Projecting over a general part of the complete system, $< n|$ and the material $|0>$, leads the following equations:

$$\begin{aligned} (\omega - H_{0\,0})\,\widehat{G}_{0\,0} - H_{0\,-1}\widehat{G}_{0\,-1} - H_{0\,1}\widehat{G}_{0\,1} = 1 \\ -H_{m\,m+1}\widehat{G}_{m+1\,0} + (\omega - H_{m\,m})\widehat{G}_{m\,0} - H_{m\,m-1}\widehat{G}_{m-1\,0} = 0. \end{aligned} \tag{A.6}$$

A notation change is appropriate here in order to better understand the self-consistent procedure:

$$\begin{aligned} \omega - H_{00} &\longmapsto \tilde{W} \\ \omega - H_{nn} &\longmapsto W \\ -H_{m\prime m} = -H_{m-\prime m} &\longmapsto \tau_{+1} \\ \widehat{G}_{m0} &\longmapsto G_m. \end{aligned} \tag{A.7}$$

So that Eqs. A.6 become:

$$\begin{aligned} \tilde{W}G_0 + \tau_1 G_{-1} + \tau_{-1} G_1 = 1 \\ \tau_{-1} G_{m+1} + W G_m + \tau_1 G_{m-1} = 0 \end{aligned} \tag{A.8}$$

It is convenient to express the Green functions connecting the material and an odd piece of the leads (G_m with m odd in the new notation) in terms of the Green implying the even pieces of the leads, that is, from:

$$\begin{aligned} \tau_{-1}G_2 + WG_1 + \tau_1 G_0 &= 0 \\ \tau_{-1}G_4 + WG_3 + \tau_1 G_2 &= 0 \\ \tau_{-1}G_6 + WG_5 + \tau_1 G_4 &= 0, \end{aligned} \tag{A.9}$$

and the equivalent Eqs. for the left lead (obtained by changing the signs of all subindices), we get:

$$\begin{aligned} G_1 &= -W^{-1}\left(\tau_{-1}G_2 + \tau_1 G_0\right) \\ G_3 &= -W^{-1}\left(\tau_{-1}G_4 + \tau_1 G_2\right) \\ G_5 &= -W^{-1}\left(\tau_{-1}G_6 + \tau_1 G_4\right) \end{aligned} \tag{A.10}$$

So far, we have used only particular cases of Eq. A.6, with m odd, plugging A.10 into the remaining (even m) cases of A.6, and after some straight forward algebra, it is found:

$$\begin{aligned} \left(\tilde{W} - \tau_1 W^{-1}\tau_{-1} - \tau_{-1}W^{-1}\tau_1\right)G_0 + &\quad (-\tau_1 W \tau_1)\,G_{-2} \quad + (-\tau_{-1}W^{-1}\tau_{-1})G_2 = 0 \\ \left(W - \tau_1 W^{-1}\tau_{-1} - \tau_{-1}W^{-1}\tau_1\right)G_2 + &\quad (-\tau_1 W \tau_1)\,G_0 \quad + (-\tau_{-1}W^{-1}\tau_{-1})G_4 = 0 \end{aligned} \tag{A.11}$$

The last Eqs. are equivalent to Eqs. A.6 for a modified system with modified couplings, where *boxes* /*pm*1, /*pm*3 have been renormalized out. This allows us to define the following recursion relations.

$$\begin{aligned} \tilde{W}^{(p)} &= \tilde{W}^{(p/2)} - \tau_{p/2}\left(W^{(p/2)}\right)^{-1}\tau_{-p/2} \\ \tau_{-p} &= -\tau_{-p/2}\left(W^{(p/2)}\right)^{-1}\tau_{-p/2} \\ \tau_p &= -\tau_{p/2}\left(W^{(p/2)}\right)^{-1}\tau_{p/2} \end{aligned} \tag{A.12}$$

No rigurous demonstration of the convergence of the method will be given here, however, note that τ_p effectively couples *boxes* p and 0 which get further apart as p grows. Therefore, it can be expected that τ_p converges to 0. For a sufficiently small τ_p, $\tilde{W}$ contains the relevant information of the Green function of the complete system (system + leads).

Appendix B

Magnetic Phases Observed in Manganites

In this Appendix we will very briefly describe the most relevant magnetic orderings experimentally observed in manganites. Due to the coupling of different degrees of freedom, often magnetic transitions appear accompanied by structural transitions. These couplings might be important to stabilize different phases. However, since other factors (such as the tolerance factor defined in Chapter **??**) are important in determining the structure of manganites, and structural and magnetic orderings are not univocally coupled, we will assume a cubic lattice, and pay little attention to the structural distortions. Anyhow, manganite's structure can be described by small distortions of a cubic structure (**??**) We will follow here the notation of Wollan and Koehler, established in [E.O.Wollan 55] a pioneer neutron diffraction study described in Chapter **??**, and today commonly accepted in manganite's literature. Let us remark, however, that not all the phases described in [E.O.Wollan 55] have been posteriorly confirmed. Wollan and Koehler also proposed some charge orderings compatible with the symmetry observed. This is a complex subject out of the scope of this little guide, so no reference to charge ordering will be given here either.

In the following, each magnetic phase is described by small scheme and the magnetic wave vector in units a pseudo-cubic lattice parameter. Almost all phases studied in this thesis have been included in the appendix. It is only intended as a short guide, so when a short description of the magnetic orderings was appropriate in the discussion, it has been given in the corresponding chapter. Some very particular phases are also described in some chapters and they will be only reference here, they are two complex to be summarized in a small scheme. In chapter 3 besides the A and E phases described here, incommensurate phases consisting in domain walls between E-ordered parts of the material appear. In Chapter **??** multilayers of different materials give rise to exotic orderings. Some can be understood as small parts of the material being CE or Ferromagnetically ordered. Some other are more complex and the periodicity of CE phase is encountered only in two directions, but not in the third (named z in this appendix, and x in chapter **??**)

B.1. Ferromagnetic.

This is the usual ferromagnetic phase. Although it is probably well known by the reader, we describe it for completeness. It has been observed in metallic and insulating samples. Although it was called *B phase* in Ref. [E.O.Wollan 55] we have used the far more common name Ferromagnetic (abbreviated FM) along the thesis.

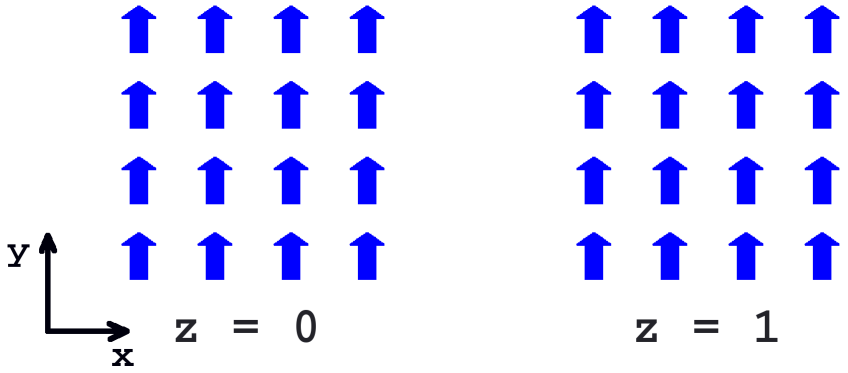

Figure B.1: Ferromagnetic phase.

Wave vector (0,0,0) (homogeneous)

B.2. A phase

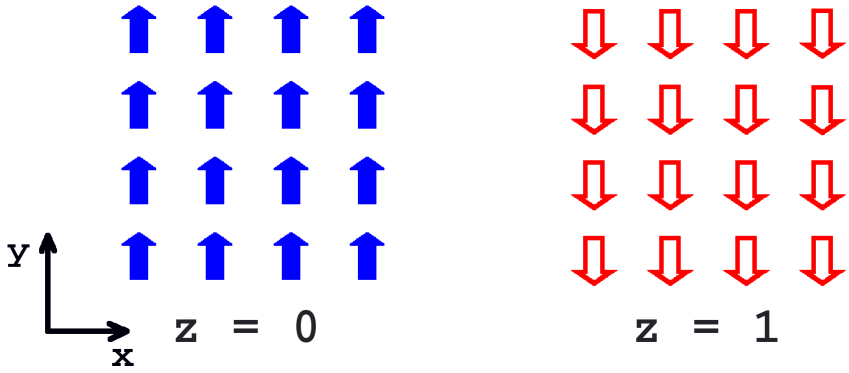

Figure B.2: A phase.

Wave vector $(0, 0, \pi)$

B.3. E phase

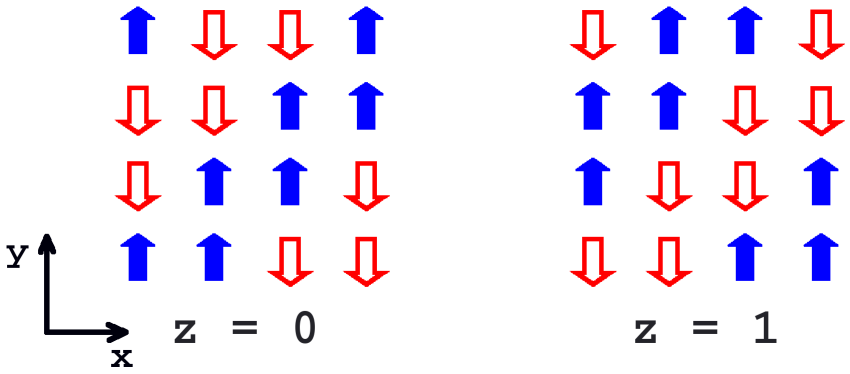

Figure B.3: E phase.

Wave vector $(\frac{\sqrt{2}}{2}\pi, \frac{\sqrt{2}}{2}\pi, \pi)$

B.4. C phase

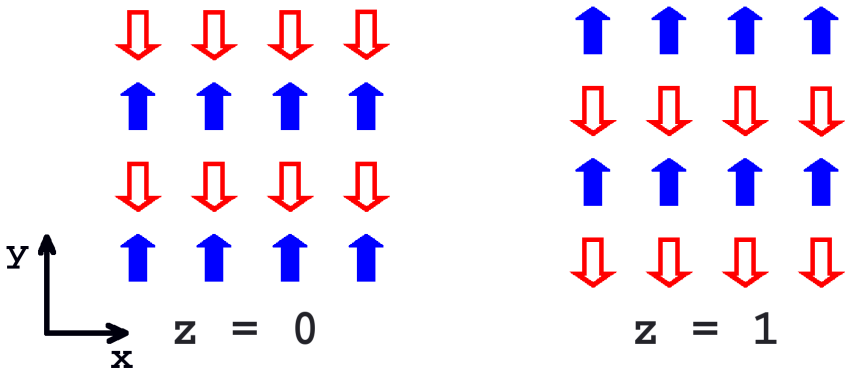

Figure B.4: C phase.

Wave vector $(0,\pi,\pi)$

B.5. CE phase

Wave vector $(\pi/2,\pi/2,\pi)$

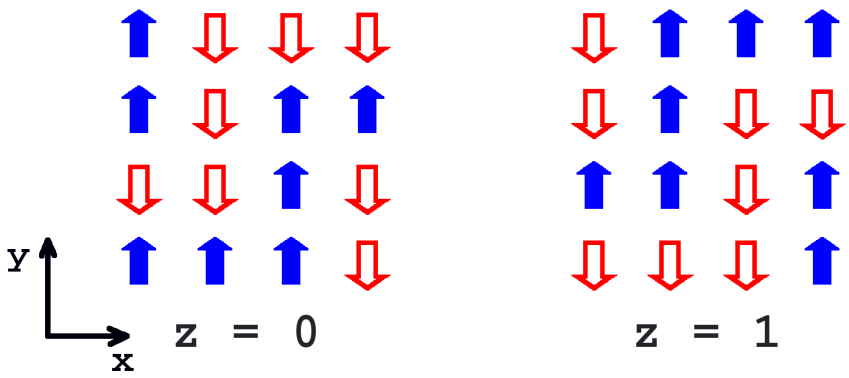

Figure B.5: CE phase.

B.6. G phase

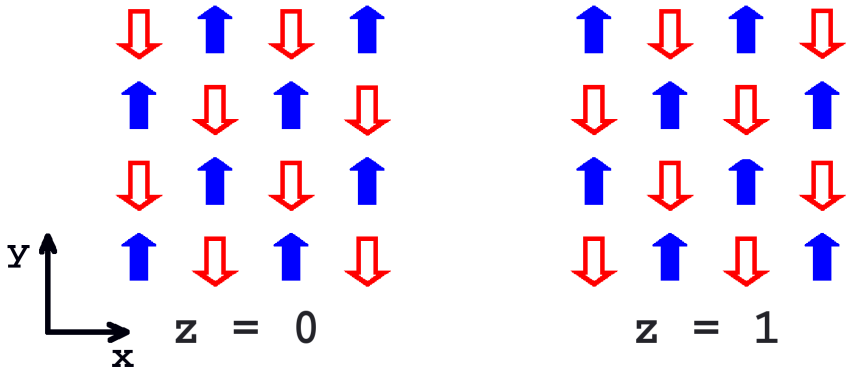

Figure B.6: G phase.

Wave vector (π,π,π)

Bibliography

[Akahoshi 03] D. Akahoshi, M. Uchida, Y. Tomioka, T. Arima, Y. Matsui and Y. Tokura. *Random Potential Effect near the Bicritical Region in Perovskite Manganites as Revealed by Comparison with the Ordered Perovskite Analogs.* Physical Review Letters, 90, 17, 177203, 2003.

[Aliaga 03] H. Aliaga, D. Magnoux, A. Moreo, D. Poilblanc, S. Yunoki and E. Dagotto. Phys. Rev. B, 68, 104405, 2003.

[Alldredge 04] LMB Alldredge and Y. Suzuki. *Colossal magnetoresistance materials-based junctions with antiferromagnetic insulating barriers.* Applied Physics Letters, 85, 437, 2004.

[Alonso 01a] J. L. Alonso, , L. A. Fernández, F. Guinea, V. Laliena and V. Martín-Mayor. Phys. Rev. B, 63, 64416, 2001.

[Alonso 01b] J. L. Alonso, J. A. Capitán, L. A. Fernández, F. Guinea and V. Martín-Mayor. Phys. Rev. B, 64, 54408, 2001.

[Alonso 01c] J.L. Alonso, J.A.Capitán, L. A. Fernández, F. Guinea and V. Martín-Mayor. Phys. Rev. B, 64, 054408, 2001.

[Alvarez 05] G. Alvarez, C. Sen, N. Furukawa, Y. Motome and E. Dagotto. Comp. Phys. Commun., 168, 32, 2005.

[Anane 99] A. Anane, J.-P. Renard, L. Reversat, C. Dupas, P. Veillet, M. Viret, L. Pinsard and A. Revcolevschi. *Colossal resistive relaxation effects in a $Pr_{0.67}Ca_{0.33}MnO_3$ single crystal.* Phys. Rev. B, 59, 1, pages 77–80, Jan 1999.

[Anderson 55] P.W. Anderson and H.Hasewaga. Phys. Rev., 100, 675, 1955.

[Arovas 98] D. P. Arovas and F. Guinea. Phys. Rev. B, 58, 9150, 1998.

[Attfield 06] J.P. Attfield. *Charge ordering in transition metal oxides.* Solid State Sciences, 8, 8, pages 861–867, 2006.

[A.Urushibara 95] A.Urushibara, Y.Moritono, T.Arima, A.Asamisu, G.Kido and Y.Tokura. *Insulator-metal transition and giant magnetoresistance in $La_{1-x}Sr_xMnO_3$.* Phys. Rev. B, 51, 20, pages 14103–14109, May 1995.

[Baibich 88] M. N. Baibich, J. M. Broto, A. Fert, F. Nguyen Van Dau, F. Petroff, P. Eitenne, G. Creuzet, A. Friederich and J. Chazelas. *Giant Magnetoresistance of (001)Fe/(001)Cr Magnetic Superlattices*. Phys. Rev. Lett., 61, 21, pages 2472–2475, Nov 1988.

[Bibes 07] M. Bibes and A. Barthélémy. *Oxide Spintronics*. IEEE Trans. Electron. Devices, 54, 1003, 2007.

[Binasch 89] G. Binasch, P. Grünberg, F. Saurenbach and W. Zinn. *Enhanced magnetoresistance in layered magnetic structures with antiferromagnetic interlayer exchange*. Phys. Rev. B, 39, 7, pages 4828–4830, Mar 1989.

[Blasco 03] J. Blasco, J. García and J. Stankiewicz. *Effects of Ga doping in La_ {2/3} Sr_ {1/3} MnO_ {3}*. Physical Review B, 68, 5, 54421, 2003.

[Bowen 03] M. Bowen, M. Bibes, A. Barthelemy, J.-P. Contour, A. Anane, Y. Lemaitre and A. Fert. *Nearly total spin polarization in La[sub 2/3]Sr[sub 1/3]MnO[sub 3] from tunneling experiments*. Appl. Phys. Lett., 82, 2, pages 233–235, 2003.

[Bransden 80] B. H. Bransden and C. J. Joaquim. *Physics of Atoms and Molecules*. Longmans, New York, 1980.

[Brey 04] Luis Brey. Phys.Rev.Lett., 92, 127202, 2004.

[Brey 07] Luis Brey. *Electronic phase separation in manganite-insulator interfaces*. Phys. Rev. B, 75, 10, 104423, 2007.

[Calderón 98] M. J. Calderón and L. Brey. Phys. Rev. B, 58, 3286, 1998.

[Calderón 99a] M. J. Calderón, L. Brey and F. Guinea. *Surface electronic structure and magnetic properties of doped manganites*. Phys. Rev. B, 60, 6698, 1999.

[Calderón 99b] M. J. Calderón, J. A. Vergés and L. Brey. *Conductance as a Function of the Temperature in the Double Exchange Model*. Phys. Rev. B, 59, 4170, 1999.

[Collado 05] J.A. Collado, C. Frontera, J.L. García-Muñoz and M.G.A. Aranda. J. Solid State Chem., 178, 1949, 2005.

[C.Sen 04] C.Sen, G.Alvarez and E.Dagotto. Phys. Rev. B, 70, 064428, 2004.

[C.Zener 51] C.Zener. *Interaction between the d-Shells in the Transition Metals. II. Ferromagnetic Compounds of Manganese with Perovskite Structure*. Physical Review, 82, 3, pages 403–405, 1951.

[dabrowski 02] B. dabrowski, O. Chmaissen, J. Mais, S. Kolesnik, , J.D. Jorgensen and S. Short. *Increase Of Magnetic Transition Temperatures By Reduction Of Local Disorder For Perovskite Manganites*. Mater. Res. Soc. Symp. Proc., 718, 169, 2002.

[Dagotto 02] E. Dagotto. *Nanoscale Phase Separation and Colossal Magnetoresistance*. Springer-Verlag, Berlin, 2002.

[Dagotto 05] Elbio Dagotto. *Open questions in CMR manganites, relevance of clustered states and analogies with other compounds including the cuprates*. New Journal of Physics, 7, 1, pages 67+, February 2005.

[Damay 97] F. Damay. *Cation disorder and size effects upon magnetic transitions in Ln [sub 0. 5] A [sub 0. 5] MnO [sub 3] manganites*. Journal of Applied Physics, 82, 12, 6181, 1997.

[D.Arovas 99] D.Arovas, G.Gómez-Santos and F.Guinea. Phys. Rev. B, 59, 13569, 1999.

[Datta 97] S. Datta. *Electronic Transport in Mesoscopic Systems*. Cambridge University Press, 1997.

[de Andrés 99] A. de Andrés, M. García-Hernández and JL Martínez. *Conduction channels and magnetoresistance in polycrystalline manganites*. Physical Review B, 60, 10, pages 7328–7334, 1999.

[de Gennes 60] P.-G. de Gennes. Phys. Rev., 118, 141, 1960.

[D.V.Efremov] D.V.Efremov and D.I.Khomskii.

[E.O.Wollan 55] E.O.Wollan and W.C. Koehler. Phys. Rev., 100, 545, 1955.

[et al. 02] R. Kajimoto et al. 2002.

[Fisher 68] M.E. Fisher and J.S.Langer. Phys. Rev. Lett., 20, 665, 1968.

[Fontcuberta 96] J. Fontcuberta, B. Martínez, A. Seffar, S. Piñol, J. L. García-Muñoz and X. Obradors. *Colossal Magnetoresistance of Ferromagnetic Manganites: Structural Tuning and Mechanisms*. Phys. Rev. Lett., 76, 7, pages 1122–1125, Feb 1996.

[Fontcuberta 98] J. Fontcuberta, V. Laukin and X. Obradors. Appl. Phys. Lett., 72, 2607, 1998.

[Furukawa 01] N. Furukawa, Y. Motome and H. Nakata. Comp. Phys. Commun., 142, 757, 2001.

[Garcia 04] V. Garcia, M. Bibes, A. Barthelemy, M. Bowen, E. Jacquet, J.-P. Contour and A. Fert. *Temperature dependence of the interfacial spin polarization of La[sub 2/3]Sr[sub 1/3]MnO[sub 3]*. Phys. Rev. B, 69, 5, 052403, 2004.

[G.DeGennes 68] P. G.DeGennes. Solid State Commun., 6, 163, 1968.

[G.D.Mahan 00] G.D.Mahan. *Many-Particle Physics.- 3rd ed.* Kluwer Academic, New York, 2000.

[Goto 04] T. Goto, T. Kimura, G. Lawes, A.P. Ramirez and Y. Tokura. *Ferroelectricity and giant magnetocapacitance in perovskite rare-earth manganites.* Phys Rev Lett, 92, 25 Pt 1, 257201, 2004.

[Griffiths 69] Robert B. Griffiths. *Nonanalytic Behavior Above the Critical Point in a Random Ising Ferromagnet*. Phys. Rev. Lett., 23, 1, pages 17–19, Jul 1969.

[Guinea 83] F. Guinea, J. Sanchez-Dehesa and F. Flores. *Schottky barrier formation. I. Abrupt metal-semiconductor junctions*. Journal of Physics C: Solid State Physics, 16, 33, pages 6499–6512, 1983.

[Guinea 00] F. Guinea, G. Gómez-Santos and D. Arovas. Phys. Rev. B, 62, 391, 2000.

[Hossain 99] AKM Akther Hossain, LF Cohen, T Kodenkandeth, J MacManus-Driscoll and NM Alford. *Influence of oxygen vacancies on magnetoresistance properties of bulk La0. 67Ca0. 33MnO3-delta*. Journal of Magnetism and Magnetic Materials, 195, 1, pages 31–36, 1999.

[Hotta 03] T. Hotta, M. Moraghebi, A. Feiguin, A. Moreo, S. Yunoki and E. Dagotto. *Unveiling New Magnetic Phases of Undoped and Doped Manganites*. Physical Review Letters, 90, 24, 247203, 2003.

[Huijben 06] M. Huijben, G. Rijnders, D. H. A. Blank, S. Bals, S. Van Aert, J. Verbeeck, G. Van Tendeloo, A. Brinkman and H. Hilgenkamp. *Electronically coupled complementary interfaces between perovskite band insulators*. Nature Materials, 5, 556, 2006.

[Iliev 04] MN Iliev, AP Litvinchuk, MV Abrashev, VN Popov, J. Cmaidalka, B. Lorenz and RL Meng. *Phonons and magnetic excitations in the Mott insulator LaTiO_ {3}*. Physical Review B, 69, 17, 172301, 2004.

[Imada 98] Masatoshi Imada, Atsushi Fujimori and Yoshinori Tokura. *Metal-insulator transitions*. Rev. Mod. Phys., 70, 4, pages 1039–1263, Oct 1998.

[Infante 07] I.C. Infante, S. Estradé, F. Sánchez, J. Arbiol, F. Peiró, V. Laukhin, J. P. Espinós, M. Wojcik, E. Jedryka and J. Fontcuberta. *Strain-driven competition between elastic and orbital ordering effects on thickness-dependent properties of manganites thin films*. 2007. arXiv:0708.3602.

[Ishii 06] Y. Ishii, H. Yamada, H. Sato, H. Akoh, Y. Ogawa, M. Kawasaki and Y. Tokura. *Improved tunneling magnetoresistance in interface engineered (La,Sr)MnO[sub 3] junctions*. Appl. Phys. Lett., 89, 4, 042509, 2006.

[Israel 07] C. Israel, M.J. Calderón and N.D. Mathur. *The current spin on manganites*. Materials Today, 10, 10, pages 24–32, 2007.

[Jahn 37] HA Jahn and E. Teller. *Stability of Polyatomic Molecules in Degenerate Electronic States. I. Orbital Degeneracy*. Proceedings of the Royal Society of London. Series A, Mathematical and Physical Sciences, 161, 905, pages 220–235, 1937.

[Jain 06] M. Jain, P. Shukla, Y. Li, M.f. Hundley, H. Wang, S.r. Foltyn, A.k. Burrell, T.m. Mccleskey and Q Jia. *Manipulating magnetoresistance near room temperature in La? 0. 67 ?Sr? 0. 33 ?MnO? 3 ?/La? 0. 67 ?Ca? 0. 33 ?MnO? 3 ?films prepared by polymer assisted deposition*. Advanced materials (Weinheim), 18, 20, pages 2695–2698, 2006.

[Jin 94] S. Jin, TH Tiefel, M. McCormack, RA Fastnacht, R. Ramesh and LH Chen. *Thousandfold Change in Resistivity in Magnetoresistive La-Ca-Mn-O Films*. Science, 264, 5157, pages 413–415, 1994.

[J.Kanamori 60] J.Kanamori. J. Appl. Phys. (Suppl.), 31, 14S, 1960.

[J.M.D.Coey 99] J.M.D.Coey, M.Viret and S.von Molnar. Adv. Phys., 48, 167, 1999.

[Jonker 50] GH Jonker and JH van Santen. *Ferromagnetic compounds of manganese with perovskite structure*. Physica, 16, 3, pages 337–349, 1950.

[Jullière 75] M. Jullière. Phys. Lett., 54A, 225, 1975.

[Kancharla 06] S. S. Kancharla and E. Dagotto. *Metallic interface at the boundary between band and Mott insulators*. Phys. Rev. B, 74, 19, 195427, 2006.

[K.H.Ahn 04] K.H.Ahn, T.Lookman and A.R.Bishop. Nature, 428, 401, 2004.

[Kim 07] Y. S. Kim, D. J. Kim, T. H. Kim, T. W. Noh, J. S. Choi, B. H. Park and J.-G. Yoon. *Observation of room-temperature ferroelectricity in tetragonal strontium titanate thin films on SrTiO[sub 3] (001) substrates*. Applied Physics Letters, 91, 4, 042908, 2007.

[Kimura 03] K. Kimura, S.Ishihara, H.Shintani, T.Arima, K.T.Takahashi, K.Ishizaka and Y.Tokura. Phys.Rev.B, 68, 060403, 2003.

[Kramer 93] B Kramer and A MacKinnon. *Localization: theory and experiment*. Reports on Progress in Physics, 56, 12, pages 1469–1564, 1993.

[Kubo 72] K. Kubo and N. Ohata. *A Quantum Theory of Double Exchange. I.* Journal of the Physical Society of Japan, 33, 1, pages 21–32, 1972.

[Kusters 89] RM Kusters, J. Singleton, DA Keen, R. McGreevy and W. Hayes. *Magnetoresistance measurements on the magnetic semiconductor Nd0.5 Pb 0.5 MnO 3*. Physica B, 155, 1-3, pages 362–365, 1989.

[L.Brey 05] L.Brey. Phys. Rev. B, 71, 174426, 2005.

[LeClair 00] P. LeClair, H. J. M. Swagten, J. T. Kohlhepp, R. J. M. van de Veerdonk and W. J. M. de Jonge. *Apparent Spin Polarization Decay in Cu-Dusted $Co/Al_2O_3/Co$ Tunnel Junctions*. Phys. Rev. Lett., 84, 13, pages 2933–2936, Mar 2000.

[Li 97] Q. Li, J. Zang, AR Bishop and CM Soukoulis. *Charge localization in disordered colossal-magnetoresistance manganites*. Physical Review B, 56, 8, pages 4541–4544, 1997.

[Li 02] H. Li, J. R. Sun and H. K. Wong. *Enhanced low-field magnetoresistance in La[sub 2/3]Ca[sub 1/3]MnO[sub 3]/Pr[sub 2/3]Ca[sub 1/3]MnO[sub 3] superlattices*. Appl. Phys. Lett., 80, 4, pages 628–630, 2002.

[Lian 99] GJ Lian, ZH Wang, J. Gao, JF Kang, MY Li and GC Xiong. *Large low-field magnetoresistance observed in heterostructure*. J. Phys. D: Appl. Phys, 32, pages 90–93, 1999.

[Lin 06] Chungwei Lin, Satoshi Okamoto and Andrew J. Millis. *Dynamical mean-field study of model double-exchange superlattices*. Phys. Rev. B, 73, 4, 041104, 2006.

[Lu 96] Y. Lu, X. W. Li, G. Q. Gong, Gang Xiao, A. Gupta, P. Lecoeur, J. Z. Sun, Y. Y. Wang and V. P. Dravid. *Large magnetotunneling effect at low magnetic fields in micrometer-scale epitaxial $La_{0.67}Sr_{0.33}MnO_3$ tunnel junctions*. Phys. Rev. B, 54, R8357, 1996.

[MARTIN 96] C. MARTIN, A. MAIGNAN and B. RAVEAU. *Effect of aluminium for manganese substitution upon the GMR properties of the praseodymium manganites*. Journal of material chemistry, 6, 7, pages 1245–1248, 1996.

[Mayr 01] Matthias Mayr, Adriana Moreo, Jose A. Vergés, Jeanette Arispe, Adrian Feiguin and Elbio Dagotto. *Resistivity of Mixed-Phase Manganites*. Phys. Rev. Lett., 86, 1, pages 135–138, Jan 2001.

[Millange 98] F. Millange, V. Caignaert, B. Domengès, B. Raveau and E. Suard. *Order-Disorder Phenomena in New LaBaMn 2 O 6-x CMR Perovskites. Crystal and Magnetic Structure*. Chemistry of materials, 10, 7, pages 1974–1983, 1998.

[Millis 96] A. J. Millis, Boris I. Shraiman and R. Mueller. *Dynamic Jahn-Teller Effect and Colossal Magnetoresistance in $La_{1-x}Sr_xMnO_3$*. Phys. Rev. Lett., 77, 1, pages 175–178, Jul 1996.

[Millis 97] AJ Millis. *Orbital ordering and superexchange in manganite oxides*. Physical Review B, 55, 10, pages 6405–6408, 1997.

[Millis 98] AJ Millis. *Lattice effects in magnetoresistive manganese perovskites*. Nature, 392, 6672, pages 147–150, 1998.

[Millis 00] AJ Millis. *Theory of CMR Manganites*, volume 53. 2000.

[Millis 03] AJ Millis. *Towards a classification of the effects of disorder on materials properties*. Solid State Communications, 126, 1-2, pages 3–8, 2003.

[Mochizuki 04] M. Mochizuki and M. Imada. *Orbital physics in the perovskite Ti oxides*. New Journal of Physics, 6, 1, 154, 2004.

[Moshnyaga 06] V. Moshnyaga, L. Sudheendra, OI Lebedev, SA Köster, K. Gehrke, O. Shapoval, A. Belenchuk, B. Damaschke, G. van Tendeloo and K. Samwer. *A-Site Ordering versus Electronic Inhomogeneity in Colossally Magnetoresistive Manganite Films*. Physical Review Letters, 97, 10, 107205, 2006.

[Motome 03] Y. Motome, N. Furukawa and N. Nagaosa. *Competing Orders and Disorder-Induced Insulator to Metal Transition in Manganites*. Physical Review Letters, 91, 16, 167204, 2003.

[Mukhopadhyay 06] S. Mukhopadhyay and I. Das. *Giant enhancement of room-temperature magnetoresistance in LaSrMnO/ NdSrMnO multilayers*. Applied Physics Letters, 88, 032506, 2006.

[Müller-Hartmann 96] Erwin Müller-Hartmann and Elbio Dagotto. *Electronic Hamiltonian for transition-metal oxide compounds*. Phys. Rev. B, 54, 10, pages R6819–R6822, Sep 1996.

[Muñoz 01] A. Muñoz, M. T. Casáis, J. A. Alonso, M. J. Martínez-Lope, J. L. Martínez and M. T. Fernández-Díaz. Inorg. Chem., 40, 1020, 2001.

[Nakatsuji 00] S. Nakatsuji and Y. Maeno. *Quasi-Two-Dimensional Mott Transition System Ca_ {2-x} Sr_ {x} RuO_ {4}*. Physical Review Letters, 84, 12, pages 2666–2669, 2000.

[Niebieskikwiat 07] D. Niebieskikwiat, M. B. Salomon, L. E. Hueso, N. D. Mathur and J. A. Borchers. *Nanoscale magnetic structure of FM/AF manganite multilayers*. 2007. cond-mat/0702350.

[not] The participations number for an eigenvector of the sytems, $|\psi>$ is defined as $P = \sum |<i|\psi>^4|$ for more details about its relation to localization see ref [Kramer 93].

[N.W.Ashcroft 76] N.W.Ashcroft and N.D.Mermin. In Solid State Physics.Saunders College Publishing, New York, 1976.

[Okamoto 04] S. Okamoto and A.J. Millis. *Electonic reconstruction at an interface between a Mott insulator and a band insulator*. Nature, 428, 630, 2004.

[Park 98a] J.-H. Park, E. Vescovo, H.-J. Kim, C. Kwon, R. Ramesh and T.Venkatesan. *Magnetic properties at surface boundary of a half-metallic ferromagnet* $La_{0.7}Sr_{0.3}MnO_3$. Phys. Rev. Lett., 81, 1953, 1998.

[Park 98b] J.-H. Park, E. Vescovo, H.-J. Kim, C. Kwon, R. Ramesh and T. Venkatesan. *Direct evidence for a half-metallic ferromagnet.* Nature (London), 392, 794, 1998.

[P.Bak 80] P.Bak and J. von Boehm. Phys. Rev. B, 21, 5297, 1980.

[Pickett 96] W. E. Pickett and D. J. Singh. *Electronic structure and half-metallic transport in the* $La_{1-x}Ca_xMnO_3$ *system.* Phys. Rev. B, 53, 1146, 1996.

[Popovic 00] Z. Popovic and S. Satpathy. *Cooperative Jahn-Teller Coupling in the Manganites.* Physical Review Letters, 84, 7, pages 1603–1606, 2000.

[P.Schiffer 95] P.Schiffer, A.P.Ramirez, W.Bao and S.-W.Cheong. *Low Temperature Magnetoresistance and the Magnetic Phase Diagram of* $La_{1-x}Ca_xMnO_3$. Phys. Rev. Lett., 75, 18, pages 3336–3339, Oct 1995.

[Ritter 97] C. Ritter, MR Ibarra, JM De Teresa, PA Algarabel, C. Marquina, J. Blasco, J. García, S. Oseroff and SW Cheong. *Influence of oxygen content on the structural, magnetotransport, and magnetic properties of LaMnO_* $\{3+\delta\}$. Physical Review B, 56, 14, pages 8902–8911, 1997.

[Rivas 00] J. Rivas, LE Hueso, A. Fondado, F. Rivadulla and MA López-Quintela. *Low field magnetoresistance effects in fine particles of La0. 67Ca0. 33MnO3 perovskites.* Journal of Magnetism and Magnetic Materials, 221, 1-2, pages 57–62, 2000.

[Rodríguez-Carvajal 98] J. Rodríguez-Carvajal, M. Hennion, F. Moussa, AH Moudden, L. Pinsard and A. Revcolevschi. *Neutron-diffraction study of the Jahn-Teller transition in stoichiometric LaMnO_* $\{3\}$. Physical Review B, 57, 6, pages 3189–3192, 1998.

[Rodriguez-Martinez 96] L.M. Rodriguez-Martinez and J.P. Attfield. *Cation disorder and size effects in magnetoresistive manganese oxide perovskites.* Physical Review B, 54, 22, pages 15622–15625, 1996.

[Salafranca 06a] J. Salafranca and L. Brey. Phys. Rev. B, 73, 024422, 2006.

[Salafranca 06b] J. Salafranca and L. Brey. *Phase diagram and incommensurate phases in undoped manganites.* Physical Review B, 73, 2, 24422, 2006.

[Salamon 02] M. B. Salamon, P. Lin and S. H. Chun. *Colossal Magnetoresistance is a Griffiths Singularity.* Phys. Rev. Lett., 88, 19, 197203, Apr 2002.

[Sawaki 00a] Y. Sawaki, K. Takenaka, A. Osuka, R. Shiozaki and S. Sugai. *Al-substitution effect on charge transport in La_ {1-x} Sr_ {x} MnO_ {3}: Incoherent metallic state in a double-exchange ferromagnet.* Physical Review B, 61, 17, pages 11588–11593, 2000.

[Sawaki 00b] Y. Sawaki, K. Takenaka, A. Osuka, R. Shiozaki and S. Sugai. *Al-substitution effect on charge transport in $La_{1-x}Sr_xMnO_3$: Incoherent metallic state in a double-exchange ferromagnet.* Phys. Rev. B, 61, 17, pages 11588–11593, May 2000.

[Sen 06a] C. Sen, G. Alvarez, H. Aliaga and E. Dagotto. Phys. Rev. B, 73, 224441, 2006.

[Sen 06b] C. Sen, G. Alvarez, Y. Motome, N. Furukawa, I. A. Sergienko, T. Schulthess, A. Moreo and E. Dagotto. Phys. Rev. B, 73, 224430, 2006.

[Sergienko] I. A. Sergienko and E. Dagotto.

[S.Kumar 03] S.Kumar and P.Majumdar. Phys. Rev. Lett., 91, 246602, 2003.

[S.Kumar 06] S.Kumar and P.Majumdar. Phys. Rev. Lett., 96, 016602, 2006.

[Teresa 97] J.M. De Teresa, M. R. Ibarra, P. A. Algarabel, C. Ritter, C. Marquina, J. Blasco, J. García, A. del Moral and Z. Arnold. Nature, 386, 256, 1997.

[T.Hotta 03] T.Hotta. Phys. Rev. B, 67, 104428, 2003.

[T.J.Sato 04] T.J.Sato, J.W.Lynn and B.Dabrowski. Phys. Rev. Lett., 93, 267204, 2004.

[Tokura 00] Y. Tokura. *Colossal Magnetoresistive Oxides.* CRC Press, 2000.

[Tomioka 96] Y. Tomioka, A. Asamitsu, H. Kuwahara, Y. Moritomo and Y. Tokura. *Magnetic-field-induced metal-insulator phenomena in $Pr_{1-x}Ca_xMnO_3$ with controlled charge-ordering instability.* Phys. Rev. B, 53, 4, pages R1689–R1692, Jan 1996.

[Trukhanov 02] SV Trukhanov, IO Troyanchuk, M. Hervieu, H. Szymczak and K. Bärner. *Magnetic and electrical properties of LBaMn_ {2} O_ {6-γ}(L= Pr, Nd, Sm, Eu, Gd, Tb) manganites.* Physical Review B, 66, 18, 184424, 2002.

[van den Brink 99a] J. van den Brink, G. Khaliullin and D. Khomskii. *Charge and Orbital Order in Half-Doped Manganites.* Physical Review Letters, 83, 24, pages 5118–5121, 1999.

[van den Brink 99b] Jeroen van den Brink, Giniyat Khaliullin and Daniel Khomskii. *Charge and Orbital Order in Half-Doped Manganites*. Phys. Rev. Lett., 83, 24, pages 5118–5121, 1999.

[van Santen 50] JH van Santen and GH Jonker. *Electrical conductivity of ferromagnetic compounds of manganese with perovskite structure*. Physica, 16, 7-8, pages 599–600, 1950.

[Van Vlek 32] J. H. Van Vlek. *The Theory Of Electric And Magnetic Susceptibilities*. Oxford At The Clarendon Press, 1932.

[Venimadhav 01] A. Venimadhav, MS Hegde, R. Rawat, I. Das and M. El Marssi. *Enhancement of magnetoresistance in La 0.67 Ca 0.33 MnO 3/Pr 0.7 Ca 0.3 MnO 3 epitaxial multilayers*. Journal of Alloys and Compounds, 326, 1-2, pages 270–274, 2001.

[Vergés 99a] J. A. Vergés. Comput. Phys. Commun., 118, 71, 1999.

[Vergés 99b] JA Vergés. *Computational implementation of the Kubo formula for the static conductance: Application to two-dimensional quantum dots*. Computer Physics Communications, 118, 1, pages 71–80, 1999.

[Vergés 02] J. A. Vergés, V. Martín-Mayor and L. Brey. Phys. Rev. Lett., 88, 136401, 2002.

[Volger 54] J. Volger. *Further Experimental Investigations on some Ferromagnetic Oxidic Compounds of Manganese with Perovskite Structure*. Physica, 20, 1954.

[von Helmolt 93] R. von Helmolt, J. Wecker, B. Holzapfel, L. Schultz and K. Samwer. *Giant negative magnetoresistance in perovskitelike La_ {2/3} Ba_ {1/3} MnO_ {x} ferromagnetic films*. Physical Review Letters, 71, 14, pages 2331–2333, 1993.

[Williams 03] AJ Williams, BM Sobotka and JP Attfield. *Charge disorder effects in 3d transition metal oxide perovskites*. Journal of Solid State Chemistry, 173, 2, pages 456–461, 2003.

[W.L.McMillan 76] W.L.McMillan. Phys. Rev. B, 14, 1496, 1976.

[W.L.McMillan 77] W.L.McMillan. Phys. Rev. B, 16, 4655, 1977.

[Yamada 04] H. Yamada, Y. Ogawa, Y. Ishii, H. Sato, M. Kawasaki, H. Akoh and Y. Tokura. *Engineered interface of magnetic oxides*. Science, 305, pages 646–648, 2004.

[Yoshizawa 96] H. Yoshizawa, H. Kawano, Y. Tomioka and Y. Tokura. *Magnetic-Field-Induced Metal-Insulator Transition in* $Pr_{0.7}Ca_{0.3}MnO_3$. J. Phys. Soc. Jpn., 65, pages 1043–+, April 1996.

[Y.Tokura 00] Y.Tokura and N.Nagaosa. Science, 288, 462, 2000.

[Zener 51] C. Zener. *Interaction Between the d Shells in the Transition Metals*. Phys. Rev., 81, 3, pages 440–444, Feb 1951.

[Zhou 06] J.S. Zhou and JB Goodenough. *Unusual Evolution of the Magnetic Interactions versus Structural Distortions in RMnO_ {3} Perovskites*. Physical Review Letters, 96, 24, 247202, 2006.

[Zutic 04] Igor Zutic, Jaroslav Fabian and S. Das Sarma. *Spintronics: Fundamentals and applications*. Rev. Mod. Phys., 76, 2, 323, 2004.